FOCAL MECHANISMS OF EARTHQUAKES IN WESTERN TURKEY AND THEIR TECTONIC IMPLICATIONS

A Dissertation
Presented to the Faculty
of the New Mexico Institute of
Mining and Technology

In Partial Fulfillment
of the Requirements for the
Degree of Doctor of Philosophy
in Geoscience

by
Ömer Alptekin
May 1973

ABSTRACT

Focal mechanisms of 10 damaging earthquakes that have occurred in the Aegean-Anatolian sector of the Alpine seismic belt were determined from an analysis of P wave first motions on the long-period seismograms of the Worldwide Standardized Seismographs. Six of these earthquakes were located in western Turkey, one in southwestern Turkey, two in the eastern Mediterranean Sea, and one in the northern Aegean Sea.

Earthquakes in western Turkey were due to normal faulting, indicative of crustal extension. Tensional axes determined for these earthquakes are nearly horizontal and perpendicular to the general east-west trend of graben structures. Fault-plane solutions for the destructive Gediz earthquake of March 28, 1970, and its aftershocks, and the complex surface faulting of the normal type associated with these shocks indicate multiple fracturing. The east-west and the southeast-northwest tectonic lines in the Gediz region were both reactivated during these earthquakes.

The focal mechanism of the Burdur earthquake of May 12, 1971, in southwestern Turkey was right-lateral strike-slip faulting and indicates that the eastern termination of the Aegean arc is an arc-to-arc transform fault.

The eastern Mediterranean earthquakes were the result of low-angle reverse faulting and indicate that the Mediterranean lithosphere is underthrusting the Aegean-Turkish block. A strike-slip solution for the northern Aegean earthquake of February 19, 1968, indicates that the right-lateral movements associated with the north Anatolian fault probably continue into the Aegean Sea.

A special study conducted during the research indicates that fault-plane solutions are strongly affected by the choice of P wave velocity at the focus. Incorrect choice of low velocity is shown to introduce a significant strike-slip component of motion in dip-slip solutions.

Seismicity, earthquake mechanisms and the geology of the eastern Mediterranean and Turkey indicate complex deformation in this region. The Aegean-Turkish block is a westward moving plate undergoing internal deformation as the result of overriding the downgoing African plate. The diffuse seismic activity within the plate is not directly related to horizontal motions but is a consequence of vertical movements inside the plate. The driving mechanism of the Aegean-Turkish plate probably is mantle convection beneath a thermal hot spot in eastern Turkey.

ACKNOWLEDGEMENTS

I am much indebted to Dr. Allan R. Sanford, my advisor and committee chairman, for his continued guidance, encouragement and generous assistance in every aspect of this study.

I would like to thank the other members of my committee, Dr. Antonius J. Budding, Dr. Marvin H. Wilkening and Dr. Charles R. Holmes, for their advice and suggestions.

I benefited much from communications with Dr. Nezihi Canitez of Istanbul Technical University during the early stages of this work.

Finally I thank my wife Meral for her patience and encouragement during the time of my graduate study.

Financial assistance for the research was provided by the Geoscience Department of the New Mexico Institute of Mining and Technology.

TABLE OF CONTENTS

LIST OF FIGURES

LIST OF TABLES

1. INTRODUCTION

Purpose of the Dissertation

The purpose of this dissertation was four-fold: (1) to determine the focal mechanisms of some recent damaging earthquakes that occurred in western Turkey, the eastern Mediterranean Sea and the northern Aegean Sea; (2) to compare the earthquake mechanisms with postulated crustal movements in the eastern Mediterranean and Turkey; (3) to investigate the possibility of deformation in the interior of a continental lithospheric plate and (4) to test the applicability of the concept of "Plate Tectonics" to the Aegean-Anatolian sector of the Mediterranean region.

Method Used

The method used to determine earthquake mechanisms is called the fault-plane solution technique. This technique was initiated by Byerly in 1926 on the basis of the fault rebound theory formulated by Reid (1910) and Nakano (1923). The method was perfected by Byerly and his students in the United States; Koning, Ritsema and Scheidegger in Europe; Hodgson, Wickens and Stevens in Canada; Honda in Japan and Keilis-Borok, et al. in the U.S.S.R. A complete bibliography on the development and applications of the fault-plane technique can be found in papers by Honda (1962), and Stauder (1962).

Because of ease in use, the fault-plane technique has received a wide scale application and therefore its impact on the development of new dynamic theories of global tectonics has been significant. Sykes (1967) used the technique to obtain positive evidence for sea-floor

spreading (Hess, 1960), and transform faults (Wilson, 1965). Despite its large scale applications, adequate attention has not been given to the difficulties involved in fault-plane solutions (Ritsema, 1967). Some of these difficulties are discussed in this dissertation.

Significance

Within the past 10 years a remarkable revolution has taken place in our understanding of the global features of the earth. A new dynamic theory, which is called "Plate Tectonics," has evolved from the earlier concepts of continental drift as published by Wegener in 1929 (Wegener, 1966) and sea floor spreading (Hess, 1960; Vine and Matthews, 1963). According to the new theory, the earth to a depth of about 100 km is made up of a number of rigid plates or blocks which are in motion relative to each other (McKenzie and Parker, 1967; Morgan, 1968). The boundaries of plates are defined by the seismic zones of the earth. Three types of plate boundaries have been recognized; rises, sinks, and the transform faults.

Rises are the sites where new lithosphere is produced. They form continuous zones along the mid-oceanic ridges and are frequently offset by transform faults. The seismic activity along mid-ocean ridges occurs at shallow depths (< 70 km) and is confined to a narrow zone. Sinks are the sites where old lithosphere is consumed. They are related to deep oceanic trenches and volcanic island-arc systems. In the sink areas, shallow, intermediate (70-300 km) or deep (300-700 km) focus earthquakes

may occur. The intermediate and deep focus earthquakes form an inclined zone underlying the active volcanic chains. These inclined seismic zones are called Benioff zones. To account for the geological observations in the sink areas, a new term "subduction zone" has been adopted.

Transform faults occur where plates slide past each other. This type of plate boundary only generates shallow focus earthquakes, and frequently these have large magnitudes.

Plate tectonics has been based mainly on the data from oceanic areas. In the oceans, earthquakes are confined to narrow zones and thus the plate boundaries are relatively simple. In the continents, however, seismic activity occurs along broad belts, indicating complex deformation. Plate boundaries and plate motions in the continental areas have been studied very little, in spite of the fact that the geology of the continents is better known than the oceans (Beloussov, 1969).

The difference between the seismicity of continents and oceans may result for two reasons (McKenzie, 1972b). First, the composition of the oceanic and the continental lithospheres are different. At low temperatures the silica-rich continental rocks may fracture more easily than the silica-poor basalts in oceanic rocks. Second, the continental lithosphere is older and contains many old faults. These old lines of weaknesses may be reactivated from the interaction of plates. These possibilities could be tested by seismological means. The first problem may be solved by laboratory studies but a further discussion of it is beyond the scope of this study.

The second problem can be investigated with the aid of seismicity and focal mechanism studies. The Aegean-Anatolian sector of the

Mediterranean region is a suitable area for such a study, because the seismicity and the geology of the area have been studied (Ergin, et al., 1967; Ketin, 1968; Galonopoulos, 1967). Focal mechanisms of earthquakes for this area have been presented in papers by Canitez and Ucer (1967), Papazachos and Delibasis (1969), McKenzie (1970) and McKenzie (1972b). Most of the fault-plane solutions given in these papers, except the last one which appeared toward the final stages of this investigation, are for earthquakes located along the boundaries of the major seismic zone in the eastern Mediterranean and Turkey. Only a few solutions are given for the continental interiors of western Turkey, an area that is seismically very active at the present time. The epicenters of many recent destructive earthquakes are located in this part of Turkey. Some of these earthquakes produced surface faulting.

McKenzie (1970) has suggested that a boundary between two plates, the Aegean and Turkish, may pass through western Turkey. Although some geologic evidence may support this hypothesis, the seismicity does not clearly substantiate the idea. In this area the earthquake activity is diffuse and therefore not typical of the majority of plate boundaries. Therefore an important question is whether the seismic activity arises from movement along a plate boundary or is the result of internal deformation within the Anatolian-Aegean block caused by vertical movements.

Study of primary vertical movements within the lithosphere, independent of their horizontal movements is a fundamental problem. An attempt was made in this research to provide evidence for vertical movements inside the Anatolian-Aegean block, using studies of earthquake

mechanism for earthquakes located in the area.

Organization

The dissertation contains five major sections and an Appendix. The introduction is followed by an informative section on the geology and tectonics of the area of study. Fault-plane solutions are presented and discussed in detail in section 3. The fundamentals of the fault-plane technique and some problems involved in the method are also discussed in this section. In section 4 the earthquake mechanisms, seismicity and geology are used to explain the current crustal motions in Turkey and adjacent areas in the eastern Mediterranean. In section 5 the dissertation is summarized and main conclusions are stated. The first motion data for the fault-plane solutions are tabulated and briefly discussed in Appendix I.

2. GEOLOGY AND TECTONICS OF TURKEY AND THE EASTERN MEDITERRANEAN

Introduction

The geology and tectonics of Turkey and the eastern Mediterranean are fairly complex and cannot be described fully in a short review. However for future reference in the dissertation, a brief summary is given here. Some structural features described in this section will be discussed in greater detail in connection with the seismicity and the earthquake mechanisms later in the dissertation. For a complete account of the geology and tectonics of Turkey and the eastern Mediterranean reference sould be made to Campbell (1971) and Ryan, et al. (1970).

Turkey

Tectonics and Geology

Turkey is an outstanding landmass in the Mediterranean sector of the Alpine orogenic belt. The main tectonic units and the major fault lines of Turkey are shown in Figures 2.1 and 2.2. The orogenic development of Turkey is similar to that of Europe but the post orogenic movements in Turkey have been quite different and more intense. Block faulting of younger age has modified the topography that was formed by the Alpine folding. There are numerous faults and grabens parallel or perpendicular to the axis of the Alpine orogeny. The Aegean and the Marmara basins were formed during the post orogenic period (Ilhan, 1971). The following structural units in the tectonics of Turkey have been recognized by Ketin (1968):

1. Metamorphic-crystalline massifs.
2. Folded Paleozoic mountain chains.
3. Folded mountains of Mesozoic and Tertiary age.
4. Major faults and overthrusts of late Alpine period.
5. Grabens and depressions of post Alpine period.
6. Active faults and main earthquake zones.

The metamorphic-crystalline massifs are composed of rocks that were subject to varying degrees of metamorphism, and of crystalline rocks of mafic and silicic composition. They form large masses in western, central and southeastern Anatolia (see Figure 2.1) and respond as rigid bodies against tectonic deformation. Some of these massifs are of Paleozoic age and formed during the Caledonian or Hercynian orogeny. Others are of Lower Mesozoic age and formed during the early stages of the Alpine orogeny.

The folded mountain chains of Paleozoic age are found mainly in northwestern Anatolia in the area surrounding the sea of Marmara. The folded mountain chains of Mesozoic-Tertiary age comprise the youngest mountains of Alpine orogeny in Turkey. The Black sea coastal mountains in the north (Pontids) and the Taurus mountains in the south are included in this group. Mafic and ultramafic rocks, like gabbro and serpentinite, have taken part in the evolution of the Alpine mountain chains in Anatolia. This ophiolitic sequence occurs over large areas and is accompanied by radiolarite and includes submarine lava flows at some places. They are the host rocks for some important mineral deposits like chromite, copper and manganese.

The last stages of Alpine orogeny are responsible for the severe overthrusting seen in large areas of Turkey. The best examples are

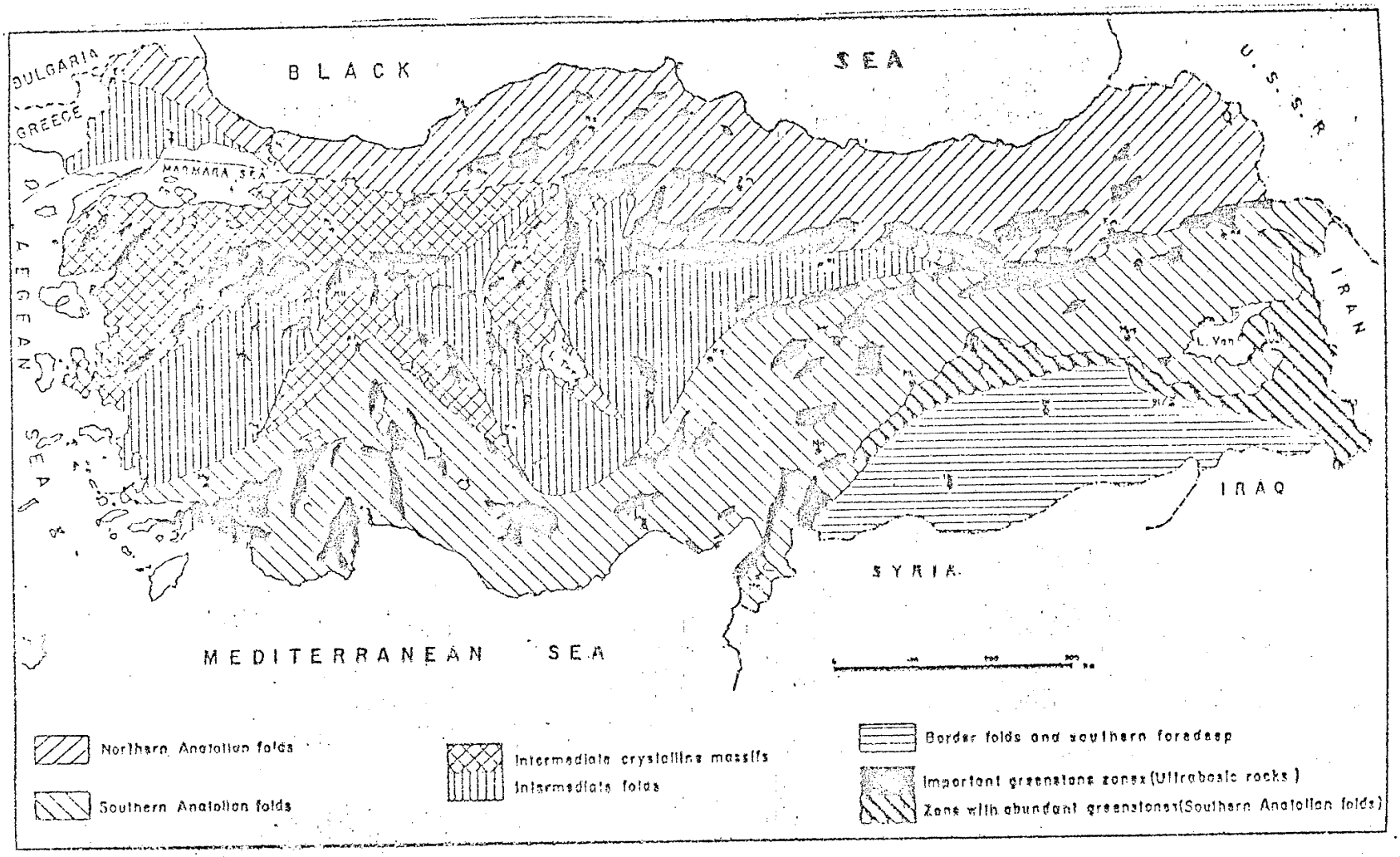

Figure 2.1. Main tectonic units of Turkey (After İlhan, 1971).

found in central, southwestern and especially southeastern Turkey.

The outstanding example of strike-slip faulting, the well-known North Anatolian fault, is a zone of depressions, grabens and faults (Figure 2.2). Its best known section extends from Abant in western Anatolia to Karliova in the eastern Anatolia (Allen, 1969). Galanopoulos (1967) suggested a continuation of this fault zone as far as the Ionian islands in the west. The eastern extension of the fault is not clearly understood but it divides into several branches. Two branches extend toward the Caucasus mountains, another branch extends into Iran. Large right-lateral movements along the North Anatolian fault have been well documented from the strong earthquakes that have occurred along it recently (Ambraseys and Zatopek, 1969). Other examples of strike-slip faulting in Turkey are seen in the southern part of the country.

Several large normal faults are found in western and central Anatolia (see Figure 2.2). Other examples of normal faulting occur in southeastern Turkey. Grabens of different size were formed in the regions of normal faulting. The low areas in these block faulted regions were filled with late Tertiary and Quaternary age sediments. Besides these depressions there are several other mobile sedimentary basins which were formed in connection with epeirogenic movements. Some of these basins have been subsiding continuously since the main phase of Alpine orogeny (Ketin, 1968).

Seismotectonics

Turkey and the adjacent areas in the eastern Mediterranean comprise the most active segment of the Mediterranean sector of the Alpine seismic

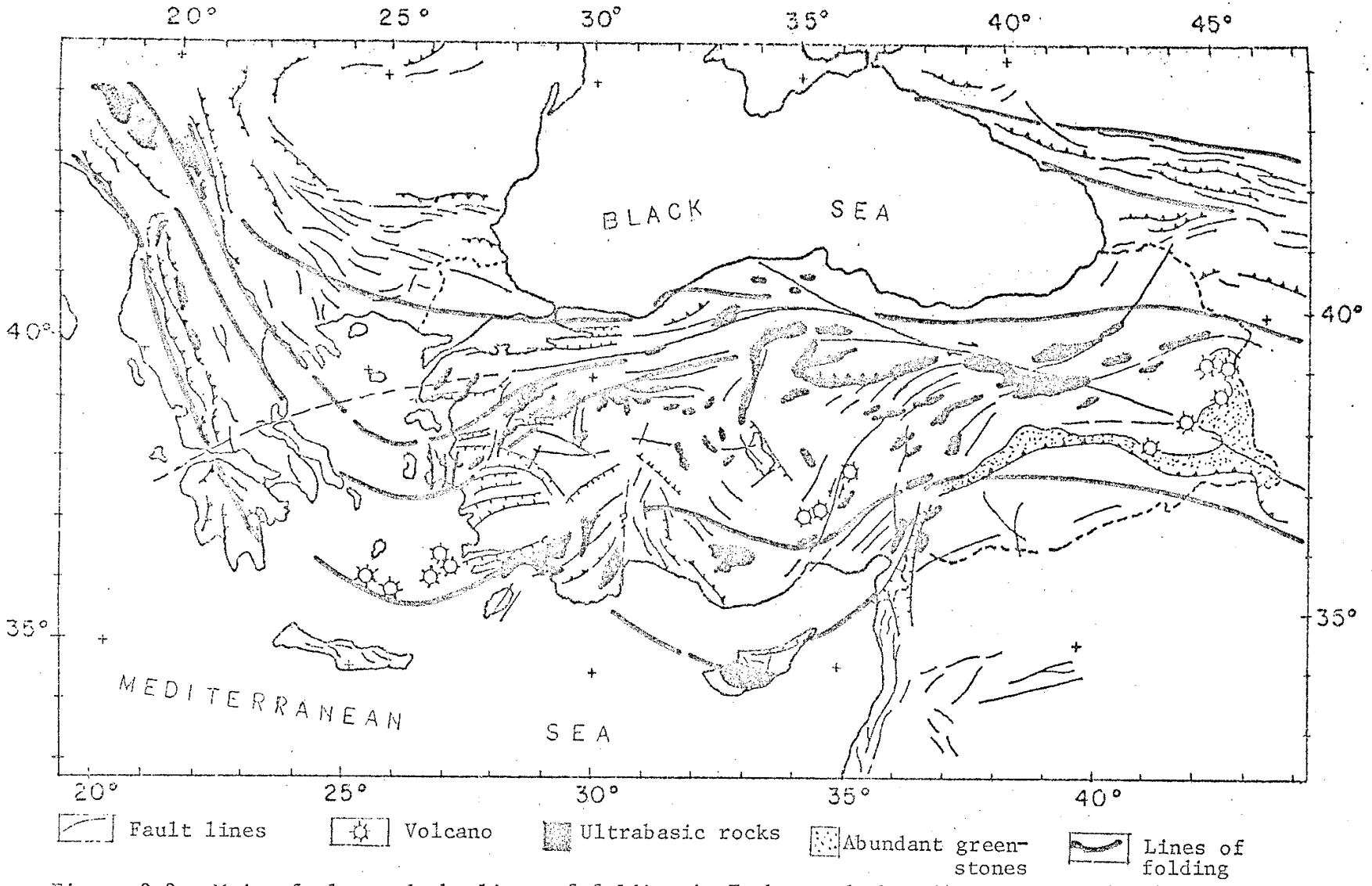

Figure 2.2. Major faults and the lines of folding in Turkey and the adjacent areas in the eastern Mediterranean (Compiled from the Geological Map of Europe (Unesco Publication), and İlhan, 1971).

belt. The most severe earthquakes in Turkey occur along the North Anatolian Fault zone and in the Aegean Rift zone in western Turkey. Areal distribution of epicenters in Turkey and the adjacent areas in the eastern Mediterranean are shown in Figures 2.3a and b. The seismic activity in Turkey appears to be related to relatively young fault lines (compare Figures 2.2 and 2.3). Most of the faults mentioned above are active. The following primary earthquake zones have been recognized in Turkey (Ilhan, 1971):

1. Aegean-Marmara zone,
2. Northern Anatolian zone,
3. Central Anatolian zone,
4. Southeastern Anatolian zone.

The seismic activity in the Aegean-Marmara zone is related to a number of east-west trending grabens. The relation of the north-south trending faults, that intersect the east-west trending grabens, to the seismicity is not clear at this time. Since the 11th century 350 major earthquakes have occurred in this zone (Ilhan, 1971).

The earthquakes in the North Anatolian zone are associated with right-lateral movements along the North Anatolian fault. Modern seismological data indicate progressive surface faulting (or a systematic migration of epicenters) toward the west. The velocity of migration has varied from 50 km/year to 145 km/year (Karnik, 1971). Recently, fault creep at a rate of 1-2 cm/year on the west central segment of the North Anatolian fault has been determined instrumentally by Nason and Aytun (Geotimes, September, 1972, p. 10). Approximately 200 major earthquakes have been reported in the North Anatolian zone since the 2nd century.

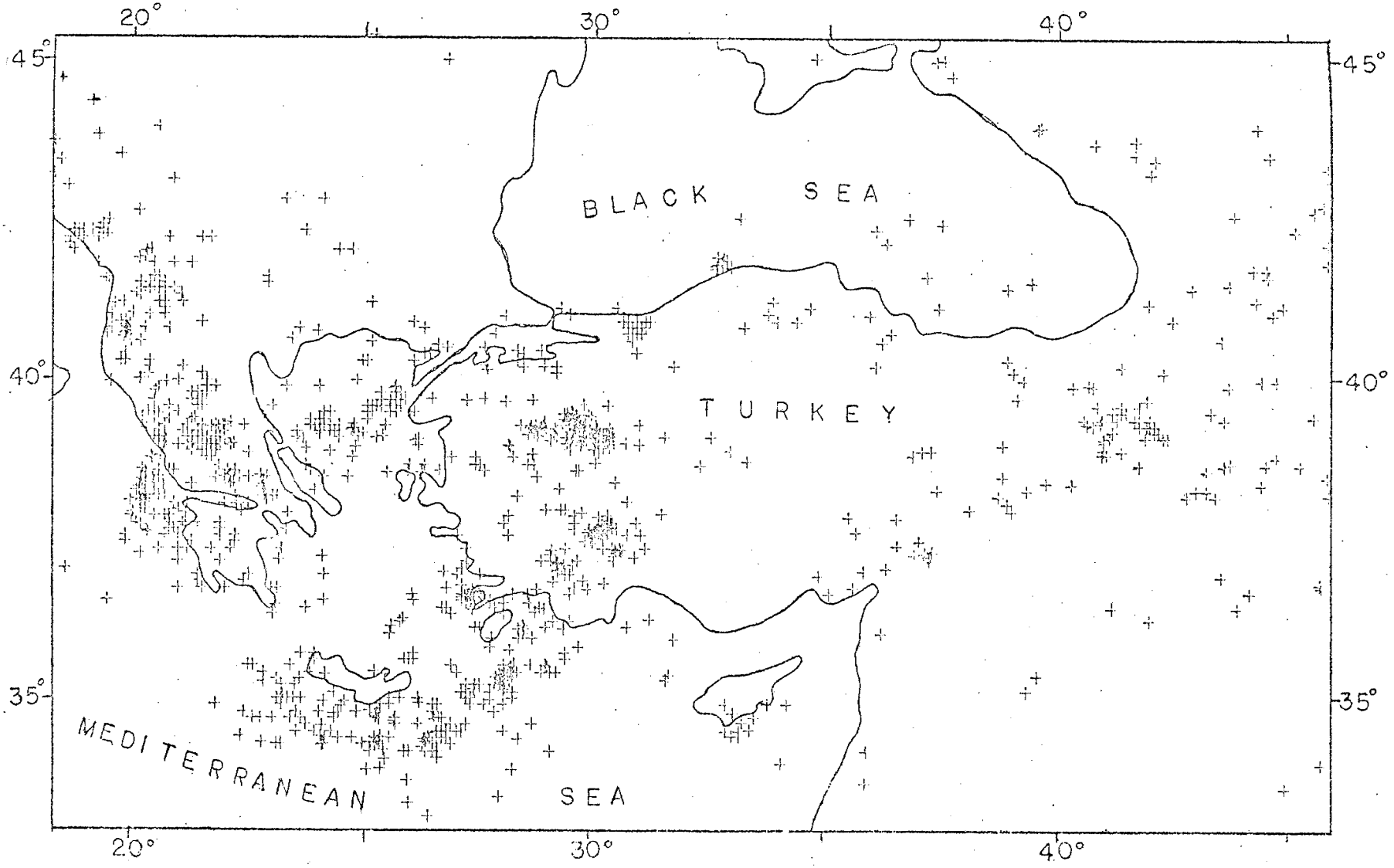

Figure 2.3a. Shallow focus ($h \leq 50$ km) seismicity of the eastern Mediterranean and Turkey from January 1, 1961 through December 31, 1971. Computer plot was made from the NOAA earthquake data file.

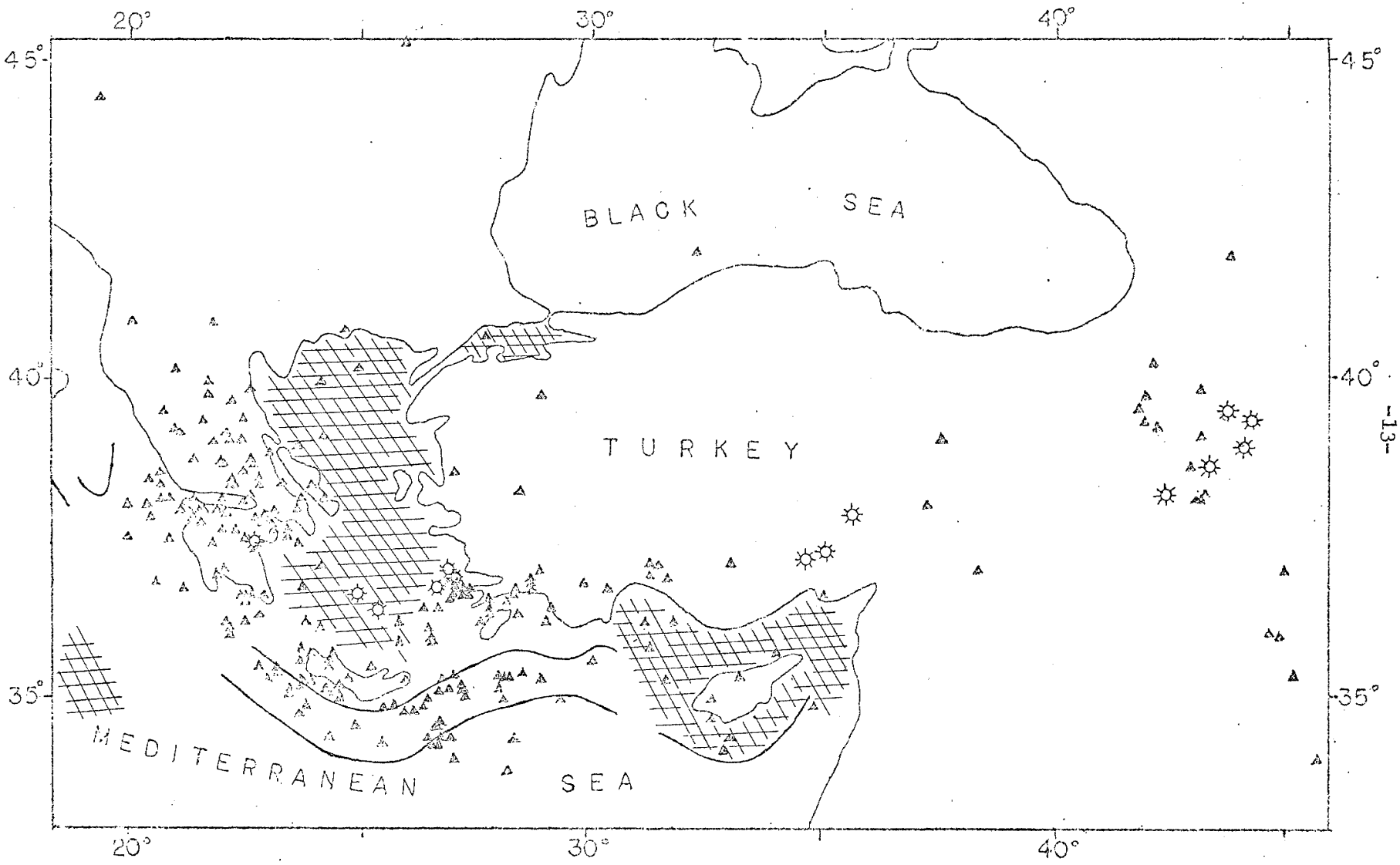

Figure 2.3b. Epicenters of intermediate focus (h > 50 km) earthquakes in the eastern Mediterranean and Turkey from January 1, 1961, through December 31, 1971. ☼ indicates volcanoes, ~ indicates axis of negative free-air gravity belt, and cross hatching indicates the presence of magnetic anomalies.

The central Anatolian zone includes the epicenters that are related to intermediate areas between northern and southern mountain ranges. Three distinct seismic zones near to Afyonkarahisar, Kirsehir and Kayseri respectively can be recognized within this region. About 50 damaging earthquakes have been reported in this region since 1205 (Ilhan, 1971).

The southeastern Anatolian earthquake zone probably represents the northern continuation of the Levant fracture zone of Syria and Lebanon into Turkey. It joins the north Anatolian earthquake zone further to the northeast (Allen, 1969). Present seismicity is not very high along this zone, however large shocks have occurred frequently in the past 2000 years (Ambraseys, 1971). About 140 damaging earthquakes have been reported since 110 A.D. (Ilhan, 1971).

Eastern Mediterranean

Tectonics and Geology

The present Mediterranean sea has been considered by many geologists as a remnant of the large Tethys ocean that existed between the Africa and Eurasia during the Cretaceous and early Tertiary time. However some other geologists (Gilluly, 1972) believe that only a small part of the present Mediterranean Sea may be a remnant of the Tethys ocean, and that most of it probably is a new sea formed by oceanization of a large amount of the continental crust that occupied the present sea areas in the past.

Tectonic movements in the Tethys ocean have varied during the Cenezoic Era. From late Eocene time to late Miocene time a phase

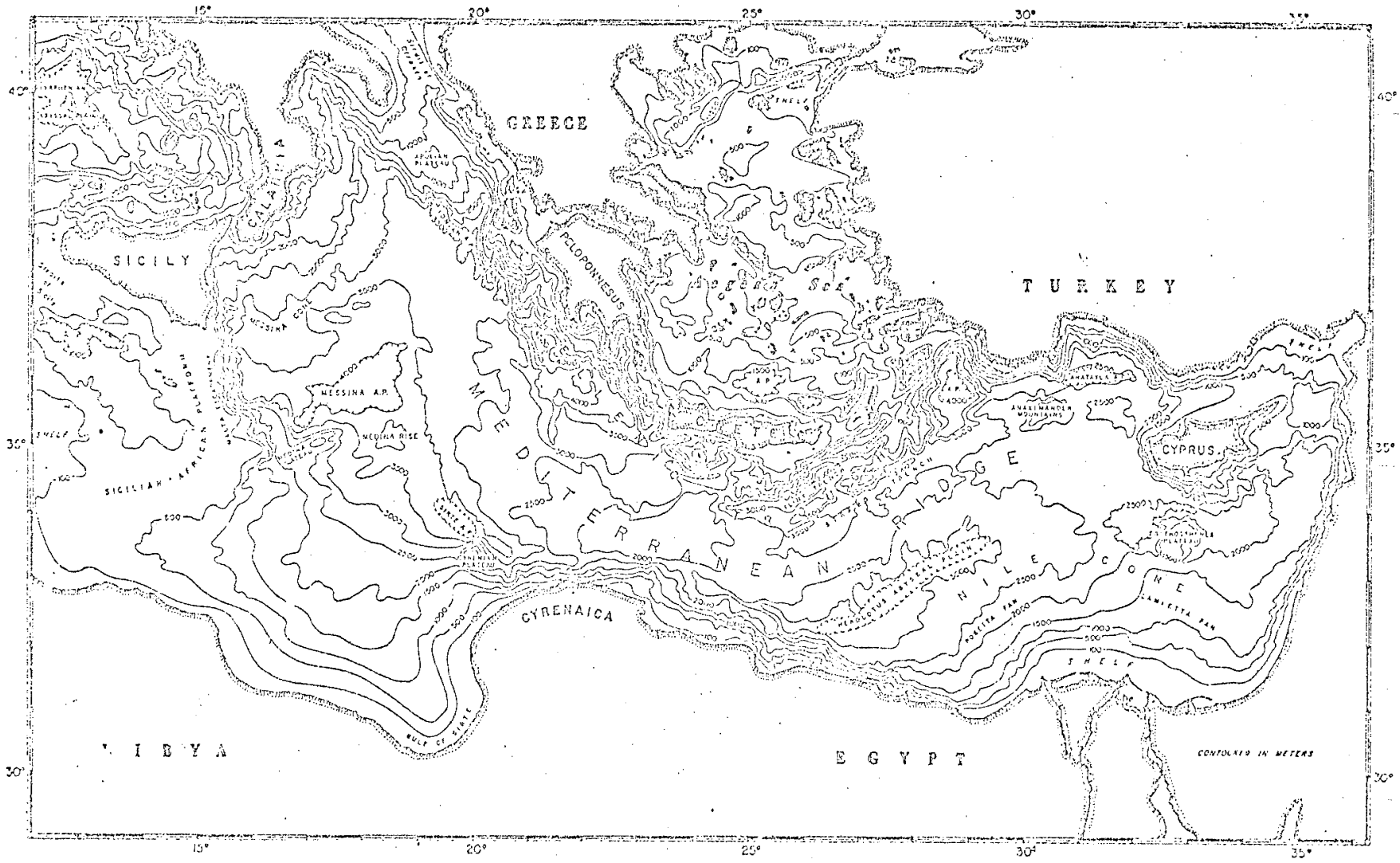

Figure 2.4. Physiography of the eastern Mediterranean and the Aegean Seas (After Ryan, et al., 1970).

of general crustal extension and rifting occurred. Some western Mediterranean basins were formed during this phase. In late Miocene to Pliocene time, the phase of extension was reversed to a phase of compression (Ryan, et al., 1970). This phase had started earlier in the eastern Mediterranean and produced underthrusting and crustal shortening. The compressional phase is still active and controls the tectonics of the eastern Mediterranean today.

The physiography of the eastern Mediterranean sea shown in Figure 2.4 is more complex than that of the western Mediterranean. In the west submarine basins and canyons are produced by sedimentary processes which suggest a lower degree of tectonic activity or very rapid accumulation of sediments. In the eastern Mediterranean however, the deformation of sediments (Ryan et al., 1970), active volcanism and high seismicity indicate recent tectonic activity.

The most outstanding physiographic features in the eastern Mediterranean are the Aegean Island Arc (the Hellenic Arc) and the Mediterranean Ridge (see Figure 2.4). The Aegean Island Arc extends from the mountain chains on the mainland of Greece and passes into Turkey through Crete and the other islands bordering the Aegean Sea in the south. Its total length exceeds 1500 km. The Mediterranean Ridge is a broad flexure that parallels the Aegean arc. The chain of depressions between the Aegean arc and the Mediterranean ridge is called the Hellenic trough and reaches to a total length of approximately 1500 km. Southeast of Rhodes a ridgelike feature separates the trenches in the Hellenic Trough. This large escarpment extends about 500 km west from the vicinity of Cyprus and is called the

Anaximander Mountains (Figure 2.4).

The structure of the Aegean Sea is not clearly known. The Hercynian granites of western Anatolia probably extend into the Aegean Sea. Several east-west trending grabens and small depressions occur in the northern part of the sea. These graben systems extend into the Sea of Marmara and the Turkish mainland.

Geophysical Anomalies

The nature of crustal structure in the eastern Mediterranean is not clearly understood at the present time. It may be oceanic, continental or transitional. Existence of a thick crust with generally low velocities however was confirmed by Payo (1967) and Papazachos (1968) on the basis of phase and group velocities of surface waves. The crust in the western Mediterranean is thin and appears to be mostly oceanic but contains transitional parts (Berry and Knopoff, 1967). Refraction measurements in the eastern Mediterranean (Gaskell, et al., 1958; Ewing and Ewing, 1959; Moskalenko, 1966) have revealed the following layers:

a) An unconsolidated layer of sediments; less than 1 km thick, that has a P wave velocity of 2.1 km/sec.

b) A layer of velocity 4.2-4.8 km/sec below the low velocity sediments. This layer was interpreted as consolidated sediments (Moskalenko, 1966).

c) A refracting interface of velocity 6.1-7.0 km/sec which may represent an extension of the crystalline African platform (Moskalenko, 1966).

Gravity and Magnetics

There are two prominent belts of negative free-air gravity anomalies in the eastern Mediterranean. These negative gravity belts parallel the Mediterranean ridge (see Figures 2.3b and 2.4). The southernmost belt extends from southwest of the Greek peninsula to west of Cyprus and is associated with the Mediterranean ridge. Free-air gravity anomalies as low as -240 mgals have been found in the areas southeast of the Rhodes (Rabinowitz and Ryan, 1970). Positive free-air gravity anomalies with magnitudes greater than +100mgals have been found in the Aegean Sea and on Cyprus (Rabinowitz and Ryan, 1970).

The magnetic field in the eastern Mediterranean is generally very smooth. The outstanding physiographic features such as the Mediterranean ridge, the Hellenic trough and the Anaximander mountains are magnetically undisturbed. Magnetic anomalies of several hundred gammas found on Cyprus, are associated with the Troodos ultra-basic complex (Vogt and Higgs, 1969). Linear magnetic anomalies of several hundred gammas are found in the northern part of the Aegean Sea (Vogt and Higgs, 1969). These anomalies trend northeast-southwest and are parallel to the structural trend of Hercynian granites.

Heat Flow and Volcanism

Heat flow in the eastern Mediterranean is remarkably uniform with an average value of 1.00 HFU (1 microcal/cm^2/sec) (Ryan, et al., 1970). This is lower than the worldwide weighted average of 1.35 HFU for oceanic areas. It is worth noting that the mean heat flow in the

western Mediterranean is considerably higher, i.e. 2.14 HFU.

The Tertiary orogeny in the Mediterranean was accompanied by two phases of igneous activity. The Oligocene-Miocene phase was dominantly andesitic volcanism. During this period, a large amount of tracyandesites erupted in central Turkey, in the islands of the Aegean Sea and in Macedonia. This phase was followed by plutonism which produced granodioritic rocks. Quaternary volcanism has been essentially basaltic. The volcanoes are found in the inner part of the Aegean island arc and in eastern Turkey (see Figure 2.3b).

Seismicity

Seismic activity in the eastern Mediterranean shows a close relation to the zones of Tertiary folding and Quaternary differential movements (Karnik, 1969). The areal distribution of epicenters in the eastern Mediterranean is shown in Figures 2.3a and b. As can be seen from these figures the majority of seismic activity takes place around the Aegean Sea. Here the seismic zone is very broad and includes both shallow and intermediate focus earthquakes. Two arcuate seismic zones are recognized in the eastern Mediterranean. One of them is the zone associated with the Aegean island arc. This zone starts from northwest of Crete and extends into the Turkish mainland northeast of the island of Rhodes. The second arcuate zone which is not defined as well as the other starts in southwestern Turkey and curves around Cyprus joining the southeastern Anatolian earthquake zone just east of the Gulf of Iskenderun. Immediately south of the junction of these arcuate zones seismic activity suddenly

disappears (see Figure 2.3). This junction must have a tectonic significance, because the deepest and strongest intermediate shocks as well as strong shallow shocks have occurred in this area (Karnik, 1969 and 1971).

The central part of the Aegean Sea appears to be aseismic. Also a noticeable seismic gap occurs along the Aegean arc to the south of Pelopennesus. A well defined east-west trending seismic zone is found in the northern Aegean Sea. This zone may be related to a westward extension of the North Anatolian Fault zone. The seismic zone in Greece and Yugoslavia is broad and follows the trend of mountain ranges. A dextral offset along this zone is noticeable immediately north of Pelopennesus. In the northernmost part of the Aegean Sea and in Bulgaria the seismic activity is scattered and may be related to a system of grabens (Karnik, 1971).

Intermediate earthquakes in eastern Mediterranean occur on the concave sides of the Aegean and the Cyprian arcs (Figure 2.3b). However earthquakes slightly deeper than normal are found in the northern Aegean Sea and in eastern Turkey (Figure 2.3b). A localized zone of intermediate earthquakes in the eastern Mediterranean region occurs in Rumania to the south of the curved section of eastern Carpathian mountains.

3. FOCAL MECHANISMS OF EARTHQUAKES

Introduction

In this section, focal mechanisms of some recent damaging earthquakes located in western Turkey, the eastern Mediterranean and the northern part of the Aegean Sea are presented. The focal mechanisms of these shocks were obtained from an analysis of the directions of initial P wave motions. Subsequently detailed discussions of focal mechanisms are presented and the limitations and the shortcomings of the method used are discussed.

Review

Historical Remarks and the Elastic Rebound Theory

Comprehensive summaries of research on the focal mechanism of earthquakes have been given by Stauder (1962), Honda (1962), and recently Evison (1970). What follows is a brief summary of the most important developments.

The focal mechanism of earthquakes has long been studied by seismologists, but with little progress before the introduction of modern seismographs. John Milne in 1891 was the first to recognize fault displacement as a possible source of seismic energy. A clear relation however, between the fault displacement and an earthquake, was first documented by B. Koto in his publication on the Mino-Owari earthquake of 1891 in Japan (Richter, 1958). After the great San Francisco earthquake of 1906, Reid (1910) firmly established the fault-earthquake relationship on the basis of geodetic observations. Reid's theory which is now known as the elastic rebound theory of earthquakes is widely accepted.

According to the elastic rebound theory the source of the energy released from earthquakes is the elastic strain energy stored in crustal blocks. If there are no preexisting faults, the stored energy is released when the shear stress exceeds the strength of the rocks and fracture occurs. If however, the accumulation of strain is along a preexisting fault, slip will occur somewhere along this fault where the shear stress exceeds the frictional resistance to sliding. Rapid displacement along a newly initiated fracture or a preexisting fault releases

the stored elastic strain energy (see Figure 3.1). Some of the energy released by the earthquake mechanism is spent to heat and deform rocks in the vicinity of the source, and the remaining energy is propagated away in the form of elastic waves. The seismic waves, both body and surface waves, carry with them a great deal of information on the nature of the earthquake source.

Observations and the Mathematical Models

Although the elastic rebound theory describes a model for an earthquake source, the actual physical mechanism is far from being clearly understood. Therefore much effort has been devoted to finding an appropriate mathematical model that satisfactorily explains the observed radiation field of an earthquake. The simplest mathematical model is a point source from which single and double-couple models have been derived (Honda, 1962). Both the single and double-couple models shown in Figure 3.2 can produce identical P wave, but different S wave, radiation fields. The single-couple model which is a non-equilibrium condition, has been completely ruled out on the basis of S wave radiation and polarization studies. The double-couple model is equivalent to two orthogonal principal stresses oriented at ±45 degrees to the fault plane. The double-couple source model has been widely accepted and its equivalence to dislocation models (Vvedenskaya, 1956) has been shown by Burridge and Knopoff (1964).

The major weakness of the point source models and the dislocation models is the assumption of the form of the source function. Randal (1964a) and Archambeau (1968) have used a more general mathematical approach and considered the source mechanism as a relaxation phenomena

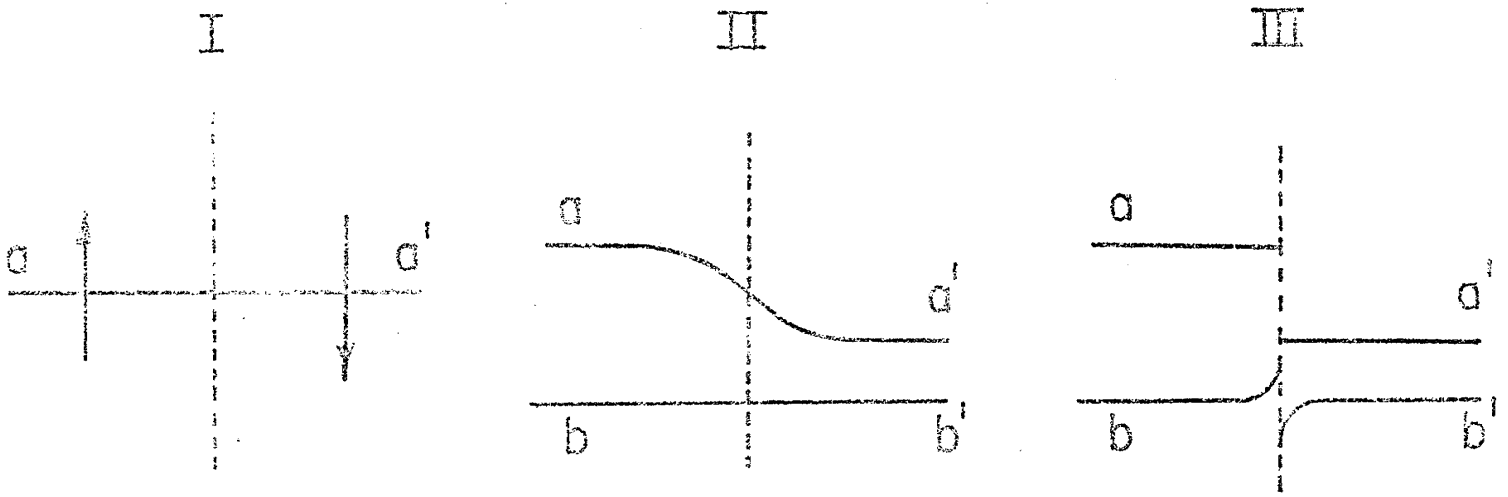

Figure 3.1. Elastic rebound model of a vertical strike-slip fault showing the horizontal deformation. I. Unstrained condition, II. Strained condition, III. Elastic strain released. aa' represents a line drawn perpendicular to the fault before deformation started; bb' represents a line drawn just before the release of elastic strain.

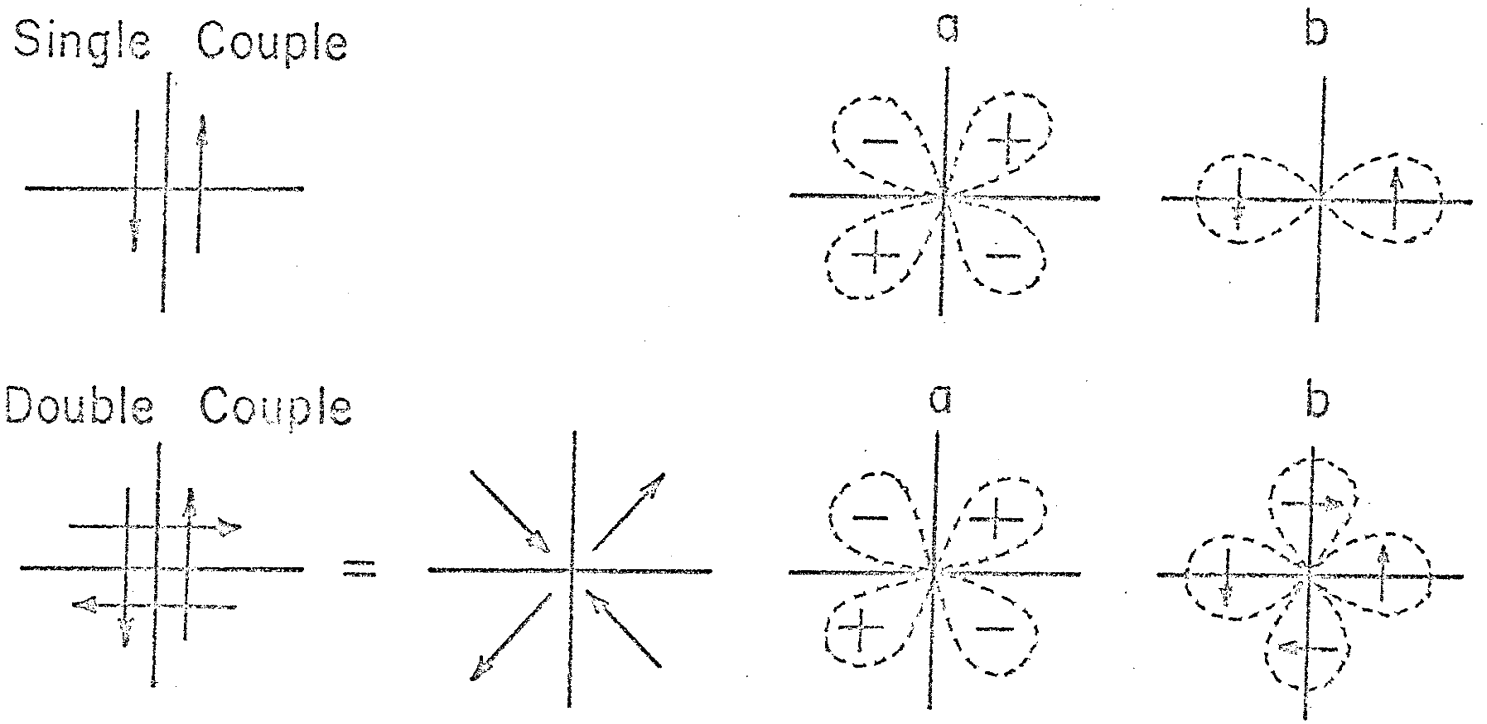

Figure 3.2. Single-couple and double-couple point source models; (a) P wave radiation pattern, (b) S wave radiation pattern; + represents compression, - represents dilatation, → represents shear type motion.

from one equilibrium state to another. This approach has led toward determination of the actual form of the source function. Recently numerical techniques have been used to describe the dynamic near field characteristics of a tensile crack (Hanson and Sanford, 1970) and a brittle shear fracture (Hanson, et al., 1971), which also give the form of the source function.

Until recently the first motions of P waves and the polarization of S waves have been the primary source of data for earthquake mechanism studies. With the recent developments in the mathematical theory of source dynamics, and the installment of WWSSN long-period seismographs, now, the amplitude and phase information from surface waves and long-period body waves can be used in source mechanism studies (Aki, 1972). The amplitude and phase equalization methods which compare the observed, and the theoretical radiation patterns are being used in source mechanism studies (Aki, 1960; Toksoz, et al., 1965; Canitez and Toksoz, 1971).

Focal Mechanism from the Initial P Wave Motion

Method

The method described in this section assumes that the source mechanism of an earthquake is faulting as described by the elastic rebound theory, and it is represented by a double-couple model. The seismic waves generated at the focus by this mechanism travel through an earth that has a complex structure and composition. Consequently a relatively simple elastic disturbance generated at the focus can become quite complex at the recording stations. The influence of travel-path and the instrument response can make the analysis of source mechanism

from amplitude and phase information difficult. However, the particle motions of P and S waves are not altered in the earth because they are in the direction of propagation and transverse to the direction of propagation respectively. P waves travel faster than S waves and the surface waves, and thus they are always responsible for the initial motion observed on a seismograph. The observed first motions of P waves provide an easy way to deduce the nature of movement at the source.

Figure 3.3 is a model of a vertical strike-slip fault showing two perpendicular planes dividing the P wave radiation field into four quadrants. In quadrants (1) and (3) the initial ground motion is toward the focus or dilatational, and in quadrants (2) and (4) the particle motion is away from the focus or compressional. The plane along which fault displacement takes place is called the "fault-plane" and the plane perpendicular to it is called the "auxiliary-plane." Theoretically these are nodal planes, or planes along which no P wave motion occurs. The orientation of fault-plane and the auxiliary-plane can be inferred from the observations of initial P wave motion at a number of seismograph stations. Several methods of presenting observations are available. The method used in this study is stereographic projection on the focal sphere (Stauder, 1962). The focal sphere is a hypothetical small sphere surrounding the focus. Rays leaving the focus pass through the focal sphere with the same angle as they leave the focus (see Figure 3.4). The focal sphere is the unit sphere of stereographic projection. For a complete description of stereographic projection reference should be made to Keilis-Borok, et al. (1960) or Ramsay (1967).

The observed first motion at a station can be plotted on the

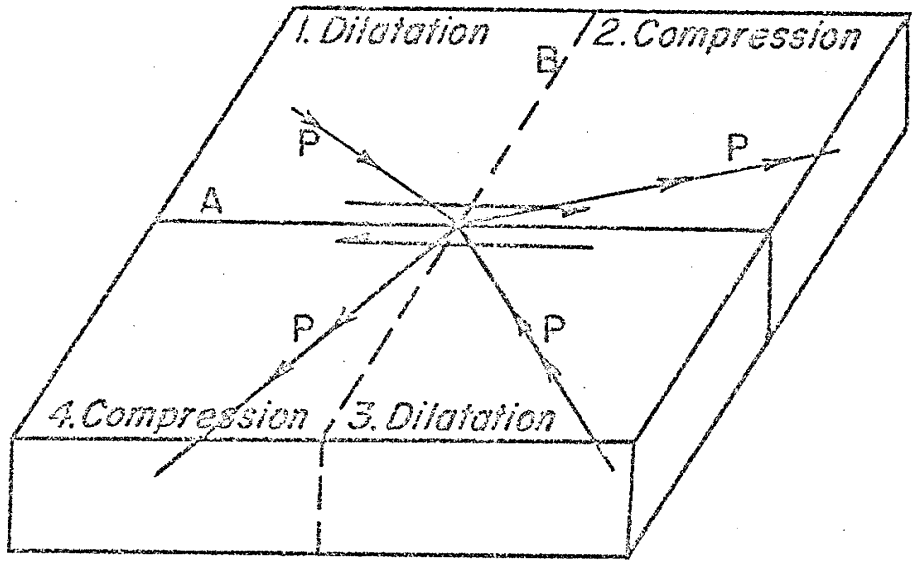

Figure 3.3. P wave radiation field from a vertically dipping strike-slip fault. The arrows on the rays indicate the initial direction of ground motion. Plane A is the fault-plane and plane B is the auxiliary-plane.

stereographic projection at the azimuth of the station with respect to the epicenter, and the angle of incidence i_h at the focus. The calculation of the azimuth with respect to the epicenter is a straightforward problem in spherical trigonometry and formulas for this purpose can be found in Bullen (1963, p. 154-155).

The angle of incidence at the focus, i_h, can be calculated from the formula given by Stauder (1962):

$$\sin i_h = (V_h) \cdot \frac{r_o}{r_o - h} \cdot (dT/d\Delta) \qquad (3.1)$$

where;

V_h: is the P wave velocity at the focus (km/sec).

r_o: is the radius of the earth (km).

h : is the depth of focus (km).

$dT/d\Delta$: is the slope of the travel-time curve for P waves (sec/km).

Equation 3.1 can easily be determined from Snell's law in spherically layered body, according to which:

$$\frac{r \sin i}{V} = p = \text{constant all along a ray.}$$

Therefore:

$$\frac{r_h \sin i_h}{V_h} = \frac{r_o \sin i_o}{V_o} \qquad (3.2)$$

Substituting the relation $\sin i_o = V_o \frac{dT}{d\Delta}$ (see Figure 3.4) in equation 3.2; equation 3.1 is obtained immediately.

After all first motions are plotted on the stereonet (Wulff stereonet) at the proper azimuth and i_h, the nodal planes are drawn on

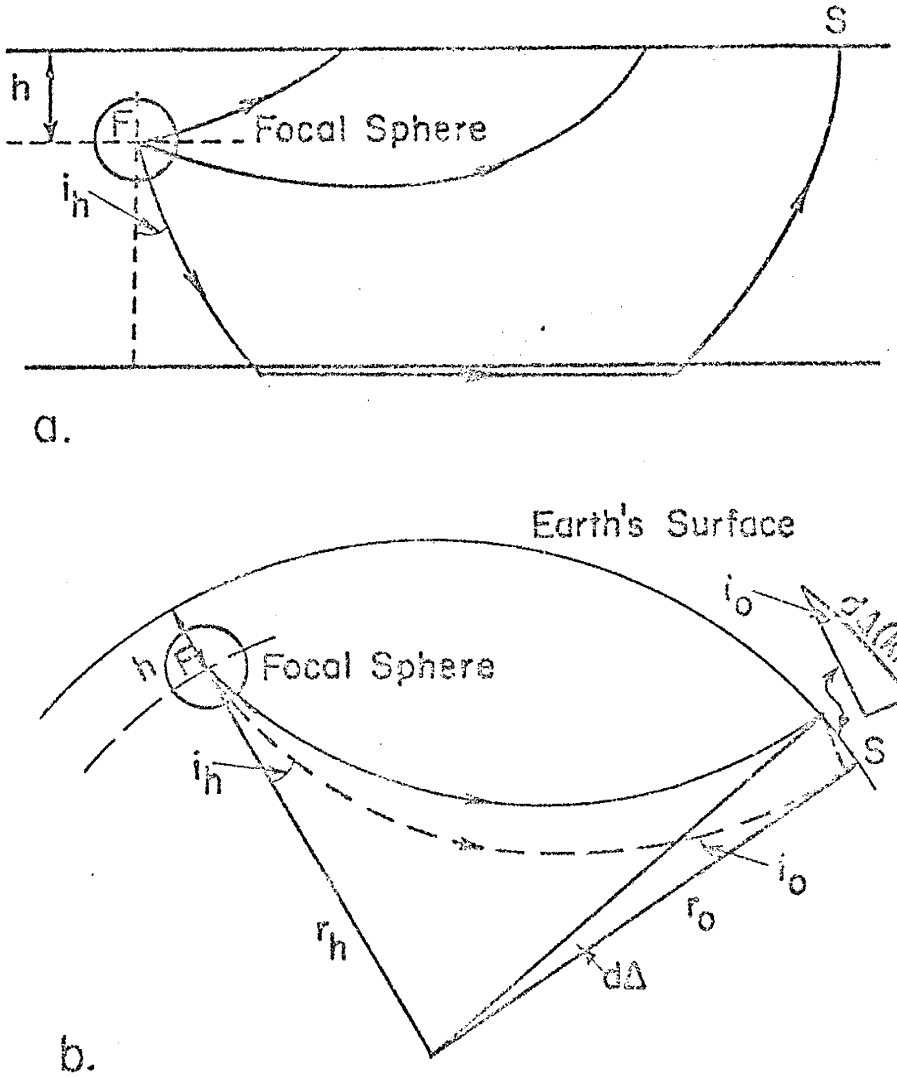

Figure 3.4. Vertical section showing the focal sphere and the travel paths of the rays leaving the focal shpere; a. ray paths to near stations, b. ray paths to distant stations; F represents focus and S represents seismograph stations.

the basis of following properties:

(1) Nodal planes separate compressions from the dilatations

(2) Nodal planes are orthogonal to each other and the orthogonality condition is given by:

$$\cos \Theta = \tan \beta / \tan \delta$$

where

Θ : is the angle between the strike of the fault-plane and the strike of the auxiliary-plane.

β : is the plunge of the motion

δ : is the dip of the fault-plane

A proof of the orthogonality condition can be found in Hodgson and Milne (1951).

The diagram finally obtained shows two perpendicular planes separating compressions from dilatations. One of these planes is the fault-plane and the other is the auxiliary-plane. Without the help of other seismological and geologic information the true fault-plane cannot be distinguished from the auxiliary-plane. This is a fundamental weakness in the method.

Interpretation of Fault-Plane Diagrams

The fault-plane diagram may represent combinations of three fundamental types of faulting:

(a) Normal faulting

(b) Reverse faulting

(c) Strike-slip faulting

A detailed description of these three types of faults can be found in De Sitter (1964). The three types of faulting produce different distribution of first motions on the fault-plane diagrams (Figure 3.5). For a strike-slip fault, a clear quadrantal pattern is apparent. For normal and reverse faults the diagram shows three wedges of dilatations and compressions. The character of first motion in the three wedges being different for the two cases. Combinations of these three cases is possible and occurs most frequently in practice.

Determination of the type and orientation of stress field at the focus from the fault-plane diagram is based on the dynamic theory of faulting (Anderson, 1951). Anderson introduced a standard stress state in which the vertical and horizontal pressures are equal everywhere inside the earth. Of course this is not the actual stress field everywhere inside the earth, however it is a useful concept to explain the formation of various types of faults. Deviations from the standard state of stress, if great enough produce faults. The three basic fault types shown in Figure 3.5 are produced by principal stress distribution shown in the figure ($\sigma_1 > \sigma_2 > \sigma_3$). In all cases, the fault-plane is oriented ±45 degrees from the greatest and the least principal stresses. This is the configuration of the greatest and least principal stresses relative to the fracture plane expected from the Navier-Coulomb criterion of brittle fracture when the angle of internal friction is zero. The intermediate stress which does not affect the faulting lies in the fault-plane and is perpendicular to σ_1 and σ_3.

Recently the relation between direction of stresses and direction of fracture assumed in the interpretation of fault-plane solutions has been

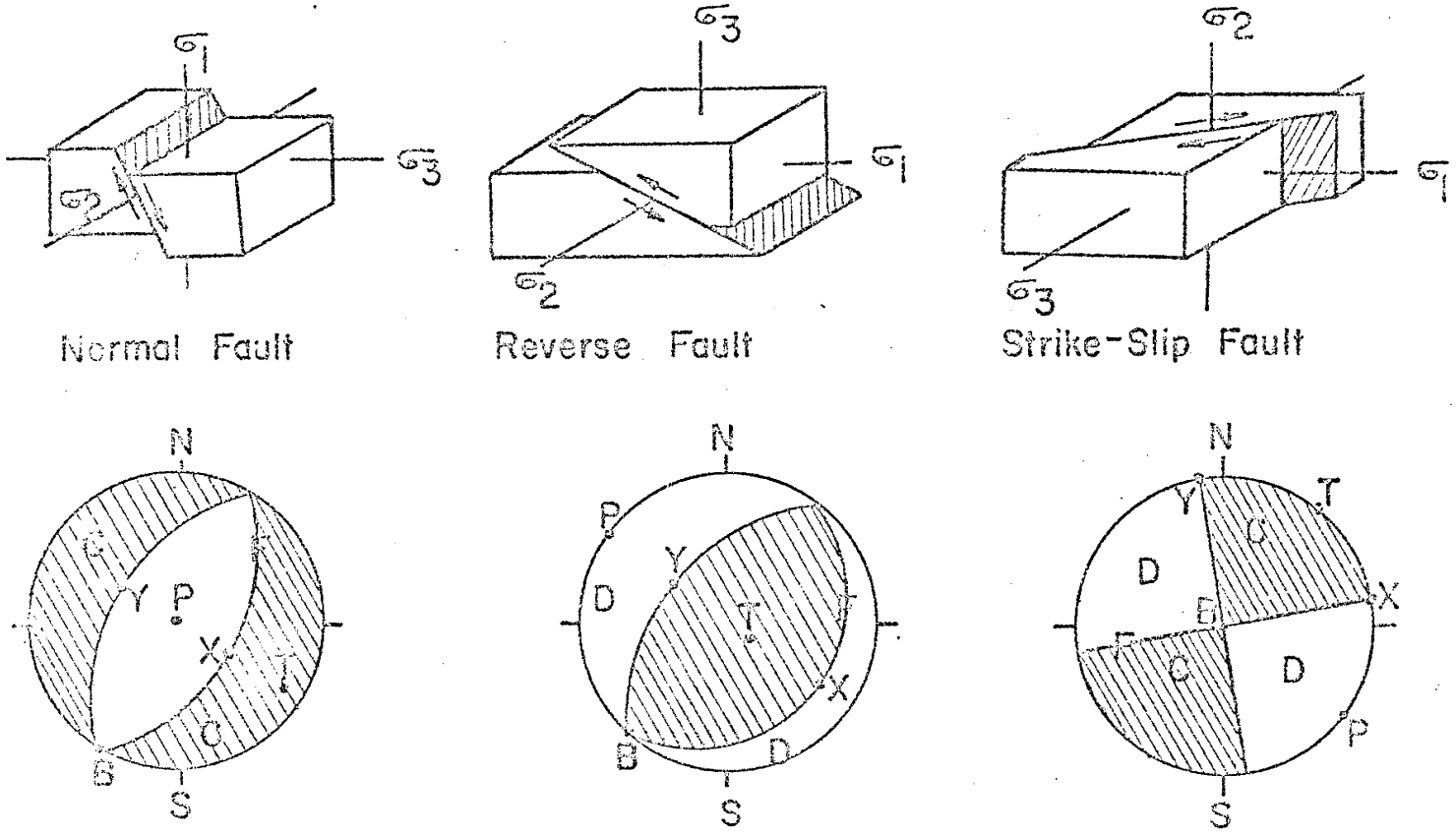

Figure 3.5. Block diagrams of three types of faulting and their mechanism diagrams. σ_1, σ_2, and σ_3 ($\sigma_1 > \sigma_2 > \sigma_3$) are the principal stresses; arrows indicate the direction of motion. Fault-plane is marked by F on mechanism diagrams; for a description of P, T, B, X and Y axes see the text.

challenged strongly by Mc Kenzie (1969) who proved mathematically that these conditions may not be satisfied in shallow earthquakes, since most shallow earthquakes occur along preexisting faults. In spite of this difficulty, pressure (P) and tension (T) axes(correspond the greatest and least principal stresses) are commonly plotted on the fault-plane diagrams.

It is convenient to introduce five axes in connection with a fault-plane solution which are called the P, T, B, X and Y axes (Figure 3.5). Their physical and geometrical meaning are:

P is the axis of greatest principal stress, oriented ±45 degrees from the fault-plane. It is always located in a region of dilatational arrivals on the focal sphere.

T is the axis of least principal stress, oriented ±45 degrees from the fault-plane. It is always located in a region of compressional arrivals on the focal sphere.

B is the axis of intermediate stress (null axis). It is located at intersection of fault-plane and the auxiliary-plane, and it is normal to the direction of motion.

X is the direction of motion. It is located in the fault-plane,and is perpendicular to the auxiliary-plane.

Y is the node of the fault-plane which lies in the auxiliary-plane, and is perpendicular to the fault-plane.

The systems P, B, T and X, B, Y form two orthogonal systems rotated around B axis by an angle of ±45 degrees with respect to each other. Note that X and Y axes can be interchanged if a choice of fault-plane has not been made.

Fault-Plane Solutions

Selected Earthquakes

Ten earthquakes from western Turkey, northern Aegean and the eastern Mediterranean were selected for the focal mechanism studies. The number of earthquakes that were sufficiently strong for the first motion study was not large. Because azimuthal coverage of near WWSSN stations was inadequate, the earthquakes with body wave magnitudes lower than 5.4 could not be considered for the study. The earthquakes selected for western Turkey belong to a remarkable sequence of earthquakes which started with the earthquake of March 23, 1969. The strongest shock in this sequence was the Gediz earthquake of March 28, 1970. High seismic activity in this area is still continuing. Epicenters of the selected earthquakes are shown in Figure 3.6 which also shows the epicenters of the shallow focus earthquakes ($h < 50$ km) in western Turkey and the Aegean region. Table 3.1 lists parameters for the earthquakes selected. Origin times, epicenter coordinates and the magnitudes given in this table were reported by NOAA. Note that the body wave magnitudes reported by NOAA are systematically low (Bune, et al., 1970). Uncertainties involved in focal depth estimates are apparent from the focal depths reported by NOAA and the BICS. All of the earthquakes selected had shallow foci and were felt over wide areas. Most of them produced considerable damage to structures and some caused heavy casualties. The earthquakes of March 28, 1969, and March 28, 1970, produced surface faulting and some field reports on these earthquakes are available (Arpat and Bingol, 1969; Ambraseys and Thalenko, 1970; Tasdemiroglu,

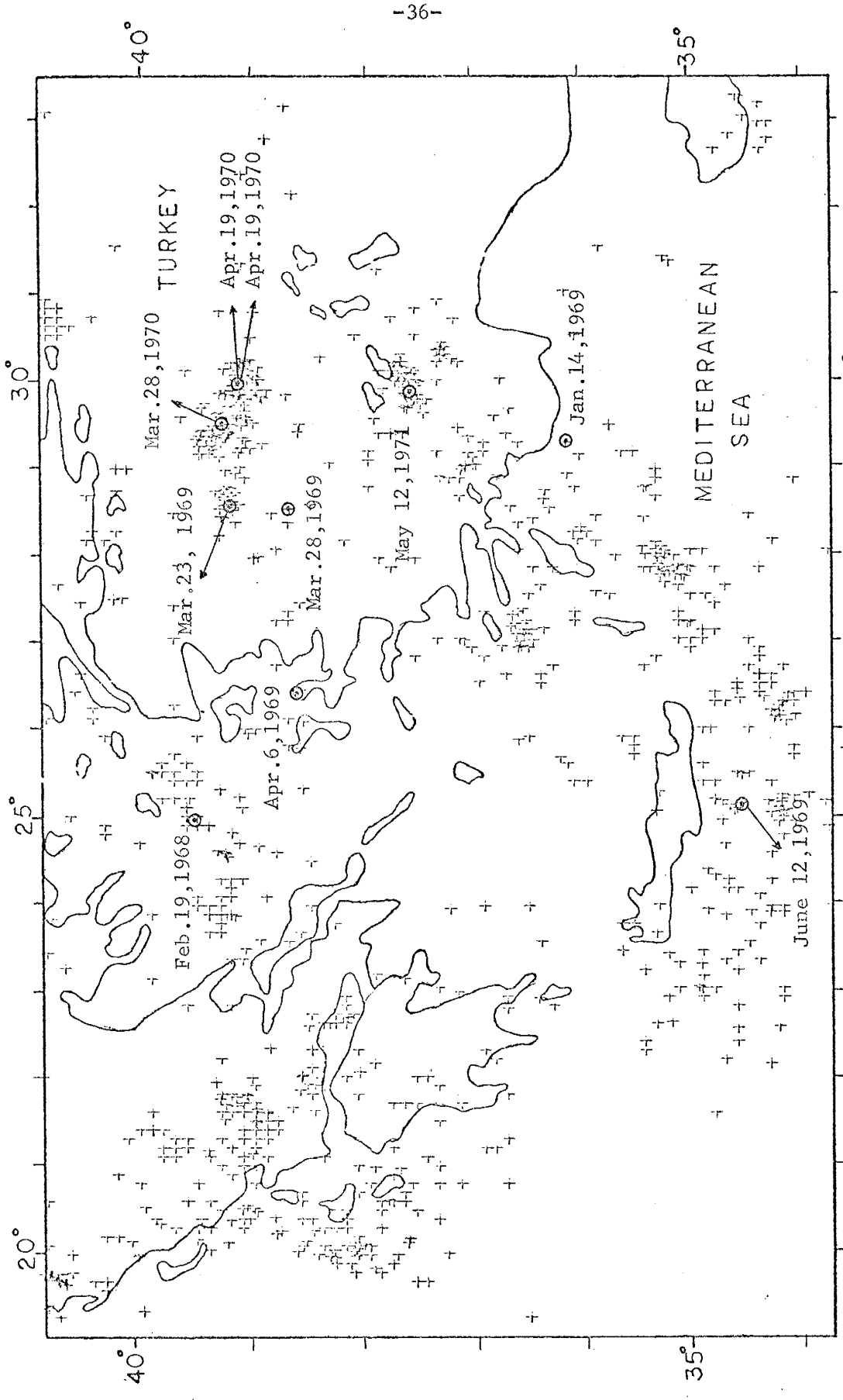

Figure 3.6. Locations of earthquakes for which focal mechanisms are determined in this study. Crosses represent the epicenters of shallow focus earthquakes that occurred in the area from January 1, 1961, to December 31, 1971.

TABLE 3.1. Date, Time, Location and Magnitude of Earthquakes Studied.*

No.	Date	Origin Time (G.M.T.)	Epicenter Lat.	Long.	Depth (km) NOAA	BCIS	Mag. m_b	M_s	Remarks
1	Feb.19,1968	22:45:41.2	39.40N	25.00E	7.	40.	5.7	7.1	Heavy damage, casualties, tsunami report.
2	Jan.14,1969	23:12:07.9	36.17N	29.20E	N.	50.	5.5	6.0	Some damage in south-western Turkey, felt widely.
3	Mar.23,1969	21:08:42.6	39.16N	28.48E	12.	--	5.6	5.6	Felt throughout western Turkey, considerable damage.
4	Mar.28,1969	01:48:30.4	38.58N	28.44E	9.	--	6.0	6.4	Heavy damage, casualties, ground break.
5	Apr. 6,1969	03:49:33.4	38.49N	26.41E	14.	--	5.5	5.5	Substantial property damage, casualties in Greece area.
6	June12,1969	15:13:31.1	34.40N	25.06E	25.	--	5.8	5.8	Felt in Crete, Alexandria in Egypt.
7	Mar.28,1970	21:02:23.4	39.18N	29.48E	20.	--	6.0	7.1	1086 killed, 1174 injured, very heavy damage in Gediz, surface faulting.
8	Apr.19,1970	13:29:36.3	39.06N	29.79E	20.	--	5.4	5.6	Felt widely.
9	Apr.19,1970	13:47:35.2	39.06N	29.83E	26.	--	5.5	5.5	Two injured, 41 houses and a mosque destroyed.
10	May 12,1971	06:25:12.9	37.58N	29.75E	23.	--	5.5	5.9	100 persons killed, many injured, heavy damage in Burdur area.

* : From NOAA Preliminary Reports
NOAA: National Oceanic and Atmospheric Administration (Formerly USCGS)
BCIS: Bureau Central International de Seismologique

1971).

Source of Data

The primary source of data for the first motion study were long-period and short-period seismograms from the Worldwide Standardized Seismograph Network (WWSSN). Negative film (70 mm) copies of the vertical, N-S, and E-W long-period records, and the vertical short-period records were obtained from the National Geophysical Data Center in Asheville, North Carolina. Additional near-station data were collected by direct correspondence with the headquarters of the seismograph networks in the U.S.S.R., Czechoslovakia, Greece and Israel. In addition a few directions of first motions were obtained from the Earthquake Data Reports of the National Ocean Survey (NOAA).

First Motions

Initial motions of P waves were directly read on the 70 mm negative film copies of the WWSSN long-period and short-period seismograms. To avoid misidentification of the first P wave arrivals, the travel times were computed from the Jeffreys-Bullen seismological tables and the beginning of the initial P wave motion on the seismograms carefully identified. In some cases, the first identifiable arrival was considerably later than the computed arrival time. First motions from these late arrivals were disregarded.

The first motion readings on the vertical components of the long-period records were essential in deciding the compressional and the dilatational nature of the first ground motion at a seismograph station. However the first motions on the vertical components of the short-p[illegible]d,

and N-S, and E-W components of the long-period records were also read and tabulated. All first motions were reexamined before deciding that initial ground motion at a seismograph was a compression or a dilatation. First motions were graded according to the quality of the initial motion and the general quality of the seismograms. A summary of first motions and their quality with other station parameters are presented in Appendix I.

Projection of First Motions

The theoretical background for the computation of station parameters; i.e., distance, azimuth and the angle of incidence at the focus was discussed previously. Here only the numerical values used in these computations are discussed. The angle of incidence at the focus was computed from equation 3.1 repeated below:

$$\sin i_h = V_h \cdot \frac{r_o}{r_o - h} \cdot \frac{dT}{d\Delta}$$

The angles determined from this equation are most strongly affected by the values of P wave velocity at the focus V_h and the slope of the travel-time curve ($dT/d\Delta$). For shallow focus earthquakes the second term on the right is approximately one. The affect of velocity is rather significant in projection of first motions and will be discussed again after the fault-plane solutions are presented. The $dT/d\Delta$ values were obtained from the Jeffreys-Bullen (1958) seismological tables. A comparison of $dT/d\Delta$ values from Jeffreys-Bullen (1958) table with those from Herrin, et al. (1968) table show no significant difference for distant stations, but small deviations for near stations. However these

latter differences were not large enough to affect the projections of first motions.

In the absence of a good knowledge of crustal structure beneath the epicenters, average values of P wave velocities were used in the angle of incidence computations. Table 3.2 presents the depths of focus and the P wave velocities used in the angle of incidence computations.

Table 3.2. Average P Wave Velocities Assumed at the Focus

Event No.	Date	Focal Depth (km)	P wave velocity (km/sec)
1	Feb. 19, 1968	7	6.6
2	Jan. 14, 1969	50	7.5
3	Mar. 23, 1969	12	6.3
4	Mar. 28, 1969	9	6.3
5	Apr. 6, 1969	14	6.6
6	June 12, 1969	25	7.5
7	Mar. 28, 1970	20	6.6
8	Apr. 19, 1970	20	6.6
9	Apr. 19, 1970	26	6.6
10	May 12, 1971	23	6.6

The focus of event 1 was located in the oceanic crust, foci of events 2 and 6 beneath the oceanic crust, and other foci in the continental crust. The slightly higher velocities used for events 2 and 6 were suggested by the crustal section for the eastern Mediterranean given by Ryan, et al. (1970).

The stereographic projections of first motions were plotted on a

Wulff stereonet. All first motions in this study were projected on the lower focal hemisphere, since all stations were thought to be beyond the critical distances. Without detailed knowledge of crustal structure beneath the epicenters the critical distances could not be determined precisely. However nearly all stations were well beyond a distance Δ of 1.5°. According to the Jeffreys-Bullen (1958) and the Herrin, et al. (1968) travel-time tables for shallow focus earthquakes, the P_n phase always precedes the P^* and the P_g phases beyond a Δ of 1.5°. Therefore it is believed there were very few if any direct P wave arrivals in the data. A few inconsistencies in first motions at near stations may be due to the fact that these stations were within the critical distance. If a station is within the critical distance, then the first arrival is a direct P wave and the resulting first motion must be projected on the upper focal hemisphere. Therefore it is important to distinguish between upgoing and downgoing rays when first motions from near stations are used (Udias, 1965).

Discussion of Fault-Plane Solutions

General Remarks

In this subsection, fault-plane diagrams are presented and their relation to local geology and tectonics discussed. The fault-plane was distinguished from the auxillary plane on the basis of one or more of the following criteria:

(1) Geology and the structural features of the area.

(2) Clustering of epicenters in the area of shock along a line parallel to the strike direction of a nodal plane.

(3) Clustering of the epicenters of the aftershocks along a line parallel to the strike direction of a nodal plane.

(4) Observed surface fractures associated with the earthquake.

(5) Resemblance of one nodal plane the faults naturally occurring in the field more closely than the other nodal plane.

The fault-planes selected on the basis of criteria (3), (4), and (5) are believed to be more certain than those based on (1) and (2). Criterion (5) is applied to normal fault solutions only.

The macroseismic observations on some of the larger earthquakes were taken from the available field reports published in foreign and domestic literature. Other primary data, i.e., locations, origin times, magnitudes, damage and intensities were obtained from the NOAA Earthquake Data Reports (EDR), and the Preliminary Bulletins of the National Seismological Observatory of Greece.

Earthquake # 1: February 19, 1968, 22:45:41.2 G.M.T.

The epicenter of this shock was located in the northern Aegean Sea at 39.4°N latitude and 25.0°E longitude (Figure 3.6). Its magnitude (Ms) was 7.1 (Table 3.1).

The earthquake was felt widely in the northern Aegean Sea and the surrounding countries. The total area of felt shaking was about 950,000 km^2. The shock caused casualties and heavy damage in Greece; 20 persons were killed, 18 severely and 21 slightly injured; 175 houses collapsed, 297 were damaged beyond repair (preliminary bulletin of the National Observatory of Greece). It was felt widely in western Turkey reaching intensities of V+ on the Modified Mercalli (M.M.) Scale.

The main reason for studying the focal mechanism of this shock is the location of the epicenter along the proposed extension of the North Anatolian fault in the Aegean Sea (Galanopoulos, 1967). Epicenters of other strong earthquakes (e.g. March 9, 1965, 39.1°N, 24.0°E; and March 4, 1967, 39.2°N, 24.6°E) in the northern Aegean Sea have also been located along the same line (Drakopoulos and Ekonomides, 1972). On the other hand McKenzie (1970) proposed the existence of a ridge in the northern Aegean Sea. The focal mechanism of this shock may allow a choice between these two possibilities.

A total of 73 P-wave first motions were available for this earthquake, of which only five were obtained from the stations outside the WWSSN. Thus the homogeneity of data was good. The shock was recorded strongly at most stations and the majority of first motions were graded excellent, very good or good (see Appendix I, Table A.I.1.).

The fault-plane diagram shown in Figure 3.7. indicates a quadrantal

distribution of compressions and dilatations. Dilatations occur from 40° to 130° and 220° to 310° and compressions occur from 130° to 220° and 310° to 40°. This distribution clearly indicates strike-slip motion during the earthquake along one of the well defined nodal planes. The parameters of the nodal planes are given in Figure 3.7. The northerly striking nodal plane defines a right-lateral strike-slip fault dipping 80° toward NW. The south-easterly striking plane on the other hand defines a left-lateral strike-slip fault dipping 86° toward NE.

On the basis of the areal distribution of the aftershocks of this earthquake (Drakopoulos and Ekonomides, 1972), shown in Figure 3.8, the nodal plane striking northeast was selected as the fault plane. This plane is more closely aligned parallel to the trend of the seismic zone in the northern Aegean Sea (Figure 3.6). The focal mechanism determined in this study is in perfect agreement with that reported by Drakopoulos and Ekonomides (1972), and also agrees with the fault-plane solutions determined by Papazachos and Delibasis (1969) for other strong earthquakes located along the same seismic zone.

The fault-plane solution defines a stress system in which the maximum principal stress (P) and the least principal stress (T) are both horizontal (Figure 3.7). The maximum principal stress is oriented in east-west and the least principal stress is oriented in the north-south direction, perpendicular to the trend of the seismic zone in the northern Aegean Sea.

The alignment of epicenters along a narrow zone (Figure 3.6) and the strike-slip fault mechanism of earthquakes found in the northern Aegean Sea support the contention that a branch of the North Anatolian

fault extends into the Aegean Sea. On the other hand however, if the ridge hypothesis of McKenzie (1970) is accepted, the focal mechanism of this earthquake may represent a transform fault associated with the ridge. Vogt and Higgs (1969), found large magnetic anomalies associated with a trough in the northern Aegean Sea. However these anomalies do not show a systematic pattern, and in the absence of other convincing evidence the existence of a ridge in the northern Aegean Sea cannot be accepted until more data to support this idea is available.

An interesting phenomenon related to the focal mechanism of this earthquake is the generation of a small tsunami. In spite of the great debate on the subject, it is usually believed that tsunamis are generated by the uplifting or subsidence of sea floor, landslides or submarine volcanoes, (Richter, 1958). Strike-slip faulting can only generate tsunamis in the case of crossing a submarine cliff or a seamount or triggering a landslide.

Event No. : 1
Date : Feb. 19, 1968
Origin time : 22:45:41.2 G.M.T.
Epicenter : 39.40N 25.00E

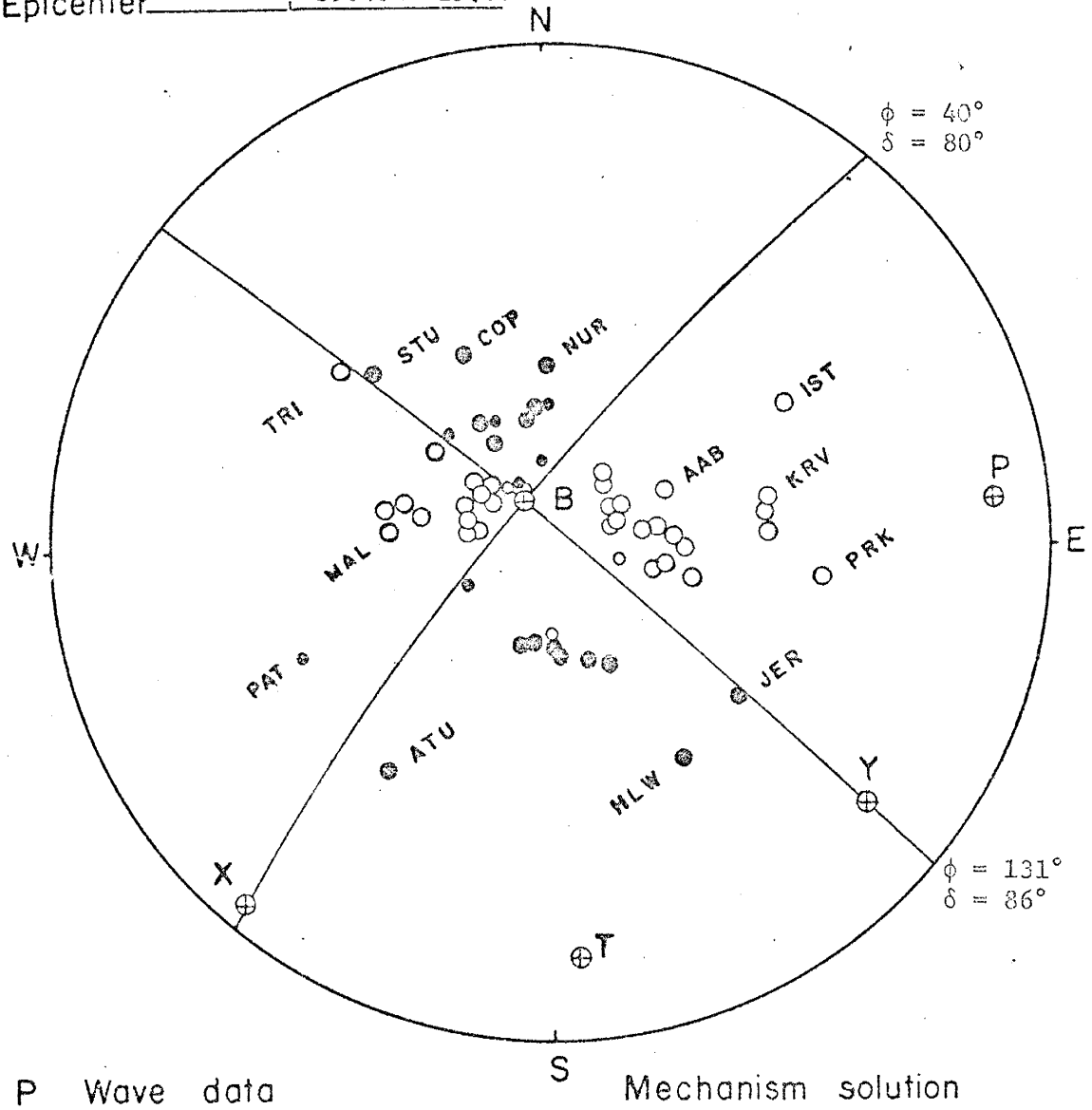

P Wave data

● Compression

○ Dilatation

Mechanism solution

Axis	P	T	B	X	Y
AZ.	35	176	333	220	130
Plunge	6	10	80	3	11

Figure 3.7. Fault-plane solution of an Aegean earthquake. Date, origin time and location are given above. A P wave velocity of 6.6 km/sec at the focus used in this projection. The larger symbols represent better quality first motions. Solution represents a strike-slip fault.

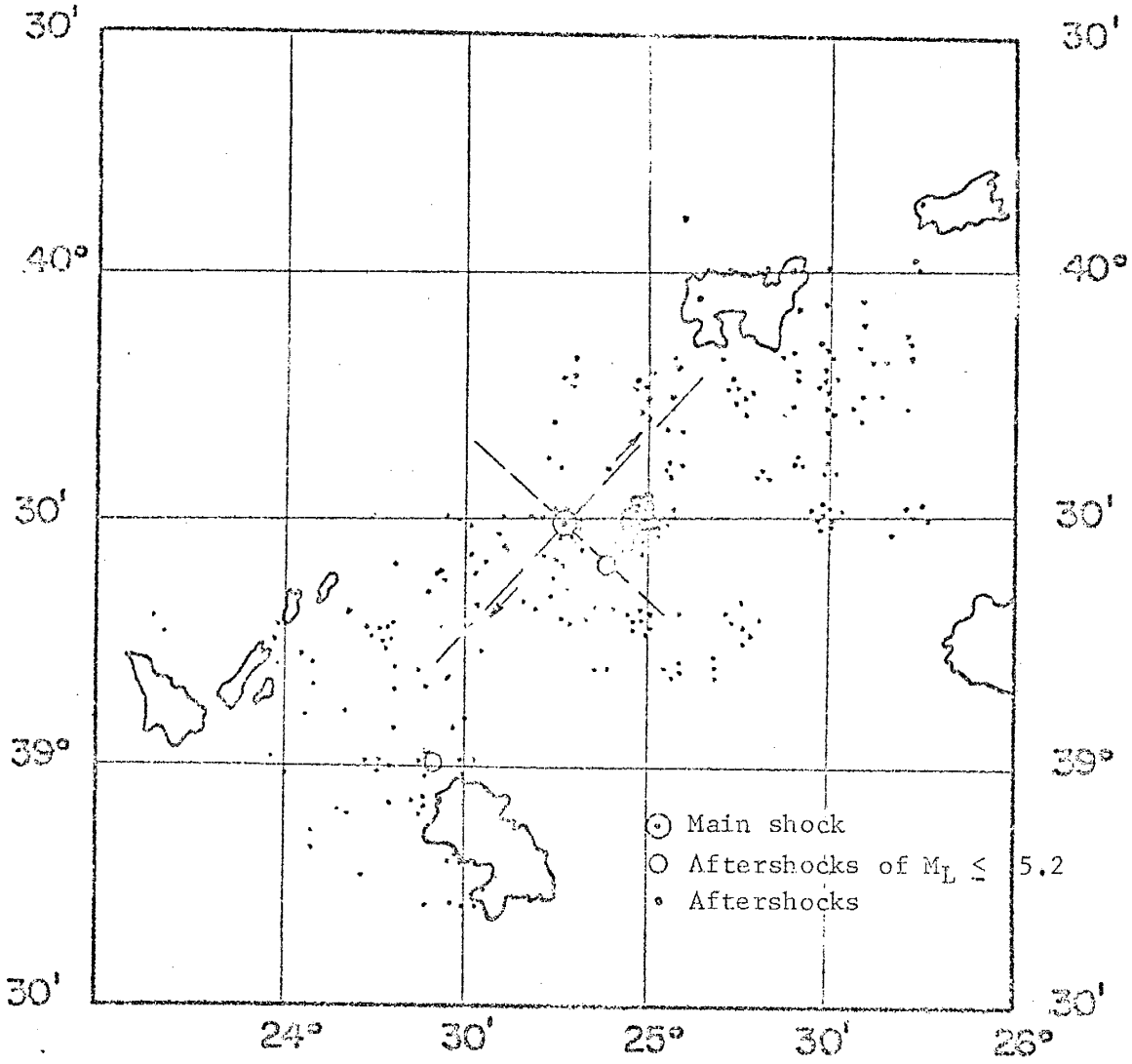

Figure 3.8. Areal distribution of the aftershocks of the Aegean earthquake of February 19, 1968, (after Drakopoulos and Ekonomides, 1972).

Earthquake # 2: January 14, 1969, 23:12:07.9 G.M.T.

The epicenter of this shock was located at 36.17°N latitude and 29.20°E longitude, near the eastern termination of the Aegean Island Arc (Figure 3.6). Its depth of focus was 50 km, and had a surface wave magnitude of 6.0 (Table 3.1).

The shock was felt throughout southwestern Turkey, and caused some damage in the coastal towns. It was also felt on the island of Rhodes with an intensity of V on the M.M. scale.

The reason for studying the focal mechanism of this earthquake is to obtain information on the Aegean Island Arc structure and the underthrusting mechanism associated with it.

The shock was recorded well on long-period instruments at many stations. A total of 63 P-wave first motions was available, all but eight from WWSSN stations (Appendix I, Table A.I.2). Forty-three first motions were graded good or better. Azimuthal distribution of stations was good.

The distribution of first motions for this shock is shown in Figure 3.9. A clear separation of compressions from the dilatations fixes the orientation of the east-west striking nodal plane fairly well. The position of the other nodal plane which strikes N 66°E is less clearly defined, and without the help of first motions at near stations IST and CMP it could be several tens of degrees in error. The mechanism indicated by the fault-plane diagram is reverse faulting. The east-west striking plane defines a steeply dipping reverse fault with a pure dip-slip motion that moved the southern block upward. The plane striking

N 66°E however, defines a low angle reverse fault (thrust fault). The motion along this fault was predominantly dip-slip (with only a very small horizontal component) with downward motion of the southern block.

On the basis of the following information the nodal plane which strikes N 66°E and dips 22°NW was selected as the fault-plane:

a) Alignment of this nodal-plane parallel to the trend of the seismic zone in the area of the shock (Figure 3.6).

b) Crustal structure inferred from the Bouger gravity anomalies (Rabinowitz and Ryan, 1970) along a profile from the Lower Nile cone to Turkey which indicates crustal shortening in the eastern Mediterranean by underthrusting and decollement.

The fault-plane solution indicates a stress system with maximum principal stress (P) about perpendicular to the trend of the seismic zone, and the least principal stress (T) in nearly vertical direction. The fault mechanism and the stress system indicated by this fault-plane solution both favor the underthrusting of the eastern Mediterranean lithosphere beneath the Aegean Sea and southwestern Anatolia.

Event No. : 2
Date : Jan. 14, 1969
Origin time : 23:12:07.88 G.M.T.
Epicenter : 36.17N 29.20E

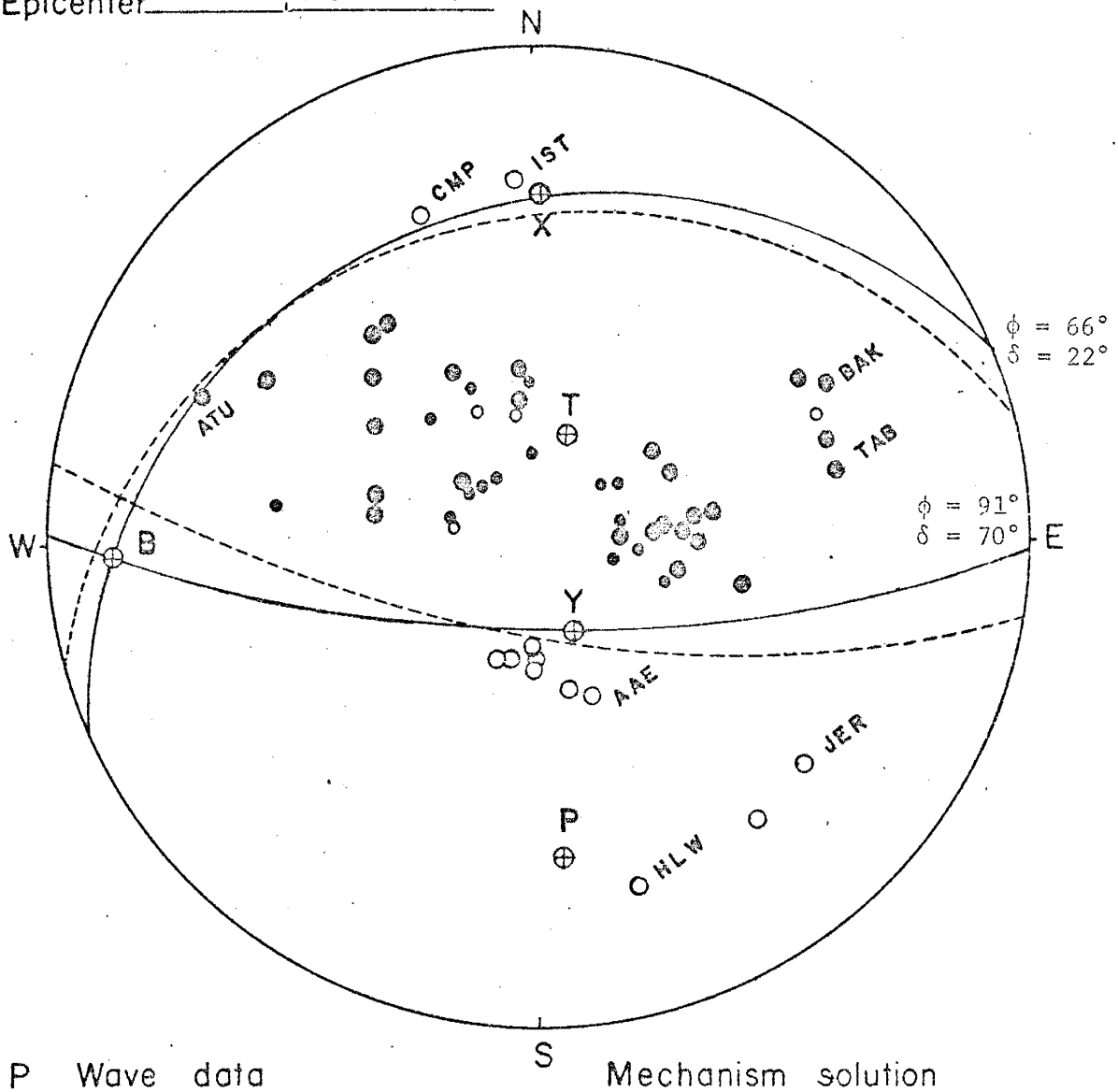

P Wave data

● Compression

○ Dilatation

Mechanism solution

Axis	P	T	B	X	Y
AZ.	176	18	268	1	157
Plunge	25	64	9	19	68

Figure 3.9. Fault-plane solution of an eastern Mediterranean shock. Date, time, and location are given above. A P wave velocity of 7.5 km/sec is used in this projection. Solution indicates a high-angle or low-angle reverse fault. Dashed lines indicate an alternate solution.

Earthquake # 3: March 23, 1969, 21:08:42.6 G.M.T.

The epicenter of this shock was located at 39.16°N latitude, and 28.48°E longitude in western Turkey (Figure 3.6). Its magnitude (Ms) was 5.6.

The shock was felt throughout western Turkey and caused considerable damage; 1100 houses were destroyed in Demirci Gordes, Sindirigi and surrounding villages. It was felt in Istanbul but caused only minor damage.

The main reason for studying the focal mechanism of this earthquake and other earthquakes from western Turkey is to understand their relation to the tectonics and the geology of western Turkey. The high seismic activity in western Turkey could be due to reactivation of old tectonic lines of weaknesses. The focal mechanism of this earthquake and others from western Turkey could decide this question. This earthquake marks the beginning of a sequence of damaging earthquakes in western Turkey.

A total of 74 P wave first motions were available for this earthquake, of which 61 were graded good, very good, or excellent (Appendix I, Table A.I.3.). However 23 of these first motions were determined from short-period records or from stations outside the WWSSN. Therefore the homogeneity of data is not as good as for the other, stronger earthquakes from western Turkey.

Figure 3.10 shows the fault-plane diagram of this shock based on all available first motions. In spite of some inconsistent first motions a wedge shaped separation of compressions and dilatations clearly indicates normal faulting. The inconsistent first motions toward the central part

of the diagram are due to observational errors introduced from the poor quality of first arrivals. To improve the quality of the fault-plane solution, a new fault-plane diagram based on first motions graded good or better was drawn (Figure 3.11). Both diagrams (Figure 3.10, and Figure 3.11) indicate the identical fault mechanism. The nodal plane striking S 71°E and dipping 58° towards the north represents a normal fault along which the northern block has moved downward with respect to the southern block. The other nodal plane striking S 26°E and dipping 42° toward the southwest, represents a normal fault, along which the western block has moved downward.

On the basis of the following information the nodal plane striking S 71°E and dipping 58° was selected as the fault-plane:

a) The epicenter of the shock is located within an east-west trending graben structure, and the fault-plane is aligned parallel to east-west trending fault lines in western Turkey see Figures 2.2 and 3.6).

b) The fault-plane is parallel to the trend of the seismic zone in the area of shock (Figure 3.6).

c) The fault-plane resembles a naturally occurring normal fault more closely than the other nodal plane. Most normal faults observed in the field dip at angles larger than 45°, most usually between 60° and 65° (Price, 1966; DeSitter, 1964). Sand box experiments have revealed similar results (Sanford, 1959). Also Navier-Coulomb fracture theory indicates that rocks break at an angle less than 45° to the maximum compressional principal stress, which is nearly vertical in

the case of normal faults.

The fault-plane solution indicates a stress field in which the maximum pressure is close to vertical, and the maximum tensile stress is nearly horizontal. The horizontal tensile stress field which is characteristic of a rift structure is perpendicular to the general trend of structure in western Anatolia.

Event No. : 3
Date : March 23, 1969
Origin time : 21:08:42.6 G.M.T.
Epicenter : 39.16N 28.48E

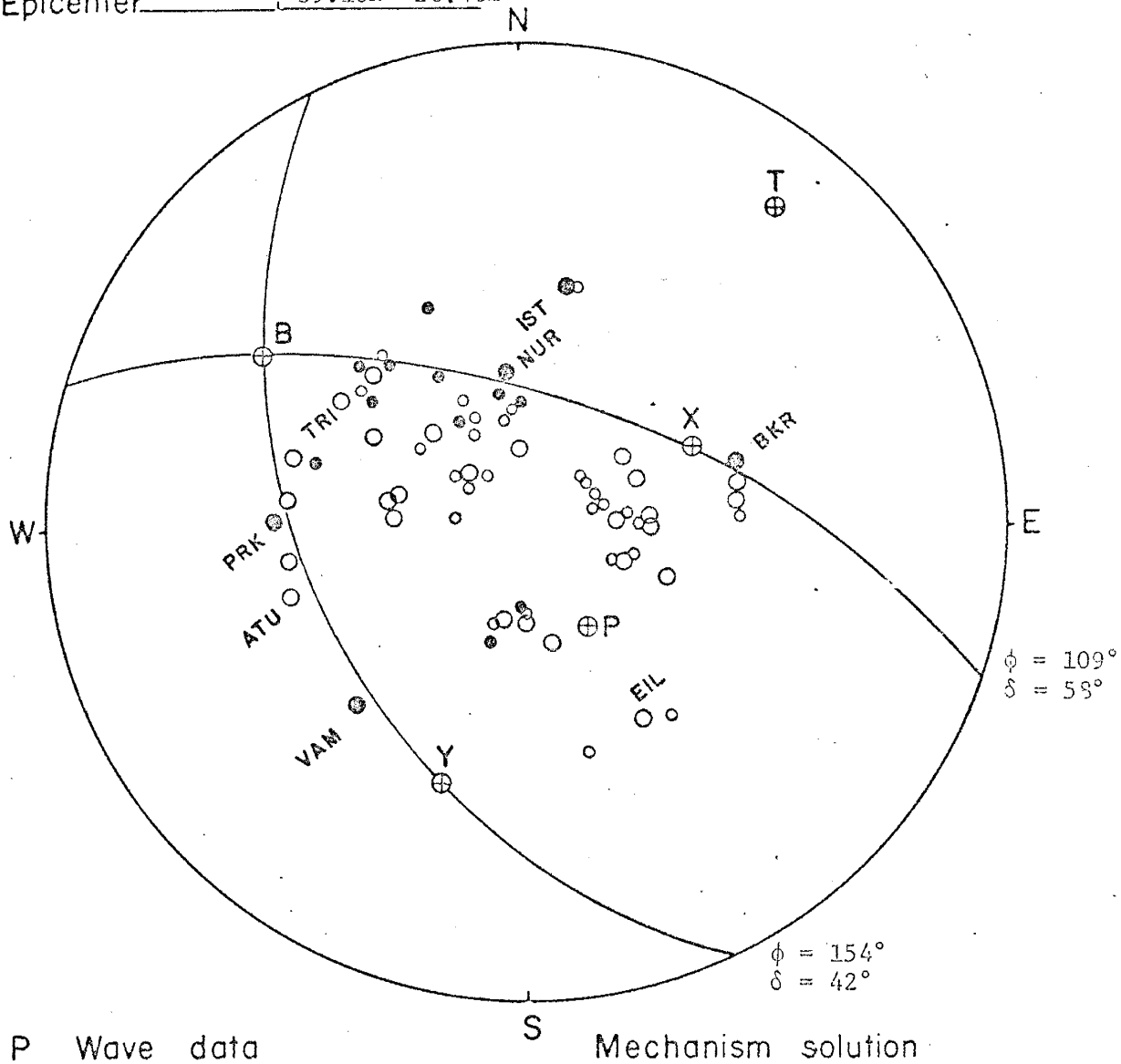

P Wave data

● Compression

○ Dilatation

Mechanism solution

Axis	P	T	B	X	Y
AZ.	148	39	305	64	198
Plunge	62	9	24	48	31

Figure 3.10. Fault-plane solution of a western Anatolian earthquake. Date, time, and epicenter are given above. The solution is based on all available first motions, and a P wave velocity of 6.3 km/sec is used in projection.

Event No. : 3
Date : March 23, 1969
Origin time : 21:08:42.6 G.M.T.
Epicenter : 39.16N 28.48E

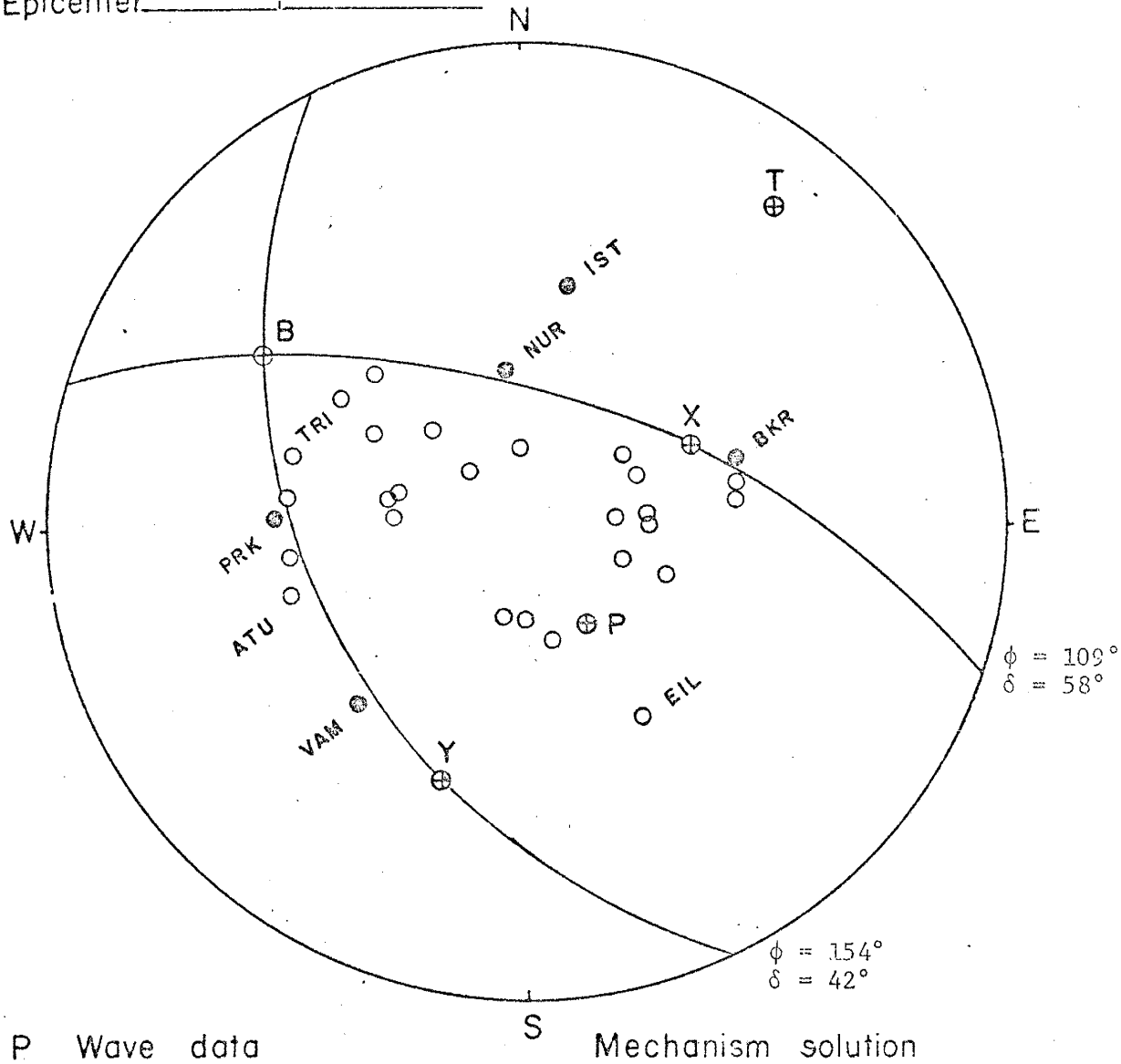

P Wave data

● Compression

○ Dilatation

Mechanism solution

Axis	P	T	B	X	Y
AZ.	148	39	305	64	198
Plunge	62	9	24	48	31

Figure 3.11. Fault-plane solution of a western Anatolian earthquake. Date, time, and epicenter are given above. The solution is based on good or better first motions, and a P wave velocity of 6.3 km/sec is used in projection.

Earthquake # 4: March 28, 1969, 01:48:30.4 G.M.T.

The epicenter of this shock was located at 38.58°N latitude, and 28.44°E longitude in western Turkey (Figure 3.6). Its surface wave magnitude was 6.4.

The earthquake caused severe damage and casualties in western Turkey. Fifty-three people were killed, and 4651 houses destroyed completely or severely damaged in Alasehir and the nearby towns. Associated with this earthquake was the development of several tension fractures in the ground the longest of which was over 12 km (Arpat and Bingol, 1969).

Like shock number 3, the main reason for studying the focal mechanism of this earthquake is to understand the relation between current earthquake motions and the tectonics of western Turkey. In addition, this earthquake is one of the few earthquakes in western Turkey that produced surface fractures and it is important to understand the relation of these surface fractures to the focal mechanism.

A total of 79 P wave first motions were available for this shock, of which 73 were rated good or better (Table A.I.4, Appendix I). The azimuthal distribution of stations and the homogeneity of data (uniformity of the source of first motions) were fairly good. The first motion diagram shown in Figure 3.12, indicates clearly a wedge shaped separation of dilatations from compressions which are relatively scarce. The fault mechanism indicated by the first motion diagram is normal faulting. One nodal plane is defined very well and represents a normal fault striking S 62°E, and dipping 64° toward the southwest. The motion along this fault would be predominantly dip-slip with the

southern block moving downward relative to the northern block. The other nodal plane striking N-S and dipping 44° to the east represents a normal fault with the eastern block moving downward relative to the western block.

On the basis of the following information the nodal plane which strikes S 62°E was selected to be the actual fault-plane:

a) The epicenter of the shock is located within the Alasehir-Salihli valley which is a NW-SE trending active graben. The strike of the fault-plane is parallel to the trend of this structure.

b) The earthquake produced tension fractures in the ground (Figure 3.13). These fractures showed continuity in NW-SE direction, and indicated dip-slip motion (Arpat and Bingol, 1969).

c) No movements occurred during the earthquake along the N-S trending older faults.

d) The fault-plane represents the naturally occurring faults more closely than the other nodal plane (see discussion for earthquake #3).

Focal mechanism of this earthquake indicates vertical crustal movements in western Turkey. The Alasehir-Salihli valley in which the epicenter was located is a typical graben structure (Figure 3.13). It is surrounded by high mountains generally made of metamorphic rocks. Block faulting has deformed the sediments in the valley and formed a stepped topography indicative of progressive subsidence. Indeed the geologic evidence suggests that the valley has subsided about 1500 m

since the end of Pliocene (Arpat and Bingol, 1969). High seismicity and Quaternary volcanism associated with the structure are indicative of present tectonic activity.

Tensional stresses are responsible for the development of a graben structure in the earth's crust (Vening-Meinesz, 1964). The focal mechanism of this earthquake was the result of such a tensional stress field. The maximum compression was nearly vertical, and the maximum tension was nearly horizontal and perpendicular to the trend of the valley.

Event No. : 4
Date : March 28, 1969
Origin time : 01:48:30.4 G.M.T.
Epicenter : 35.58N 28.44E

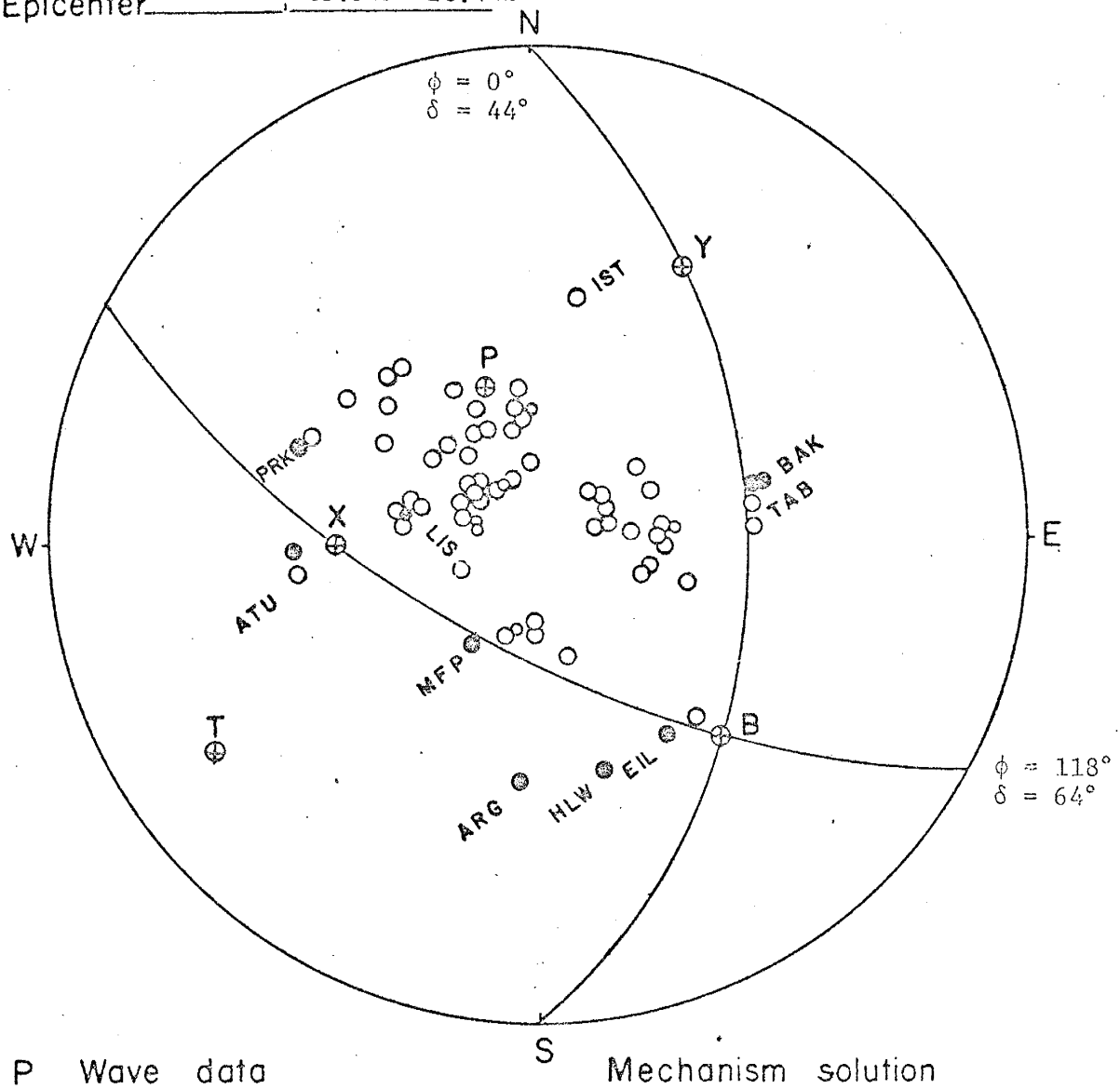

P Wave data

● Compression

○ Dilatation

Mechanism solution

Axis	P	T	B	X	Y
AZ.	343	236	139	268	29
Plunge	54	13	32	46	25

Figure 3.12. Fault-plane solution of a west Anatolian earthquake. Date, time, and location are given above. A P wave velocity of 6.6 km/sec is used in the projection. The solution represents normal faulting.

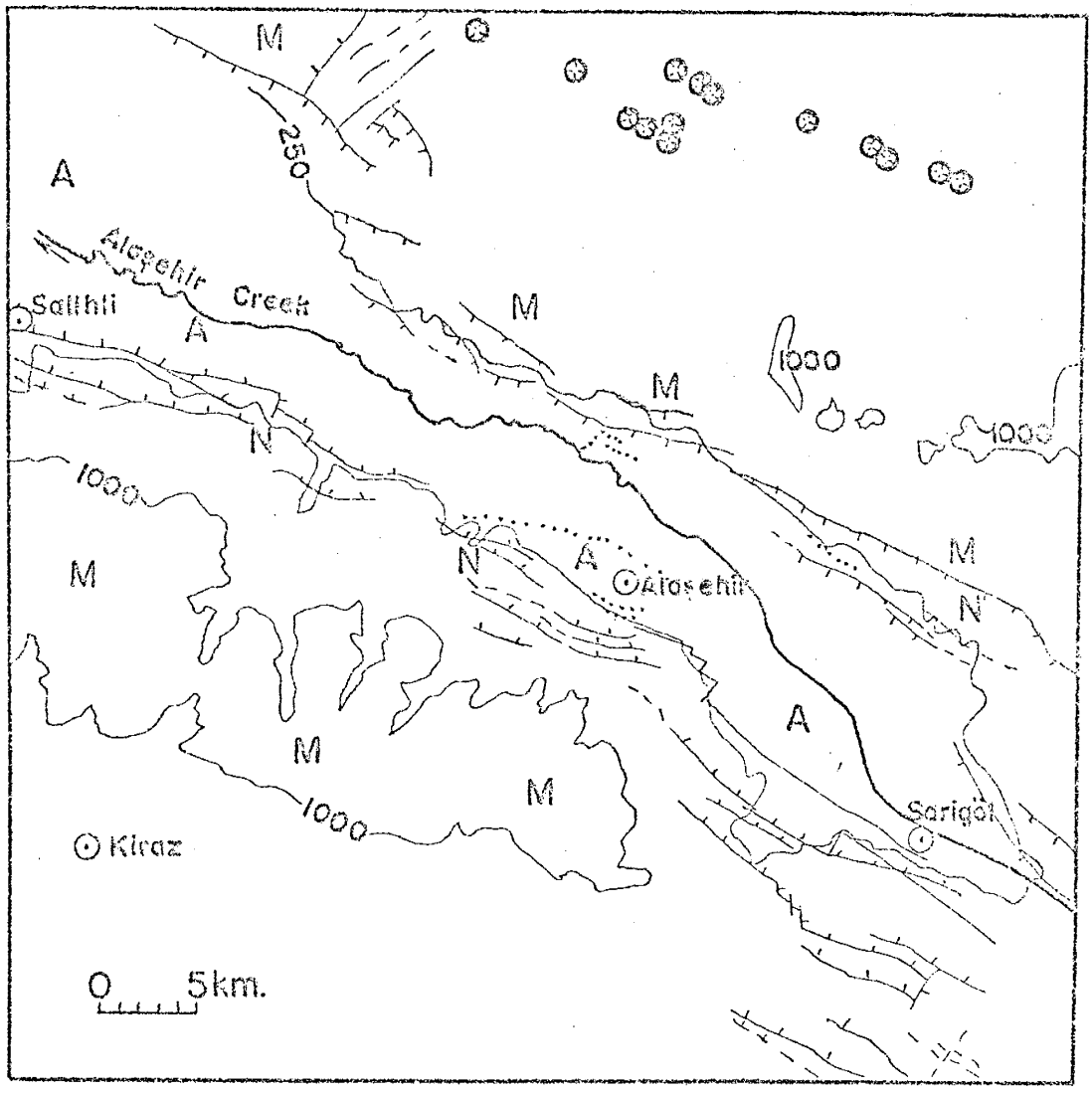

Figure 3.13. The main structural feature of the Alasehir-Salihli valley; A = alluvium, N = coarse clastic materials, M = metamorphics, certain normal faults, uncertain normal faults, ⊕ = Quaternary volcanics, ····· = surface breaks associated with the earthquake of March 28, 1969, (after Arpat and Bingol, 1969).

Earthquake # 5: April 6, 1969, 03:49:33.48 G.M.T.

The epicenter of this earthquake was located at 38.49°N latitude, and 26.41°E longitude at the Aegean coast of western Turkey. Its magnitude (Ms) was 5.5.

The shock caused substantial property damage in the coastal areas of western Turkey. There were 443 completely destroyed houses in Karaburun and Cesme. Slight damage occurred on the Aegean islands. The total area of felt shaking was about 140,000 km^2.

The main reason for studying the focal mechanism of this earthquake was to investigate whether or not the east-west trending graben systems of western Anatolia extend into the Aegean Sea. Also, the focal mechanism of this shock could decide if the north-south trending faults in the area of the earthquake (Figure 2.2) have been reactivated during the earthquake.

A total of 66 P wave first motions were available for this earthquake (Appendix I, Table A.I.5). Unfortunately the shock was not recorded very well on long-period instruments and therefore 27 first motions had to be obtained from short-period records or from stations outside WWSSN. Thus the homogeneity of data was not very good.

The fault-plane solution, based on all available first motions, is shown in Figure 3.14. All inconsistent first motions, except the one at PLG, arise from the poor quality of first arrivals. The first motion at PLG, obtained from the preliminary bulletin of the National Observatory of Greece, was reported as an iPn arrival. However this inconsistency may result from that station being located close to a nodal plane. To improve the quality of the fault-plane solution, another fault-plane

diagram based on first motions rated good or better was prepared (Figure 3.15). A comparison of both solutions (Figure 3.14, and Figure 3.15) does not show any great difference in the orientations of the nodal planes.

The focal mechanism described by the fault-plane diagrams is normal faulting. One nodal plane strikes S 79°E, and dips 66° toward the north. This plane represents a normal fault upon which the motion is dominantly dip-slip with the northern block moving downward with respect to the southern block (Figure 3.15). The other nodal plane striking N 41°E, and dipping 40° toward the southeast also represents predominantly dip-slip motion on a normal fault with downward motion of the eastern block relative to the western block.

On the basis of the following criteria, the east-west striking nodal plane was selected as the fault-plane:

a) The selected plane is aligned parallel to the trend of graben structures in western Turkey (Figure 2.2).

b) The selected plane strikes parallel to the trend of seismic zone in the area where the shock is located (Figure 3.6).

c) The motion along the north-easterly striking nodal plane would indicate subsidence of the Anatolian side. Geologic evidence however indicates the opposite (Ilhan, 1971).

d) The selected plane represents the naturally occurring faults better than the other nodal plane (see earthquake #3).

e) The epicenters of earthquakes from the same area in the days following the occurrence of this shock showed a gradual shift from west to east, and were aligned parallel to the strike of

the selected fault-plane. (In the absence of a detailed aftershock study however, it cannot be confirmed if they were the aftershocks of this earthquake.)

The focal mechanism of this earthquake supports the contention that the west Anatolian graben systems extend into the Aegean Sea. The present seismic activity along the Aegean coasts of western Turkey probably represent the tectonic activity along the extension of these grabens. The fault-plane solution indicates a tensional stress field with a different orientation from that indicated by other west Anatolian earthquakes to the east. The maximum pressure still maintains its nearly vertical position and the maximum tension is still close to the horizontal but its orientation is NW-SE rather than NE-SW.

Event No. : 5
Date : April 6, 1969
Origin time : 03:49:33.5 G.M.T.
Epicenter : 38.49N 26.41E

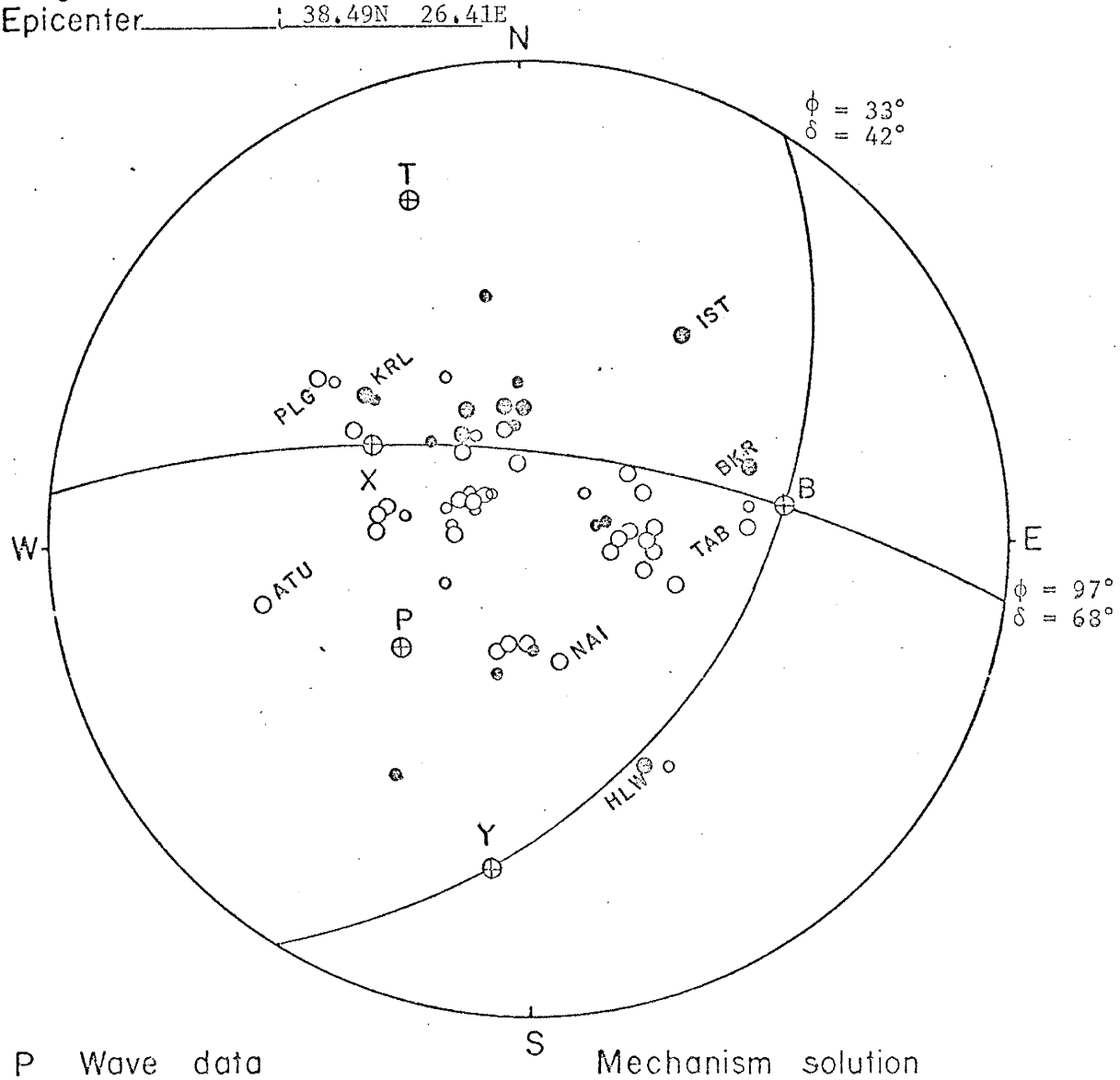

P Wave data

● Compression

○ Dilatation

Mechanism solution

Axis	P	T	B	X	Y
AZ.	210	343	82	304	186
Plunge	53	15	-33	48	22

Figure 3.14. The fault-plane solution of an Aegean earthquake. Date, time, and location are given above. The solution is based on all available first motions and a P wave velocity of 6.6 km/sec is used in the projection.

Event No. : 5
Date : April 6, 1969
Origin time : 03:49:33.5 G.M.T.
Epicenter : 38.49N 26.41E

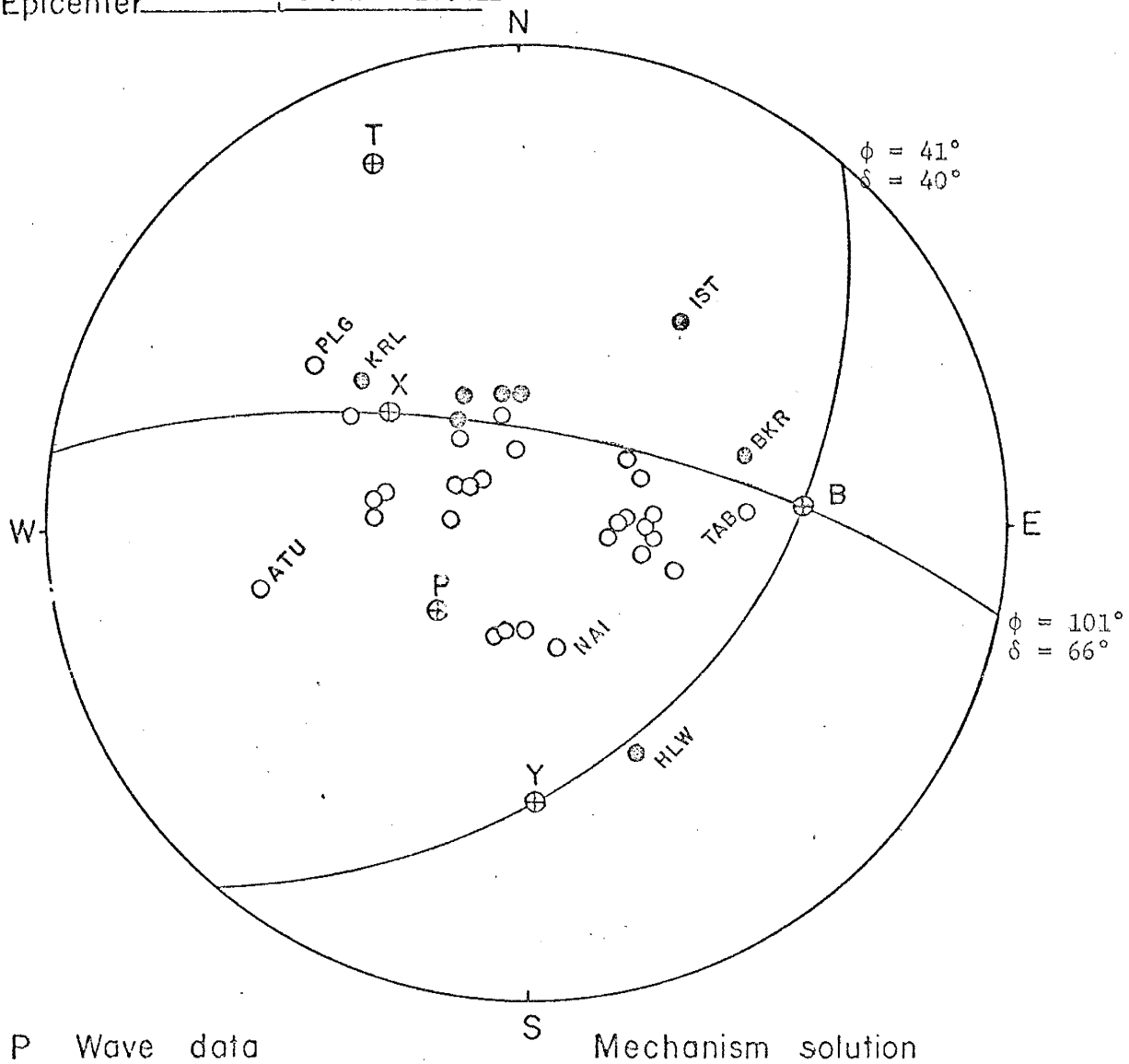

P Wave data

Compression

Dilatation

Mechanism solution

Axis	P	T	B	X	Y
AZ.	227	339	86	312	178
Plunge	62	11	30	50	30

Figure 3.15. The fault-plane solution of an Aegean earthquake. Date, time, and location are given above. The solution is based on first motions graded good or better. A P wave velocity of 6.6 km/sec is used in projection.

Earthquake # 6: June 12, 1969, 15:13:31.10 G.M.T.

The epicenter of the shock was located at 34.40°N latitude and 25.06°E longitude in the Mediterranean Sea south of the Crete island (Figure 3.6). Its magnitude (Ms) was 5.8.

The shock was felt in Crete, and at Alexandria in Egypt. The total area of felt shaking was 375,000 km^2.

The reason for studying the focal mechanism of this earthquake was to determine if fault motions conform to the proposed underthrusting mechanism in the eastern Mediterranean, suggested by seismic, gravity, and other geophysical and geological data (Caputo, et al., 1970; McKenzie, 1970; Ryan, et al., 1970).

A total of 72 P wave first motions were available for this earthquake, all but 15 from the WWSSN stations (Appendix I, Table A.I.6). Sixty-three first motions were graded good or better. The first motion diagram shown in Figure 3.16 presents a clear separation of compressions from the dilatations that is indicative of reverse fault motion during the earthquake. The nodal plane striking N 76°E, and dipping 74° toward the south, represents nearly pure dip-slip motion (upward on the southern block) on a reverse fault. The other nodal plane striking N 54°E and dipping 18° toward the northwest represents predominantly dip-slip motion on a thrust fault.

A choice of the fault-plane in this case was difficult. Focal mechanism studies of shallow focus earthquakes at the Tonga-Kermadec arc (Isacks, et al., 1969), and along the Aleutian arc (Stauder, 1968) have shown that dip-slip motion is predominant at island arcs. The thrust fault mechanism is characteristic of the area immediately behind islands

and normal faulting is characteristic of the area on the seaward side of the arcs (Isacks, et al., 1968). Thrusting and normal faulting are believed to be a natural mechanical consequence of bending and pushing lithospheric plates into the mantle. Accepting that these conclusions apply to all island arc areas, it appears more likely that thrust faulting rather than high-angle reverse faulting was the actual mechanism for this earthquake.

The greatest principal stress (P) axis defined from the fault-plane solution is perpendicular to the strike of the Aegean arc in the area of the earthquake. The least principal stress (T) is nearly vertical, and the intermediate stress (B) is parallel to the arc as found in other island arc areas (Isacks, et al., 1968).

Event No. : 6
Date : June 12, 1969
Origin time : 15:13:31.10 G.M.T.
Epicenter : 34.40N 25.06E

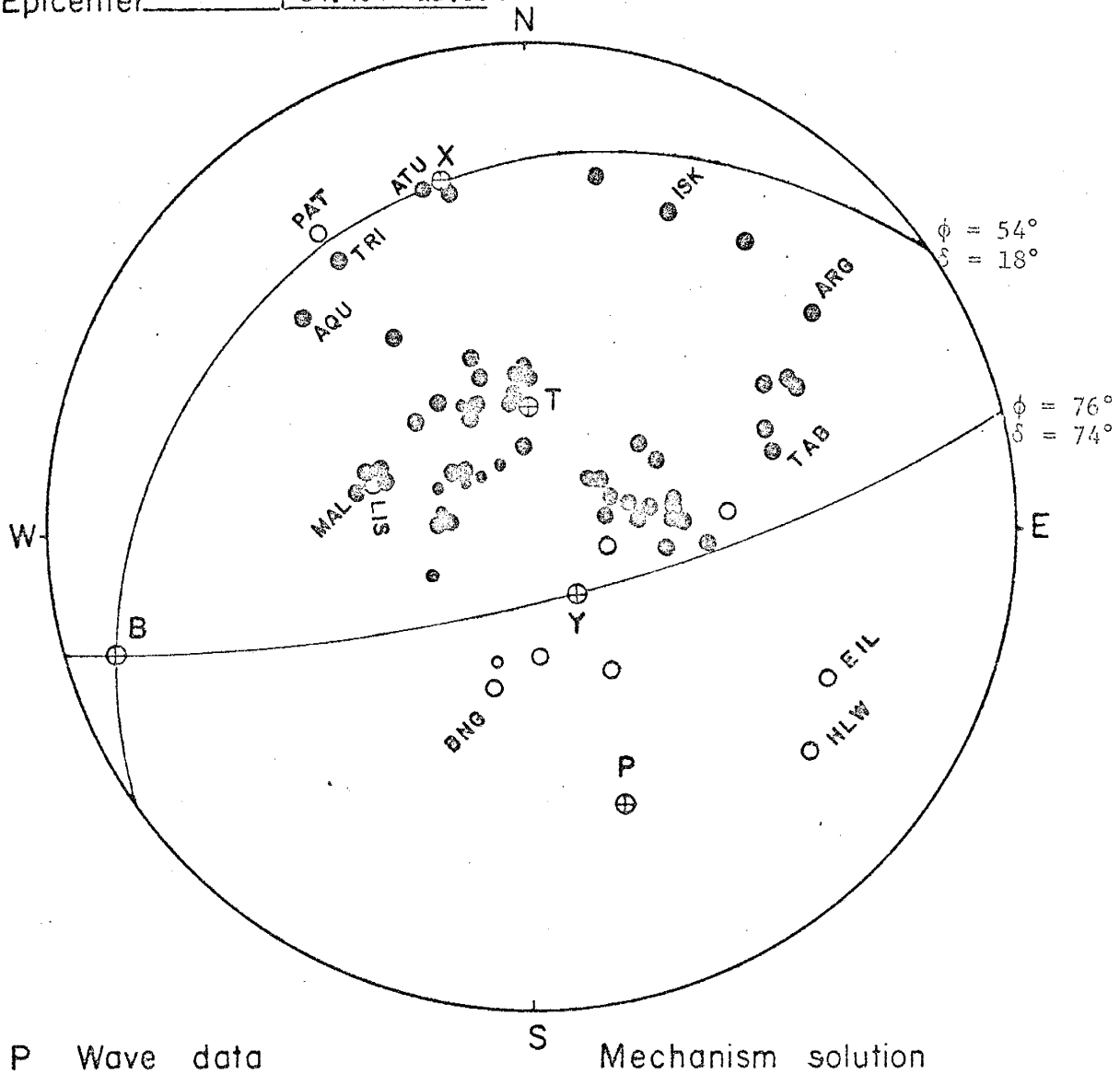

P Wave data

● Compression

○ Dilatation

Mechanism solution

Axis	P	T	B	X	Y
AZ.	161	359	254	347	143
Plunge	28	61	6	16	72

Figure 3.16. Fault-plane solution of an eastern Mediterranean earthquake. Date, time, and location are given above. A P wave velocity of 7.5 km/sec was used in the projection. The preferred solution indicates underthrusting of the Mediterranean lithosphere beneath the Aegean Sea.

Earthquake # 7: March 28, 1970, 21:02:23.4 G.M.T.

The epicenter of this disastrous earthquake was located at 39.18°N latitude, and 29.48°E longitude (Figure 3.6), just northeast of a small town in western Turkey called Gediz from which the earthquake derives its name. Its surface wave magnitude was 7.1.

The Gediz earthquake was felt throughout Turkey and on the Aegean islands. The total area of felt shaking was about 1,130,000 km^2 (Preliminary Bulletin of the Seismological Observatory of Greece). Maximum reported intensities around the epicentral area were IX on the M.M. scale. In Gediz and surrounding villages this earthquake killed 1086 people and injured 1174; destroyed completely 8226 buildings, and damaged 5586 severely. The earthquake made 80,000 people homeless in 254 villages (Ambraseys and Thalenko, 1970). The estimated damage was about 24 million dolars. Damagingly strong aftershocks followed the major shock.

Reasons for studying the focal mechanism of the Gediz earthquake were numerous. First of all, the historical records indicate that this is the strongest earthquake to occur in the Gediz region since 1700. Table 3.3 is a listing of damaging earthquakes that have occurred in the Gediz region since the 17th century. Intensities given in this table indicate that the Gediz earthquake was at least one intensity unit stronger than any previous shock in this region. Secondly, the Gediz earthquake was associated with surface faulting and caused landslides, rock falls, sand ejections, and changes in the level of ground water. Surface faulting was rather complex, and its relation to the main shock and the aftershocks is an important question that must be answered.

Also the focal mechanisms of the Gediz earthquake and its aftershocks could decide whether the east-west or southeast-northwest tectonic lines in the Gediz region (Figure 3.19) have been reactivated during the earthquake. Thirdly, the focal mechanism of the Gediz earthquake will provide additional information to relate the tectonic activity to earthquake movements in western Turkey.

A total of 91 P wave first motions was used to determine the fault-plane solution for the Gediz earthquake. Sixty-nine first motions were graded good, very good or excellent (Appendix I, Table A.I.7). Because of relative scarcity of compressions, it was necessary to use the first motions at near stations outside the WWSSN. In spite of this disturbance in the homogeneity of data, the distribution of first motions, shown in Figure 3.17, clearly indicates a wedge-shaped separation of dilatations from compressions. Thus the nodal lines were drawn with reasonable accuracy. A few inconsistent first motions toward the central portion of the diagram are thought to be either observational errors, or errors introduced instrumentally (e.g. a reversal in the polarity of instrument). The inconsistency found at the nearest station, IST, was not the result of that station being located close to a nodal plane because the first motion at this station was a strong and well-defined dilatation. Therefore, it was suspected that the first motion observed at IST might have arisen from a direct P wave arrival rather than from a head or refracted wave arrival. To check this possibility, the P wave velocity for a direct ray path was computed. From the observed travel time and the distance to the hypocenter, a P wave velocity of 6.3 km/sec was obtained. This value is very close to P wave velocities observed in the crust, and thus supports the possibility that the first

motion at station IST could have been generated by a direct P wave.

The inconsistent first motion at station VAM in the southwestern quadrant of the first motion diagram was obtained from the preliminary bulletin of the National Observatory of Greece, and may be incorrect, because the same station reported compressional first motions for the shocks following the main shock.

The source mechanism described by the first motion diagram is normal faulting. One nodal plane strikes N 81°E and dips 36° toward the north and represents a low-angle normal fault. The motion along this fault would be predominantly dip-slip, with the northern block moving downward relative to the southern block. The other nodal plane striking S 50°E and dipping 64° to the southwest represents a normal fault with the southwestern block moving downward relative to the northeastern block. In both cases, the motion along the fault has a small strike-slip component.

On the basis of the following criteria the nodal plane striking S 50°E and dipping 64° to the southwest was selected as the fault-plane:

a) The earthquake produced surface faulting reaching to a total cumulative length of 61 km (Tasdemiroglu, 1971). These faults, generally striking in the E-W and NW-SE directions (Figure 3.18), had predominantly dip-slip motion.

b) The dip of the fault-plane is close to the observed dips of surface fractures (Ambraseys and Thalenko, 1970). (For further discussions see earthquake #3).

c) The tectonics of the Gediz region is characterized by block faulting. The faults generally strike in the E-W, and NW-SE

directions (Figure 3.19).

d) The fault-plane strikes parallel to the NW-SE trending seismic zone (Figure 3.6) in the area of the earthquake. Distribution of the preliminary aftershocks (Ambraseys and Thalenko, 1970) also suggests a NW-SE alignment.

Figure 3.18 shows surface faulting that accompanied the Gediz earthquake. A complete description of these faults was given by Tasdemiroglu (1971). Most faults occurred in the sedimentary terrain, but a few of them penetrated into the crystalline rocks. Most of them were reactivated faults that had earlier histories of displacements (e.g. some faults in the Pinarbasi area (Figure 3.18) have moved during the 1944 earthquake listed in Table 3.3 (Tasdemiroglu, 1971)).

The sense of motion along these faults was predominantly dip-slip with the largest displacements (275 cm) occurring on the breaks located northwest of Gediz (Table 3.4 and Figure 3.18). A small left-lateral component of motion was present on all faults, which is indicated also from the fault-plane solution.

The complexity of surface breaks and presence of secondary strong shocks suggest multiple fracturing associated with the Gediz earthquake. Therefore the certainty of the selected fault-plane is not large. However, the fault-plane solution for the earthquake suggests that the main shock occurred probably on the faults located northwest of Gediz. Movements along east-west trending faults may be associated with the strong aftershocks.

The focal mechanism of the Gediz earthquake indicates that the vertical movements which produced block faulting in western Turkey are still continuing. The stress field indicated from the solution is in

good agreement with the active tectonics. The greatest principal stress (P) is nearly vertical, and the least principal stress (T) is near to horizontal, being perpendicular to the general trend of structures.

TABLE 3.3. Damaging Earthquakes That Have Occurred in the Gediz Region Since 1700 (Mainly from Tasdemiroglu, 1971, with a few additions and omissions).

No.	Date	Macroseismic Epicenter	Damaged Area	Max. Int. (MM Scale)	Reference*
1	1700	39.42N 29.98E	Kutahya	VI	T.D.I.K.
2	1795	38.76N 30.50E	Afyon	VIII	"
3	1859	39.42N 29.97E	Kutahya	VI	"
4	1866,Sep.18	39.40N 29.20E	Usak-Bursa	VI	"
5	1875,May 11	38.10N 30.20E	Bursa	VI	"
6	1866,Oct.6	39.55N 28.95E	Tavsanli	VII	"
7	1896,Apr.16	39.30N 29.20E	Emet	VII	"
8	1901,March	38.20N 29.40E	Usak	VI	"
9	1912	38.20N 30.00E	Usak	VI	"
10	1928,May 6	39.80N 30.50E	Eskisehir	VI	"
11	1930	39.34N 29.25E	Emet	VI	"
12	1934,June 10	38.70N 30.00E	Usak	VII	"
13	1941,Jan.29	38.76N 30.50E	Afyon	V	"
14	1941,July 3	38.67N 29.40E	Usak	VI	"
15	1942,Jan.18	38.76N 30.50E	Afyon	V	"
16	1943,Apr.14	39.34N 29.25E	Kutahya-Bursa		I.S.S.
17	1944,June 25	39.04N 29.40E	Usak-Gediz	VII	"
18	1949,Feb. 5	39.91N 29.20E	Harmancik	VII	B.C.S.I.
19	1949,May 10	38.54N 28.65E	Kula	VI	T.D.I.K.
20	1969,Mar.23	39.19N 28.43E	Demirci	VII	M.R.R.
21	1970,Mar.28	39.18N 29.48E	Gediz	IX	N.O.A.A.
22	1971,May 25	39.02N 29.23E	Eskisehir	VII	N.O.A.A.

* T.D.I.K. = Turkiye Depremleri Izahli Katalogu (Pinar and Lahn, 1952).

I.S.S. = International Seismological Summary.

B.C.S.I. = Bureau Central Internationale de Seismologie.

M.R.R. = Ministry of Reconstruction and Resettlement of Turkey.

N.O.A.A. = National Oceanic and Atmospheric Administration (Formerly U.S.C.G.S.).

TABLE 3.4. A Summary of Fault Movements Associated with the Gediz Earthquake of March 28, 1970 (From Tasdemiroglu, 1971).

No.*	Name of Fault	Maximum Displacements (cm)		Length (km)	Sense of Movements	
		Vertical	Horizontal		Horizontal	Vertical
1	Ayikayasi	275	30	5	Left-lateral	West up
2	Dikmen Tepe	150	10	6	Left-lateral	West up
3	Tuzluburun Tepe	120	--	4	---	West-East up
4	Nennikiri Tepe	110	50	10	Left-lateral	East up
5	Pinarbasi	60	10	3	Left-lateral	North up
6	Erdogmus	75	35	19	Left-lateral	South up
7	Sazkoy	10	small	3	Left-lateral	South up
8	Muratdag	60-35	80-30	7.5	Left-Right lateral	South up
	Others	---	---	3.5	---	West up

* Numbers refer to the fault numbers shown in Figure 3.18.

Event No. : 7
Date : March 28, 1970
Origin time : 21:02:23.4 G.M.T.
Epicenter : 39.18N 29.48E

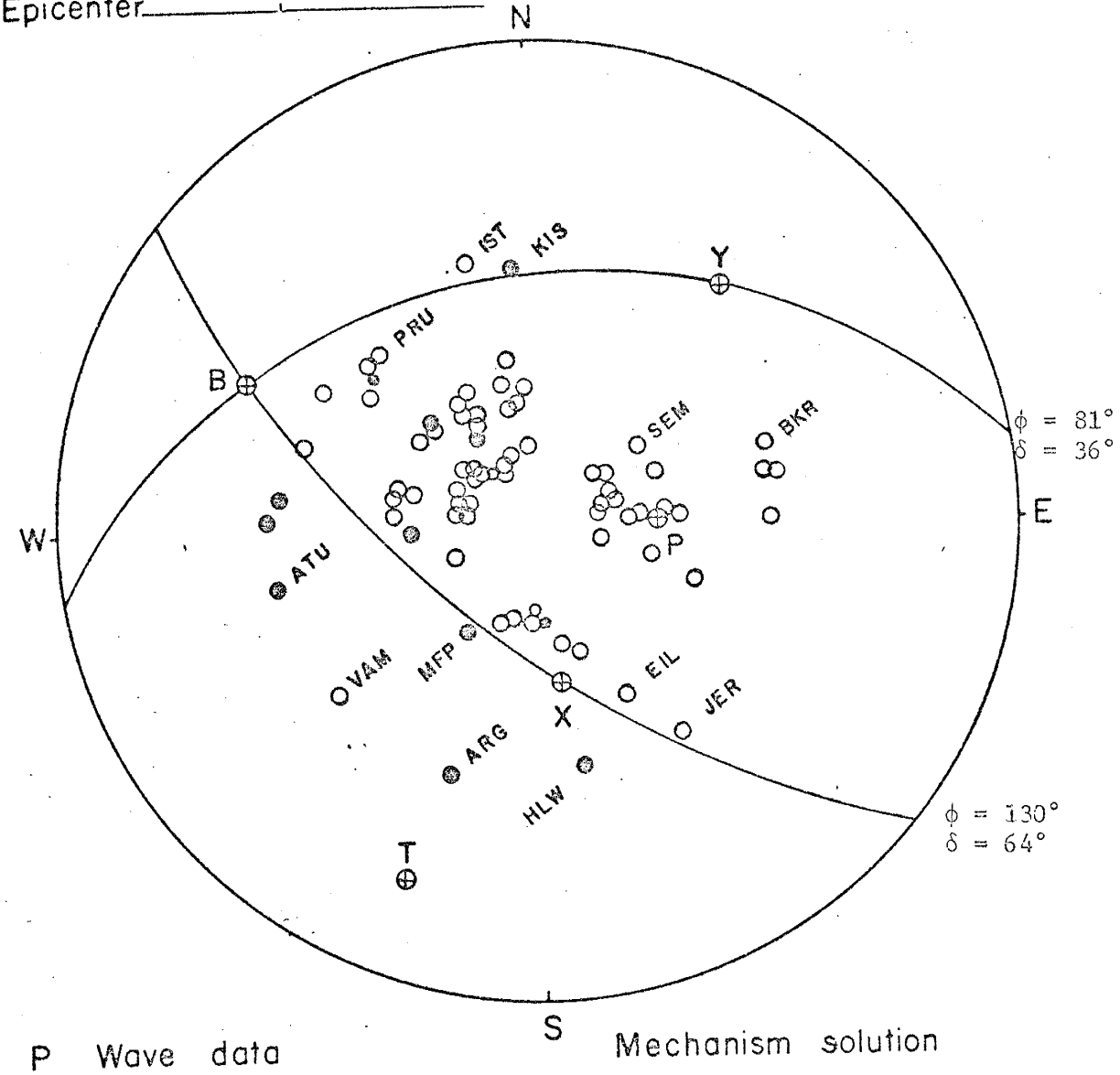

P Wave data

● Compression

○ Dilatation

Mechanism solution

Axis	P	T	B	X	Y
AZ.	90	200	297	174	40
Plunge	62	13	23	53	26

Figure 3.17. Fault-plane solution of the Gediz earthquake. Date, time, and location are given above. A P wave velocity of 6.6 km/sec is used in this projection. The solution indicates a normal fault.

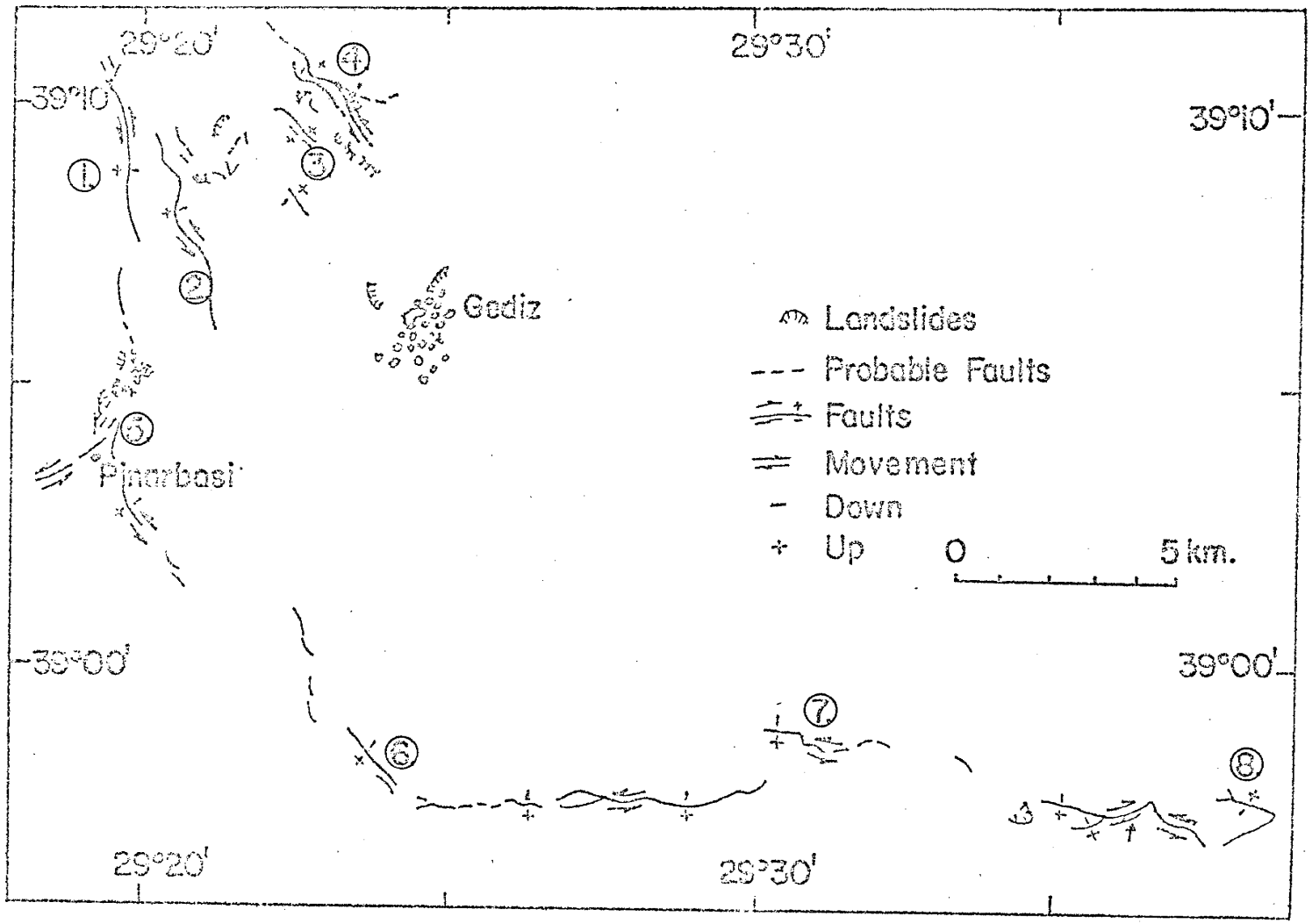

Figure 3.18. Locations of faults that have moved during the Gediz earthquake of 1970. The circled numbers indicate the faults listed in Table 3.6. (After Tasdemiroglu, 1971).

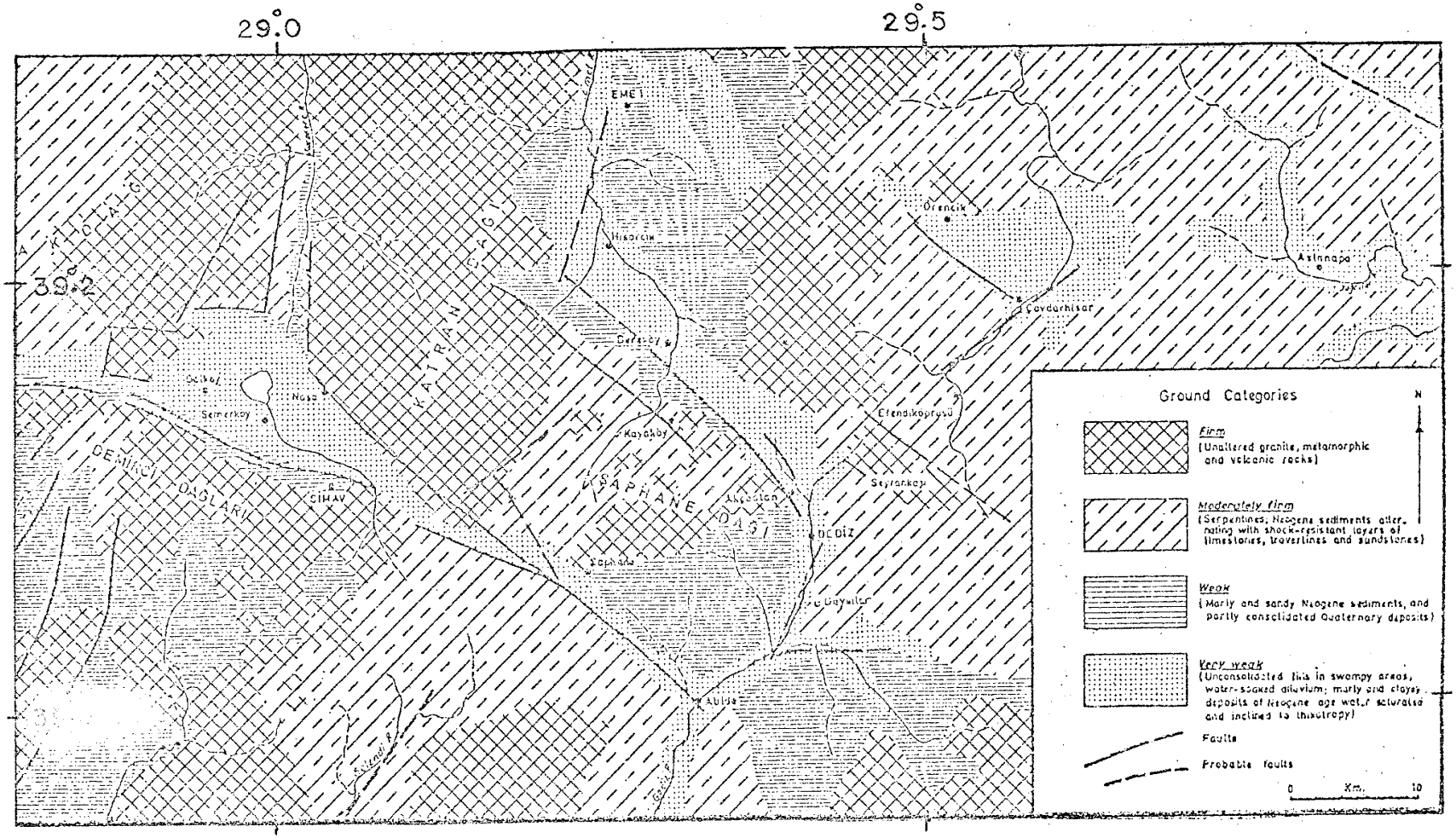

Figure 3.19. Geologic map of the Gediz region (After Erinc, 1971).

Earthquakes # 8 and # 9, April 19, 1970, 13:29:36.36 G.M.T. and 13:47:35.23 G.M.T.

Both events were located at 39.06°N latitude and 29.81°E longitude, which is approximately 35 km southeast of the epicenter of the Gediz earthquake of March 28, 1970 (Figure 3.6). Their surface wave magnitudes were 5.6 and 5.5 respectively.

Both shocks were felt widely in western Turkey. Two persons were injured, and 41 houses and a mosque were destroyed at the village of Cavdarhisar.

The main reason for studying the focal mechanisms of these earthquakes was to investigate their relation to the focal mechanism of the destructive Gediz earthquake. Their date, locations, and the focal depths (Table 3.1) suggest that they could be associated with the Gediz earthquake. The other reasons for studying the focal mechanism of these shocks were to examine their duplicate nature, and provide additional information on the relation between earthquake mechanism and the tectonics of western Turkey.

The quality and the homogeneity of first motion data for these earthquakes were not very good. Both shocks were not recorded very well on all the long-period records, and consequently it was necessary to incorporate first motions observed on the short-period records in the analysis. On the long-period records earthquake # 9 was superposed on earthquake # 8 but the two events were clearly separated on short-period records. Surprisingly, some good first motions were found for both earthquakes on the long-period records.

A total of 69 P wave first motions for shock # 8 (Table A.I.8,

Appendix I), and 58 P wave first motions for shock # 9 (Table A.I.9, Appendix I) were used to determine the fault-plane solutions shown in Figure 3.20 and Figure 3.21. These diagrams indicate the same focal mechanism for both earthquakes. Therefore they were considered to be duplicate earthquakes generated by the same motion on the same fault. Their duplicate nature was also indicated by the identical seismograms written for these shocks at several WWSSN stations. Sample long-period records showing the similarity of ground motion are shown in Figure 3.22.

Since these earthquakes were duplicates the composite fault-plane solution shown in Figure 3.23 was prepared. The solid lines in this diagram represent the best fitting nodal planes to the first motion data. The dashed lines indicate the alternate solutions, and thus some indication of the error involved in determining the nodal planes. At a few stations near the nodal planes, the first motions for the two shocks were of opposite polarity. In such cases, the first motions that were consistent with the composite fault-plane solution were used. A few inconsistent first motions toward the center of the diagrams were thought to be observational errors.

The source mechanism indicated by the composite first motion diagram is normal faulting. The nodal plane that strikes S 80°E, and dips 70° to the north, represents a normal fault with downward motion of the northern block with respect to the southern block. The other nodal plane represents a normal fault striking S 22°E, and dipping 34° to the southwest with a downward motion of the southwestern block. In both cases the fault motion would be predominantly dip-slip with a small strike-slip component.

The fault-plane solutions definitely indicate a similarity between the focal mechanisms of these earthquakes and the Gediz earthquake. However, it is obvious that they have not occurred on the same fault. On the basis of the following criteria the nodal plane striking S 80°E was selected as the fault-plane for the earthquakes # 8 and #9:

a) The selected fault-plane more closely resembles the normal faults commonly observed in the field (for further discussion see earthquake # 3).

b) The surface faulting associated with the Gediz earthquake indicates that the faults located south or southeast of Gediz generally trend in the E-W direction (Figure 3.18). The strike of the fault-plane is parallel to them.

c) The fault-plane strikes parallel to the trend of seismic zone in the area of the shock (Figure 3.6).

The focal mechanism and the time of occurrence of these earthquakes suggest that they were triggered by the Gediz earthquake. Perhaps the stresses in this area are propagating (McKenzie, 1972b) in the manner described by Elsasser (1967), and Savage (1971).

A tensional stress field almost identical to that found at the focus of the Gediz earthquake was responsible for these earthquakes. The maximum principal stress is nearly vertical and the least principal stress is almost horizontal and aligned perpendicular to the general trend of structure.

Focal mechanisms of these earthquakes and the Gediz earthquake suggest that both tectonic lines (the NW-SE and the E-W trending lines (Figure 3.19)) in the Gediz region have been reactivated during these earthquakes.

Event No. : 8
Date : April 19, 1970
Origin time : 13:29:36.36 G.M.T.
Epicenter : 39.06N 29.79E

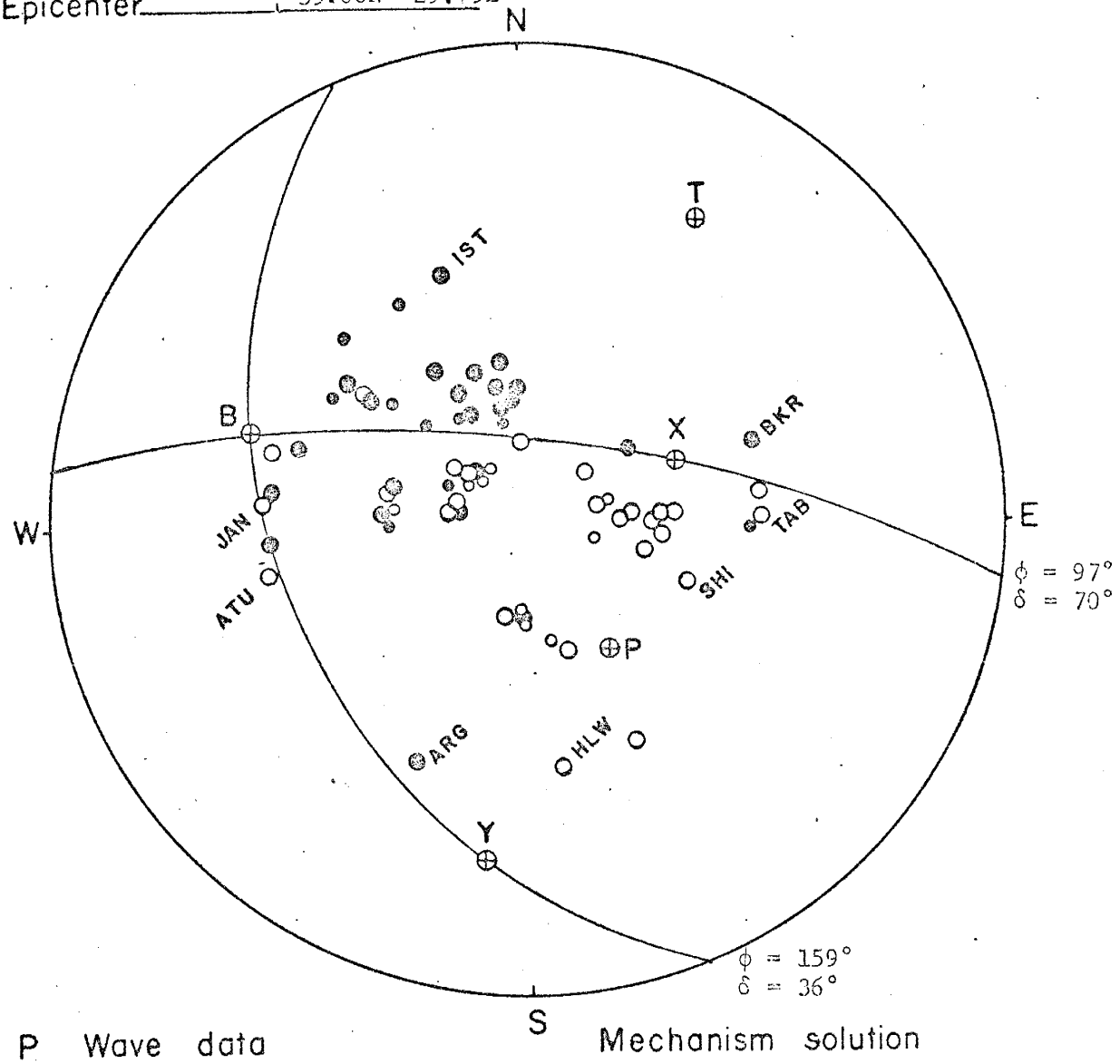

P Wave data

● Compression

○ Dilatation

Mechanism solution

Axis	P	T	B	X	Y
AZ.	145	30	290	67	189
Plunge	55	17	28	52	20

Figure 3.20. Fault-plane solution for a western Anatolian earthquake. Date, time, and location are given above. A P wave velocity of 6.6 km/sec is used in this projection. The solution indicates a normal fault.

Event No. : 9
Date : April 19, 1970
Origin time : 13:47:35.23 G.M.T.
Epicenter : 39.06N 29.83E

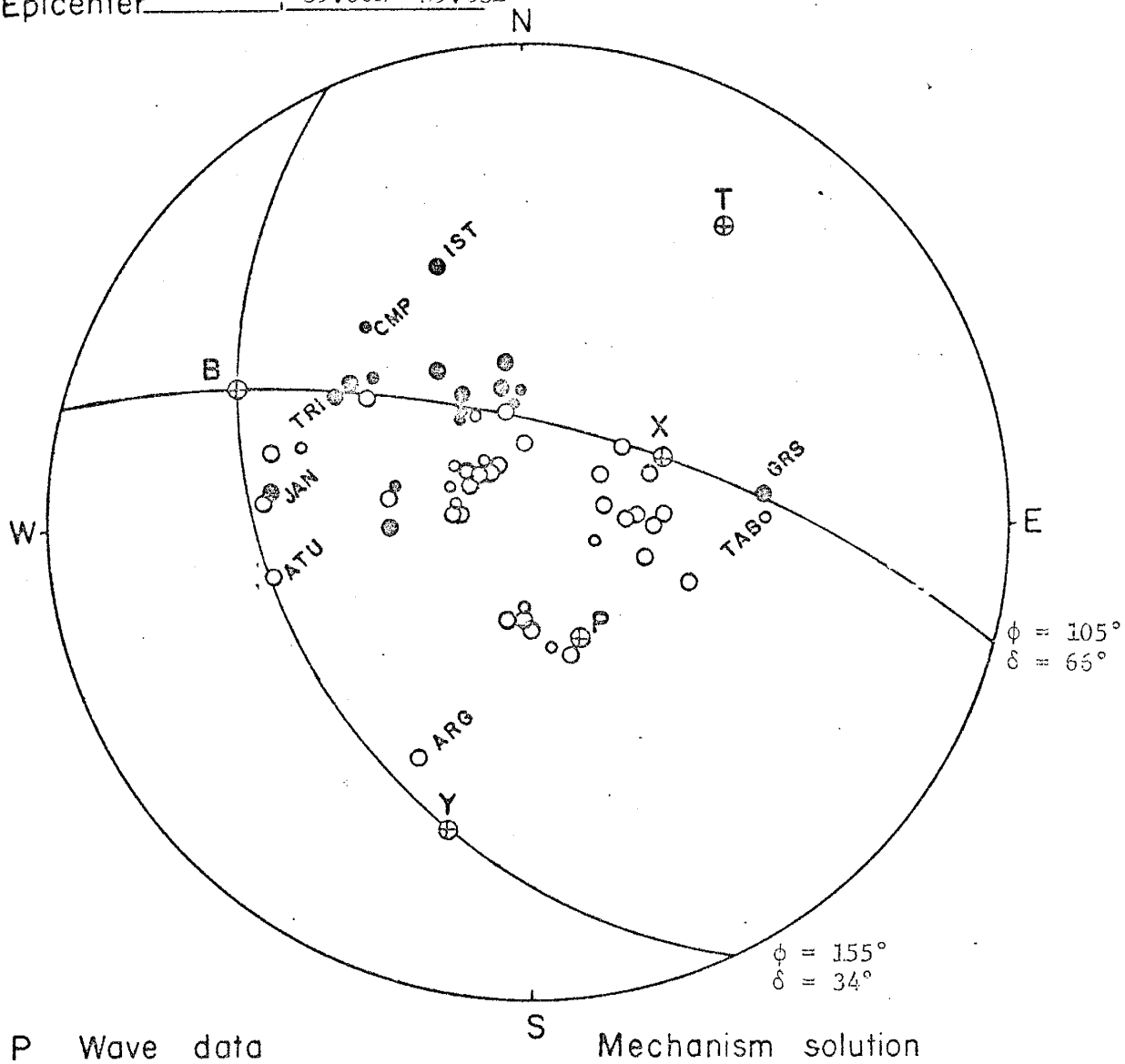

P Wave data

● Compression

○ Dilatation

Mechanism solution

Axis	P	T	B	X	Y
AZ.	156	34	296	65	196
Plunge	60	17	22	55	23

Figure 3.21. Fault-plane solution for a western Anatolian earthquake. Date, time, and location are given above. A P wave velocity of 6.6 km/sec is used in this projection. The solution indicates a normal fault.

Earthquake # 8

April 19, 1970

12:29:36.36 G.M.T.

39.06°N 29.79°E

Earthquake # 9

April 19, 1970

13:47:35.23 G.M.T.

39.06°N 29.83°E

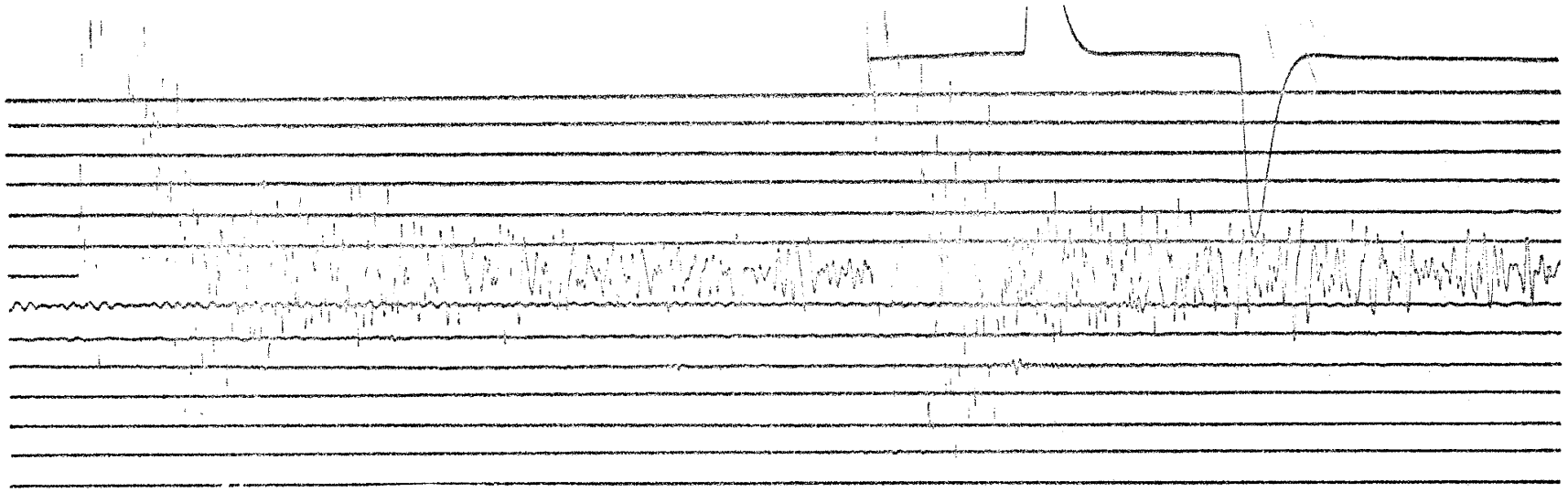

Figure 3.22. A long-period seismogram recorded at IST showing the duplicate characteristics of earthquakes # 8 and # 9.

Event No. : 8 and 9 Composite
Date : April 19, 1970
Origin time : 13:29:36.36 and 13:47:35.23 G.M.T.
Epicenter : 39.06N 29.79E

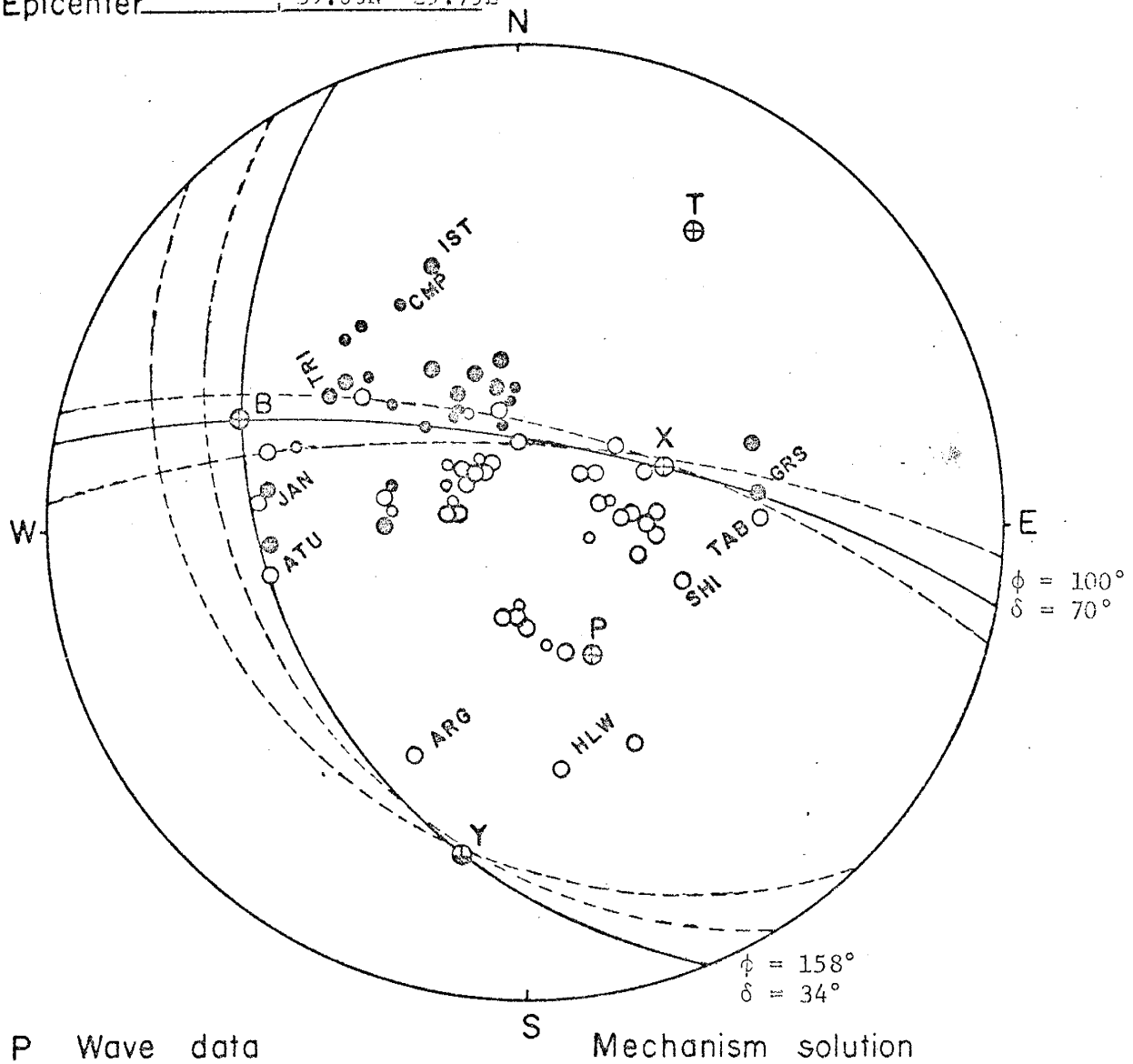

P Wave data

● Compression

○ Dilatation

Mechanism solution

Axis	P	T	B	X	Y
AZ.	152	30	291	67	190
Plunge	57	18	25	55	21

Figure 3.23. Composite fault-plane solution for the duplicate shocks # 8 and # 9. Date, times, and the common epicenter are given above. The solid lines represent the best fitting nodal planes. The solution represents a normal fault.

Earthquake # 10: May 12, 1971, 06:25:12.98 G.M.T.

This shock was located at 37.58°N latitude, and 29.75°E longitude, in southwestern Turkey (Figure 3.6). Its surface wave magnitude was 5.9.

The shock was felt in western and central Turkey and on the Aegean islands. The total area of felt shaking was about 410,000 km^2. The earthquake caused casualties and severe damage in southwestern Turkey. In Burdur, a small town with a population of 25,000 located approximately 50 km northeast of the epicenter, there were 100 people killed, many injured, and severe damage to structures. It is not usual for an earthquake of this magnitude to cause casualties and severe damage 50 km away from the epicenter. Nevertheless this may be explained by the ground conditions at Burdur or a possible error in the location of the earthquake. However if there was an error in the location, this did not affect the fault-plane solution. A small change in the location of the shock does not alter the positions of stations on the first motion diagram noticeably.

The main reason for studying the focal mechanism of this earthquake was to investigate the presence and the nature of strike-slip faulting in southwestern Turkey. A noticeable change in the trend of faults from E-W in western Anatolia to NW-SE in central Anatolia has been recognized by several investigators (Arpat and Bingol, 1969; Ilhan, 1971). Arpat and Bingol (1969) suggested that this change might be due to a transform fault. On the other hand McKenzie (1970) proposed a plate boundary in western Turkey that brings the Aegean and Turkish plates into contact. The nature of this boundary, however, was unexplained. The focal mechanism of the Burdur earthquake would help to answer these questions.

The Burdur region of southwestern Turkey has experienced other damaging earthquakes in the past. They are listed in Table 3.5. The strongest of the shocks listed in Table 3.5 occurred in 1914, and was associated with surface faulting. The epicenter of this shock was related to a longitudinal fault in the Burdur basin. It is quite possible that the Burdur earthquake of 1971 was also associated with this fault.

A total of 73 P wave first motions was available for this shock, all but 19 from the WWSSN stations (Table A.I.10, Appendix I). The Burdur shock was not an outstandingly well recorded earthquake at the WWSSN stations, however, the first motions were fairly good at many stations. There were 40 first motions that were graded good or better. The azimuthal distribution of stations was good; all quadrants except the southwestern quadrant were very well represented. The azimuthal distribution of first motions shown in Figure 3.24 indicates a well defined quadrantal pattern of compressions and dilatations. The dilatations occur from 27° to 109° and from 207° to 289°, and compressions occur from 109° to 207°, and from 289° to 27°. The source mechanism indicated from the first motion diagram is strike-slip faulting. One nodal plane strikes N 27°E and dips 66° to the northwest. This plane represents a right-lateral strike-slip fault. The other nodal plane, which strikes S 71°E and dips 72° to the south, also represents a strike-slip fault but with left-lateral motion on it. In both cases, a very small dip-slip component of motion is present.

The nodal plane that strikes N 27°E was selected as the fault-plane. The structural geology of southwestern Turkey favors this selection.

The most outstanding structural unit in southwestern Turkey is the Taurus mountains. The Taurus mountains are structurally asymmetrical. In the north of the Gulf of Antalya, near Isparta and Burdur, a junction named "Courbure d' Isparta" by Blumenthal (1947) separates two branches of the western Taurids. The eastern branch is oriented in a northwest-southeast direction and is called "Taurus Occidental" (Blumenthal, 1947). The western branch is oriented in a northeast-southwest direction and is named the Lycian Taurus. These two branches contain complicated nappe structures. A detailed geological study of this section of the Taurus mountains (Burnn, et al., 1971) indicates that the asymmetrical structure found here was not related to the initial development of these mountain chains but formed from later tectonic activity that might be as young as Miocene. A north-south left-lateral strike-slip fault at the junction of two branches has been suggested by Arpat and Bingol (1969). Other faults in the Burdur region occur along the edges of sedimentary basins and generally trend in a north-south direction. The available tectonic maps indicate no east-west trending faults in the Burdur region. A northeast-southwest alignment of epicenters (Figure 3.6) in the north of the Gulf of Antalya also favors the choice of the northerly striking nodal plane as the true fault-plane.

The sense of motion indicated from the fault-plane solution is opposite to that inferred from the geology of the area (Arpat and Bingol, 1969), and from the plate tectonics model of McKenzie (1970). The focal mechanism of this shock therefore does not represent the motion between overriding plates in the eastern Mediterranean but represents the motion on an arc-to-arc transform fault (Wilson, 1965; Stauder, 1968; McKenzie, 1972a) between the Aegean and the Cyprian arcs (see section 2). Supporting

TABLE 3.5. Damaging Earthquakes Occurred in Central Southwestern Turkey (Historical Data taken from Ilhan, 1971).

No.	Year	Location	Remarks
1	60	Denizli	Hierapolis (Pamukkale) and two other towns destroyed; extensive damage in eastern Aegean region.
2	1914	Burdur 38°N 30°E	Heavy damage at Burdur, Isparta and Dinar; 40 km long fissures occurred in the Burdur plain. Epicenter was associated with a longitudinal fault in the Burdur basin. Intensity IX, magnitude: 7.1 (Gutenberg and Richter, 1954).
3	1963	Denizli-Burdur 37°.8N 29°.0E	Strongly felt in Burdur, Denizli, and Isparta. Two persons injured, 50 houses and 4 schools damaged in the villages surrounding Denizli. M = 5.9.
4	1964	Isparta 37°.3N 29°.0E	Strongly felt at Isparta and Karamanli, slight damage occurred. M = 5.5.
5	1965	Denizli 37°.8N 29°.4E	Felt in a large portion of the western Turkey, 2 persons killed, 3 injured and 300 houses were destroyed. M = 5.9.
6	1971	Burdur 37°.6N 29°.7E	100 people killed, many injured, and severe damage occurred in Burdur. Ms = 5.9.

evidence for this interpretation are the seismicity and the earthquake mechanisms to the north and south of the central southwestern Turkey.

Focal mechanism of the Burdur earthquake indicated a different orientation of principal stresses at the focus from that obtained for earthquakes to the north and south. The greatest principal stress (P) is oriented in the NE-SW direction and has a considerable vertical component. The least principal stress (T) is horizontal in the NW-SE direction (Figure 3.24).

This completes the description of fault-plane solutions.

Event No. : 10
Date : May 12, 1971
Origin time : 06:25:12.98 G.M.T.
Epicenter : 37.58N 29.75E

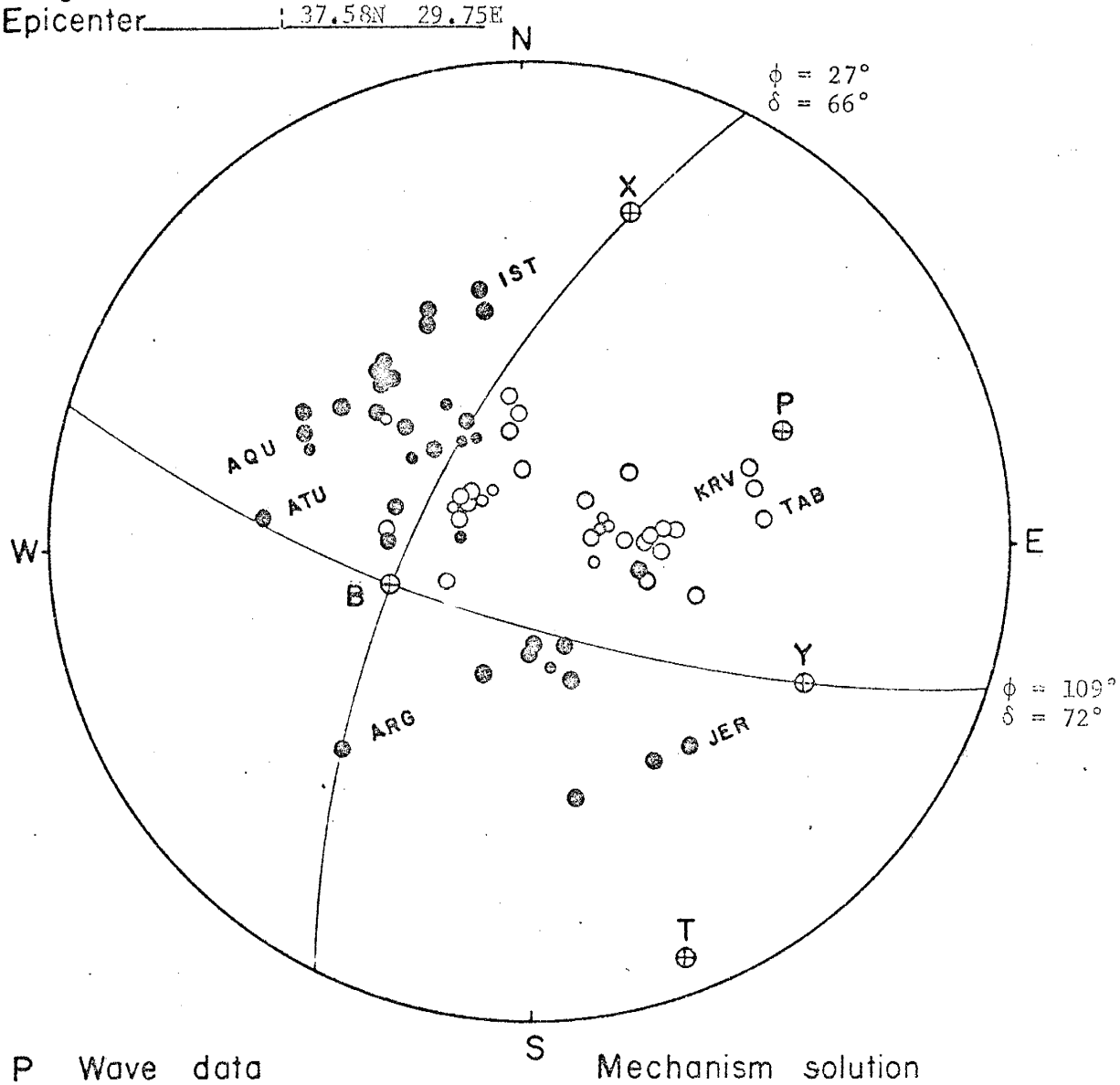

P Wave data

● Compression

○ Dilatation

Mechanism solution

Axis	P	T	B	X	Y
AZ.	66	159	255	18	118
Plunge	29	5	59	17	24

Figure 3.24. Fault-plane solution of the Burdur earthquake of south-western Turkey. Date, time, and location are given above. A P wave velocity of 6.6 km/sec was used in this projection. The solution indicates a strike-slip fault.

Reliability and Shortcomings of Fault-Plane Solutions

Reliability

Some of the weaknesses and problems of the fault-plane method mentioned previously, are now discussed in greater detail. The main parameters that affect the fault-plane solution are the magnitude and the focal depth. The quality of the fault-plane solution improves with increasing magnitude because the number of stations available for the study increases. As the strength of the quake increases, the predominant period representative of motion over the entire fault surface also increases. For this reason first motions of strong shocks record best on long-period instruments, and first motions of weaker shocks record best on short-period instruments.

A comparison between the first motions recorded on long-period and short-period instruments was made in this study. Figure 3.25 illustrates the comparison for different earthquakes at stations in different azimuthal directions. The first three examples are for relatively large shocks. The poor quality of short-period first motions for these shocks is clear. As can be seen from the last example, the quality of short-period first motions improve as the magnitude decreases. With a few exceptions, however, the quality of long-period first motions was always superior to short-period first motions within the magnitude ranges ($5.4 \leq m_b \leq 6.0$) of this study. The good quality of long-period first motions observed in this study for shocks with $m_b \leq 5.5$ is somewhat surprising. Cash (1971) found long-period first motions unsatisfactory for an earthquake of $m_b \cong 5.5$ in northern New Mexico. The reason for

Long-Period Short-Period

Event No.	Date	Magnitude M_b	Magnitude M_s	Station	Dist. (deg.)	Az.	Mechanism
1	Feb.19,1968	5.7	7.1	JER	11.25	130.	Strike-slip
6	June12,1969	5.8	5.8	ATH	3.73	344.	Thrust
7	Mar.28,1970	6.0	7.1	GDH	51.36	333.	Normal
2	Jan.14,1969	5.5	6.0	BUL	56.31	181.	Thrust

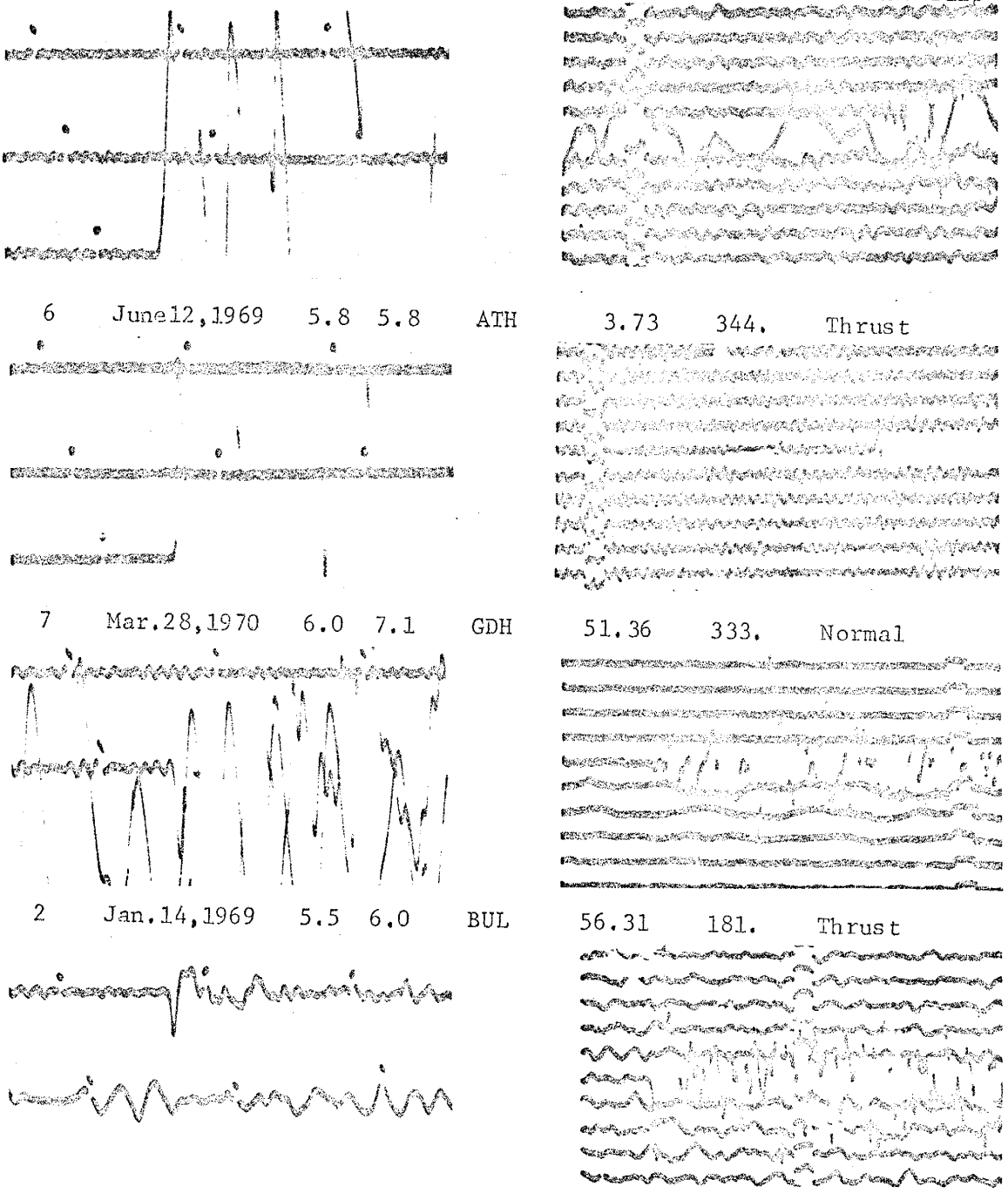

Figure 3.25. Comparison of first motions recorded on short-period and long-period instruments. Except for the last sample, the poor quality on the short-period records is clear.

this discrepancy is that m_b magnitudes for the Turkish shocks are not an accurate gauge of their true strengths.

The effect of depth of focus on fault-plane solutions is indirect. Fault-plane solutions are dependent on the P wave velocity at the focus. The velocity at the focus for a particular earthquake depends on the crustal structure and the position of the focus in that structure. The effect of velocity at the focus is most pronounced for near stations. Table 3.6 presents the angles of incidence for two distances and three different P wave velocities at the focus. Note that a change of 1.0 km/sec in velocity changes the angle of incidence and consequently the projection of first motions at near stations considerably whereas it has little effect at the distant stations.

Table 3.6. Variation of Angle of Incidence at the Focus with P Wave Velocity.

P Wave Velocity (km/sec)	Angle of Incidence at the Focus	
	$\Delta = 9.0°$ $dT/d\Delta = 13.80$	$\Delta = 62°$ $dT/d\Delta = 6.6$
6.0	48.3°	20.8°
6.5	54.0°	22.8°
7.5	69.0°	25.5°

The effect of velocity on strike-slip and dip-slip fault-plane solutions is illustrated by the fault-plane diagrams shown in Figures 3.26 to 3.30. As can be seen from these diagrams the velocity has little effect on strike-slip solutions, whereas it affects the dip-slip solutions significantly. A high P wave velocity at the focus introduces a strong

Event No. : 1
Date : Feb. 19, 1968
Origin time : 22:45:41.2 G.M.T.
Epicenter : 39.40N 25.00E

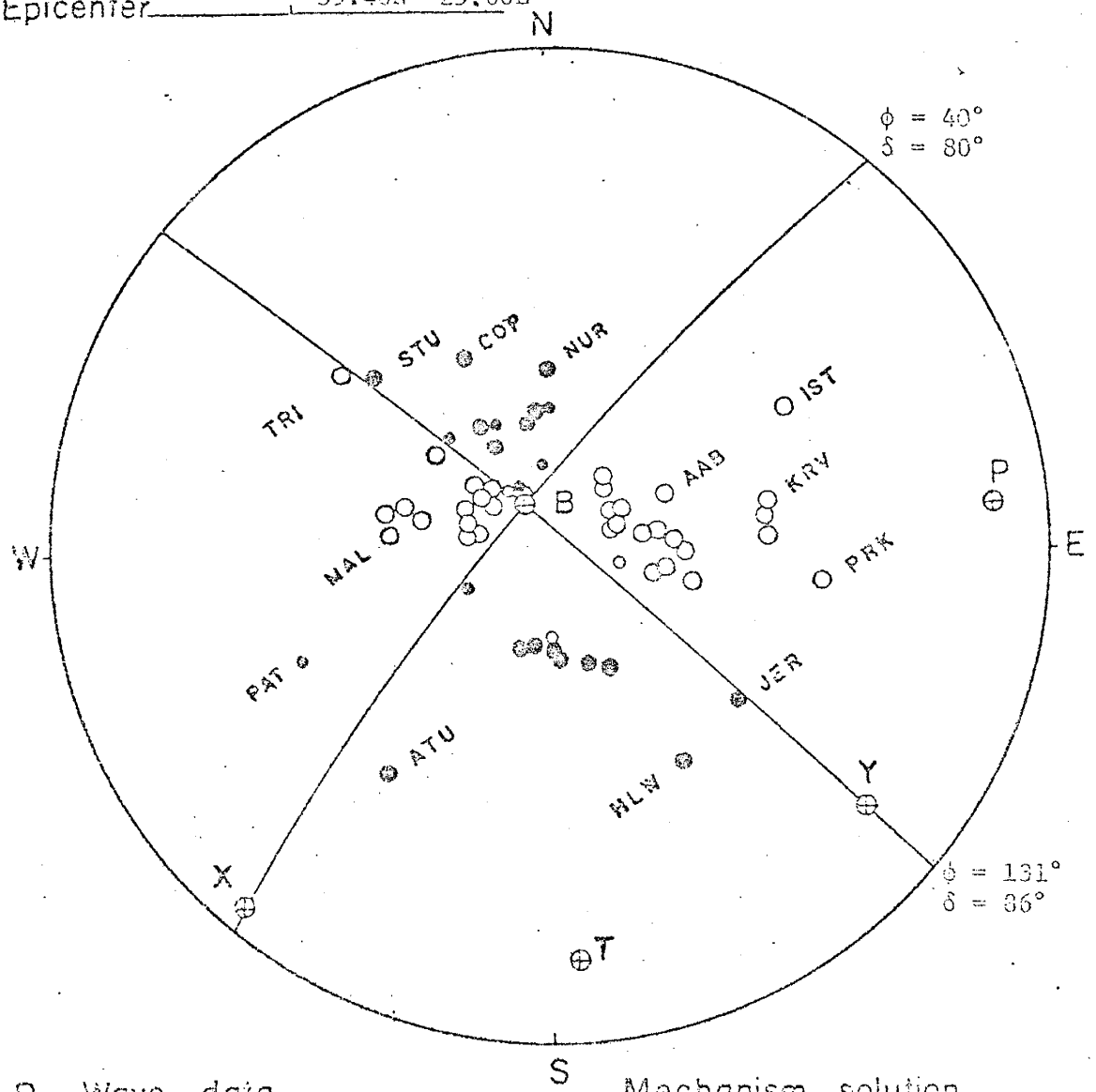

P Wave data

Compression

Dilatation

Mechanism solution

Axis	P	T	B	X	Y
AZ.	85	176	268	220	130
Plunge	6	10	80	3	11

Figure 3.26a. Fault-plane solutions indicating the effect of P wave velocity on a strike-slip solution. P wave velocities of 6.6 km/sec and 7.5 km/sec were used in the projections for the diagrams (a) and (b), respectively.

Event No.	1
Date	Feb. 19, 1958
Origin time	22:45:41.2 G.M.T.
Epicenter	39.40N 25.00E

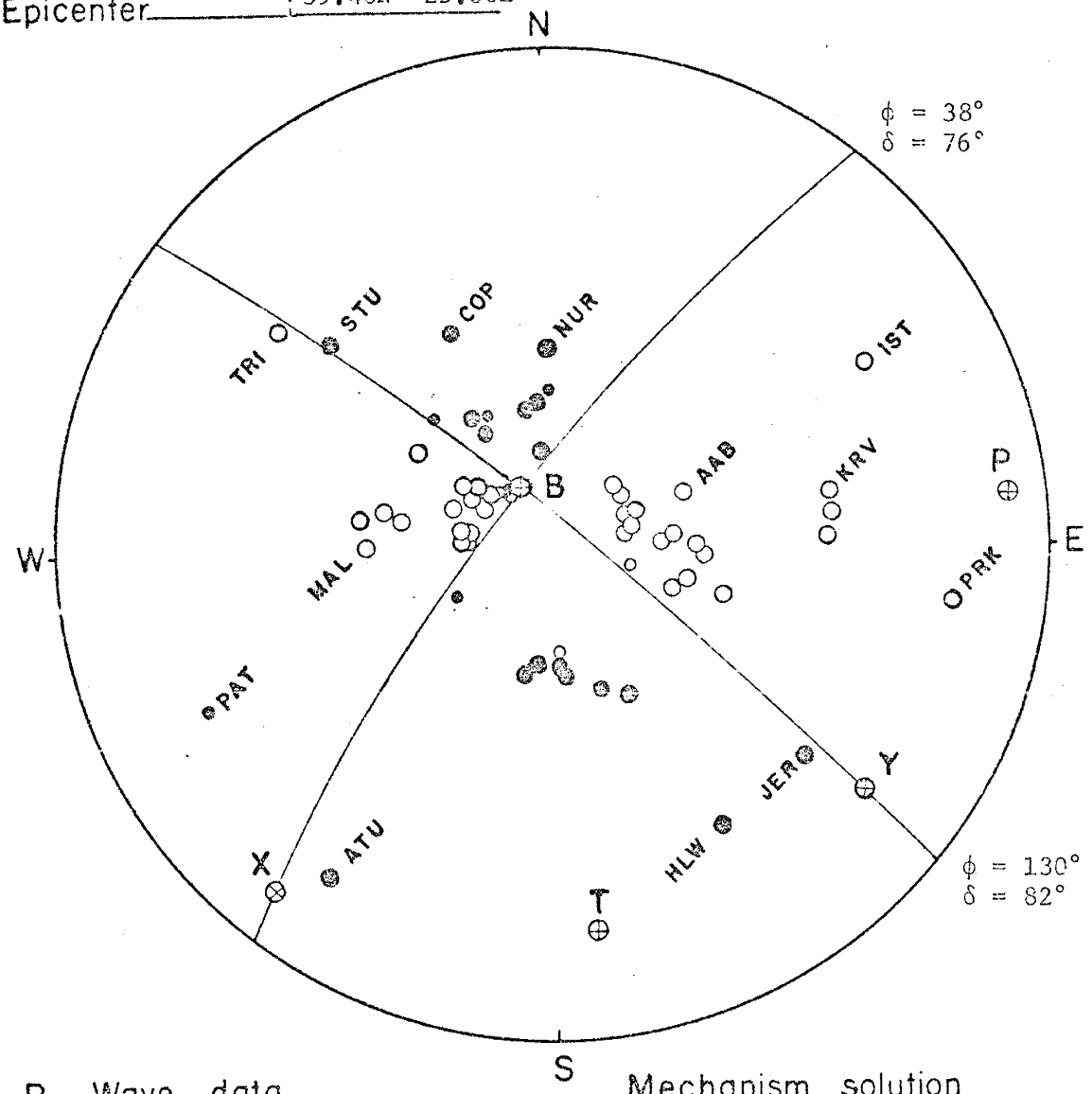

P Wave data

● Compression

o Dilatation

Mechanism solution

Axis	P	T	B	X	Y
AZ.	83	174	337	220	128
Plunge	5	14	73	7	14

Figure 3.26 b. (See figure caption for Figure 3.26a).

Event No. : 10
Date : May 12, 1971
Origin time : 06:25:12.98 G.M.T.
Epicenter : 37.58N 29.75E

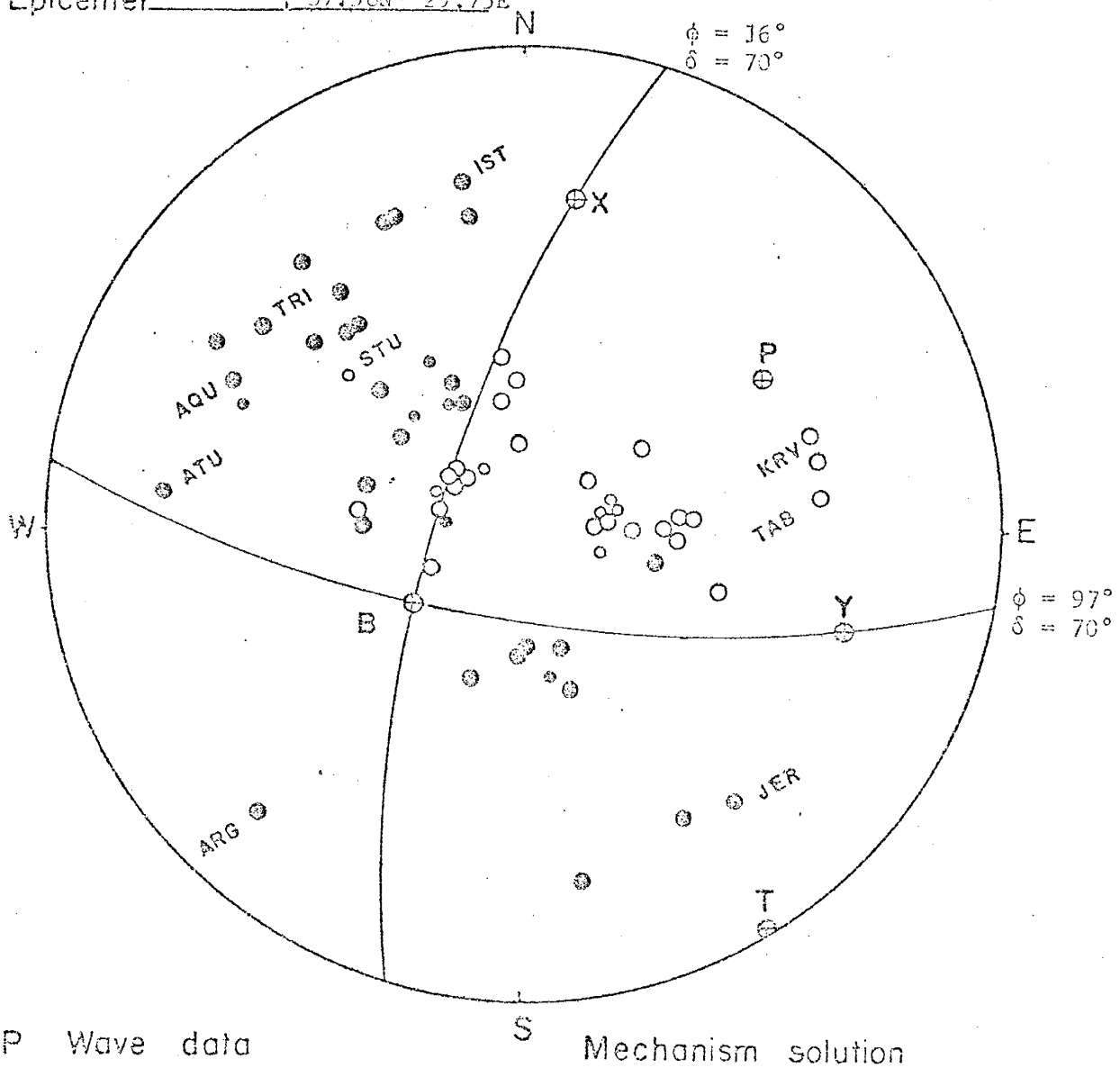

P Wave data

● Compression

○ Dilatation

Mechanism solution

Axis	P	T	B	X	Y
AZ.	57	140	237	9	107
Plunge	28	1	60	30	20

Figure 3.27a. Fault-plane solutions indicating the effect of P wave velocity on a strike-slip solution. P wave velocities of 6.6 km/sec and 7.5 km/sec were used in the projections for the diagrams (a) and (b), respectively.

Event No. : 10
Date : May 12, 1971
Origin time : 06:25:12.98 G.M.T.
Epicenter : 37.58N 29.75E

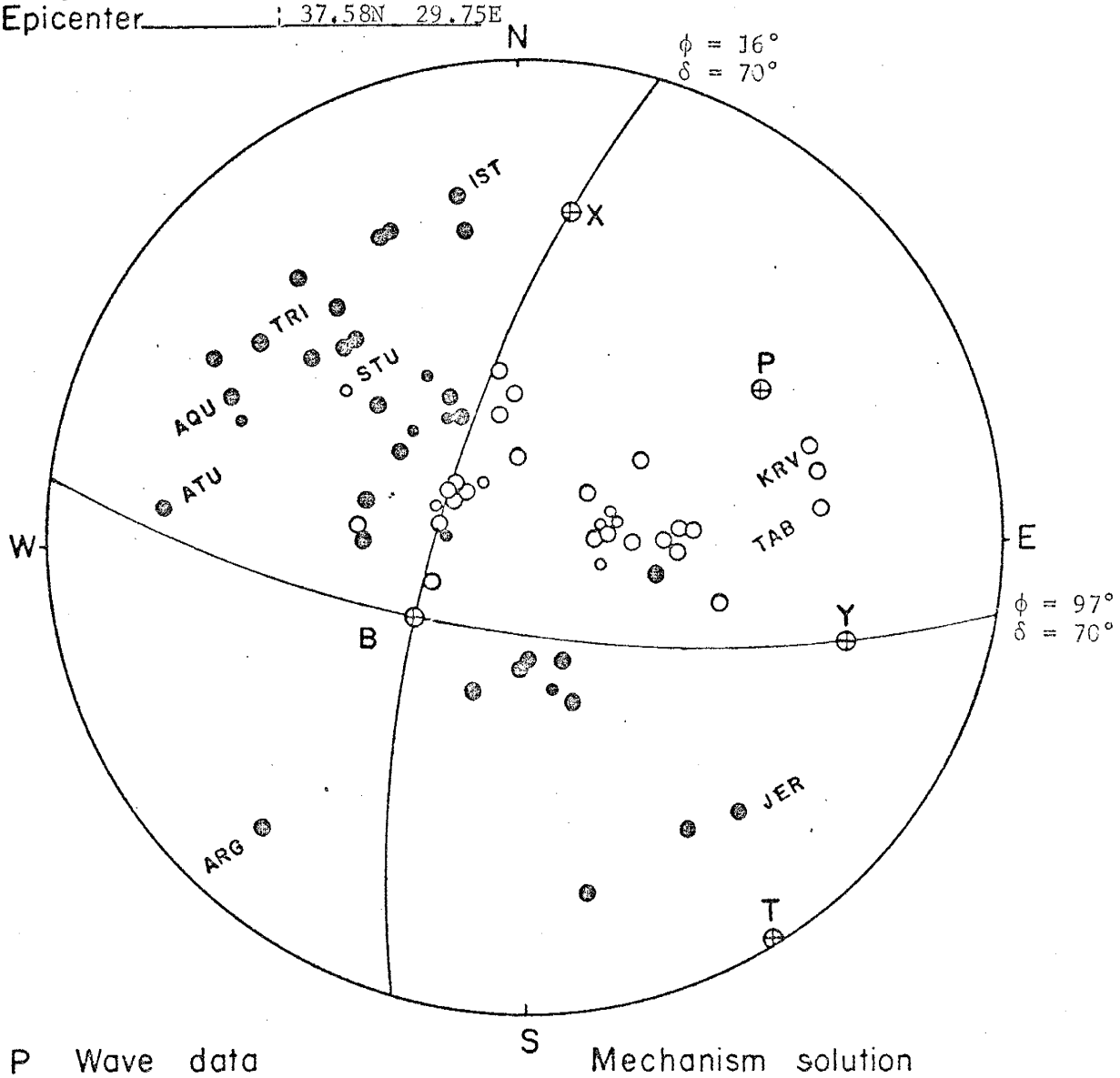

P Wave data

● Compression

○ Dilatation

Mechanism solution

Axis	P	T	B	X	Y
AZ.	57	149	237	9	107
Plunge	28	1	60	20	20

Figure 3.27b. (See figure caption for Figure 3.27a.)

Event No. : 2
Date : Jan. 14, 1969
Origin time : 23:12:07.88 G.M.T.
Epicenter : 36.17N 29.20E

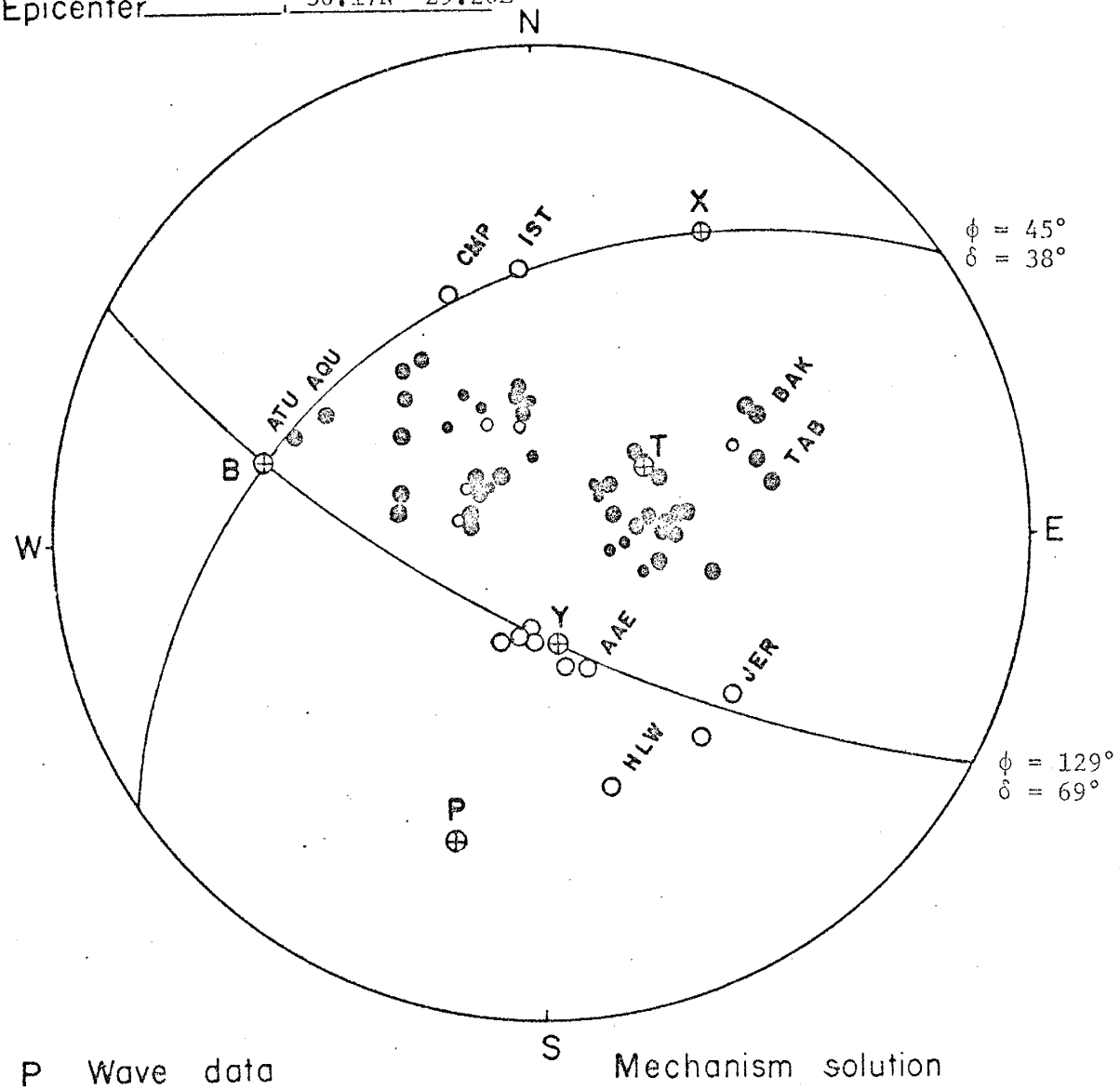

P Wave data

● Compression

○ Dilatation

Mechanism solution

Axis	P	T	B	X	Y
AZ.	196	57	286	29	170
Plunge	24	60	30	19	54

Figure 3.28a. Fault-plane solutions indicating the effect of P wave velocity on a reverse fault solution. P wave velocities of 6.6 km/sec and 7.5 km/sec were used in the projections for the diagrams (a) and (b) respectively. Notice the stronger component of dip-slip motion in (b).

Event No. : 2
Date : Jan. 14, 1969
Origin time : 23:12:07.88 G.M.T.
Epicenter : 36.17N 29.20E

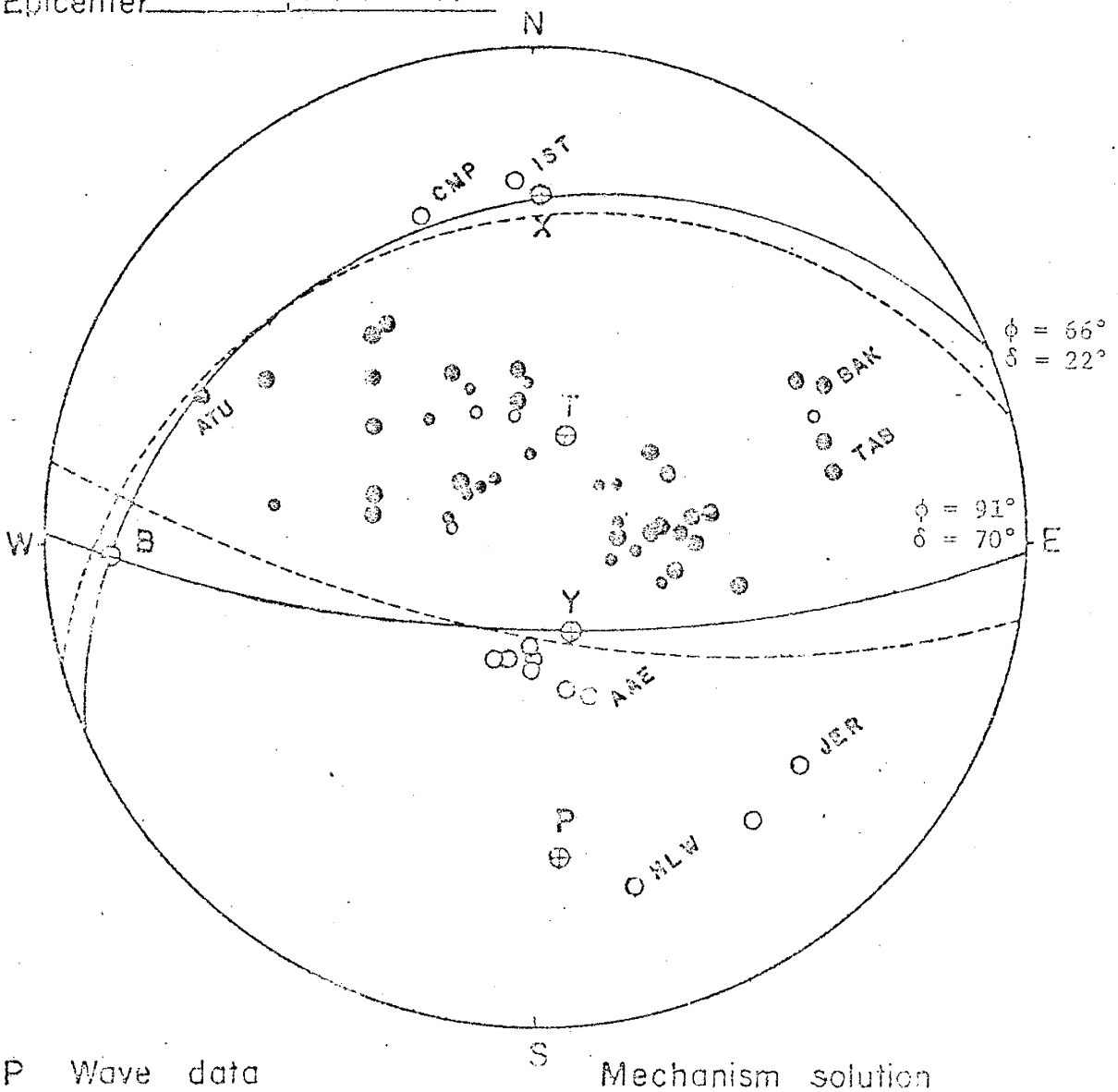

P Wave data

⊙ Compression

○ Dilatation

Mechanism solution

Axis	P	T	B	X	Y
AZ.	176	18	268	1	157
Plunge	25	64	9	19	63

Figure 3.28b. (See figure caption for Figure 3.28a.)

Event No. : 4
Date : March 28, 1969
Origin time : 01:48:30.4 G.M.T.
Epicenter : 35.58N 28.44E

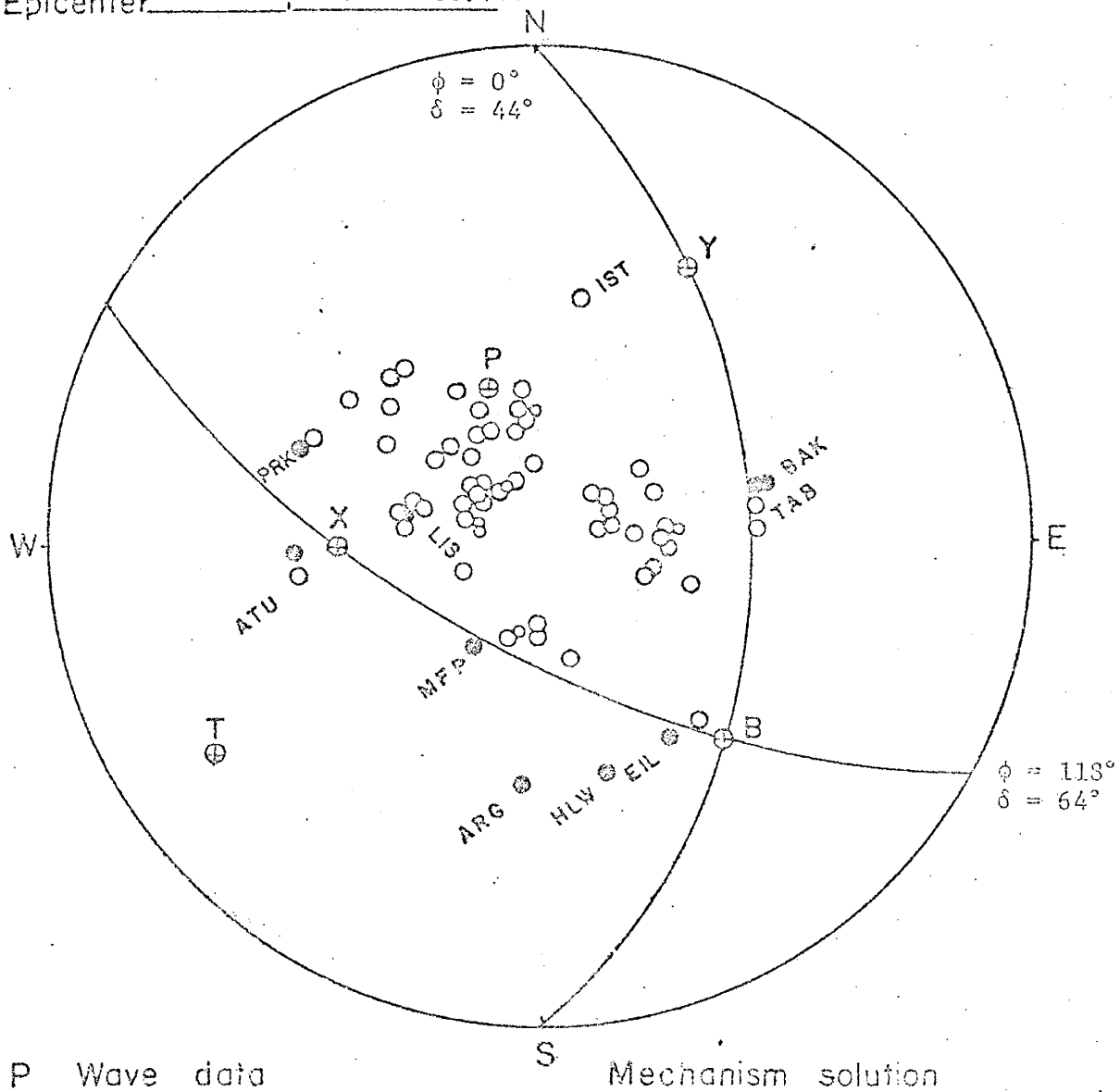

P Wave data

⊕ Compression

○ Dilatation

Mechanism solution

Axis	P	T	B	X	Y
AZ.	343	226	139	269	29
Plunge	54	13	32	46	25

Figure 3.29a. Fault-plane solutions indicating the effect of P wave velocity on a normal fault solution. P wave velocities of 6.6 km/sec and 7.5 km/sec were used in the projections for the diagrams (a) and (b) respectively. Notice the stronger component of dip-slip motion in (b).

Event No. : 4
Date : March 28, 1969
Origin time : 01:48:30.4 G.M.T.
Epicenter : 35.58N 28.44E

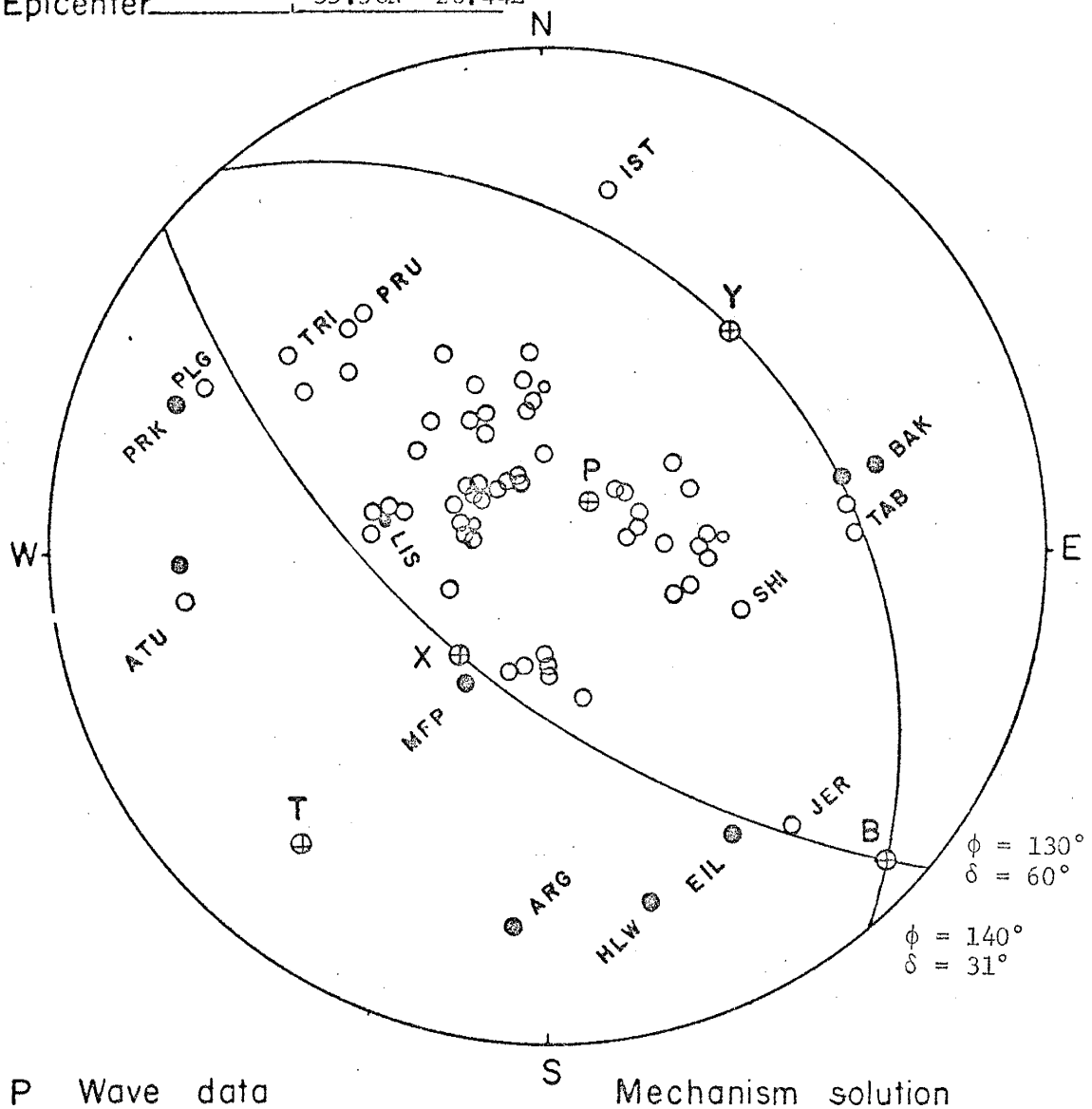

P Wave data

● Compression

○ Dilatation

Mechanism solution

Axis	P	T	B	X	Y
AZ.	38	220	133	219	40
Plunge	75	15	5	60	30

Figure 3.29b. (See figure caption for Figure 3.29a.)

Event No. : 7
Date : March 28, 1970
Origin time : 21:02:23.4 G.M.T.
Epicenter : 39.1°N 29.4°E

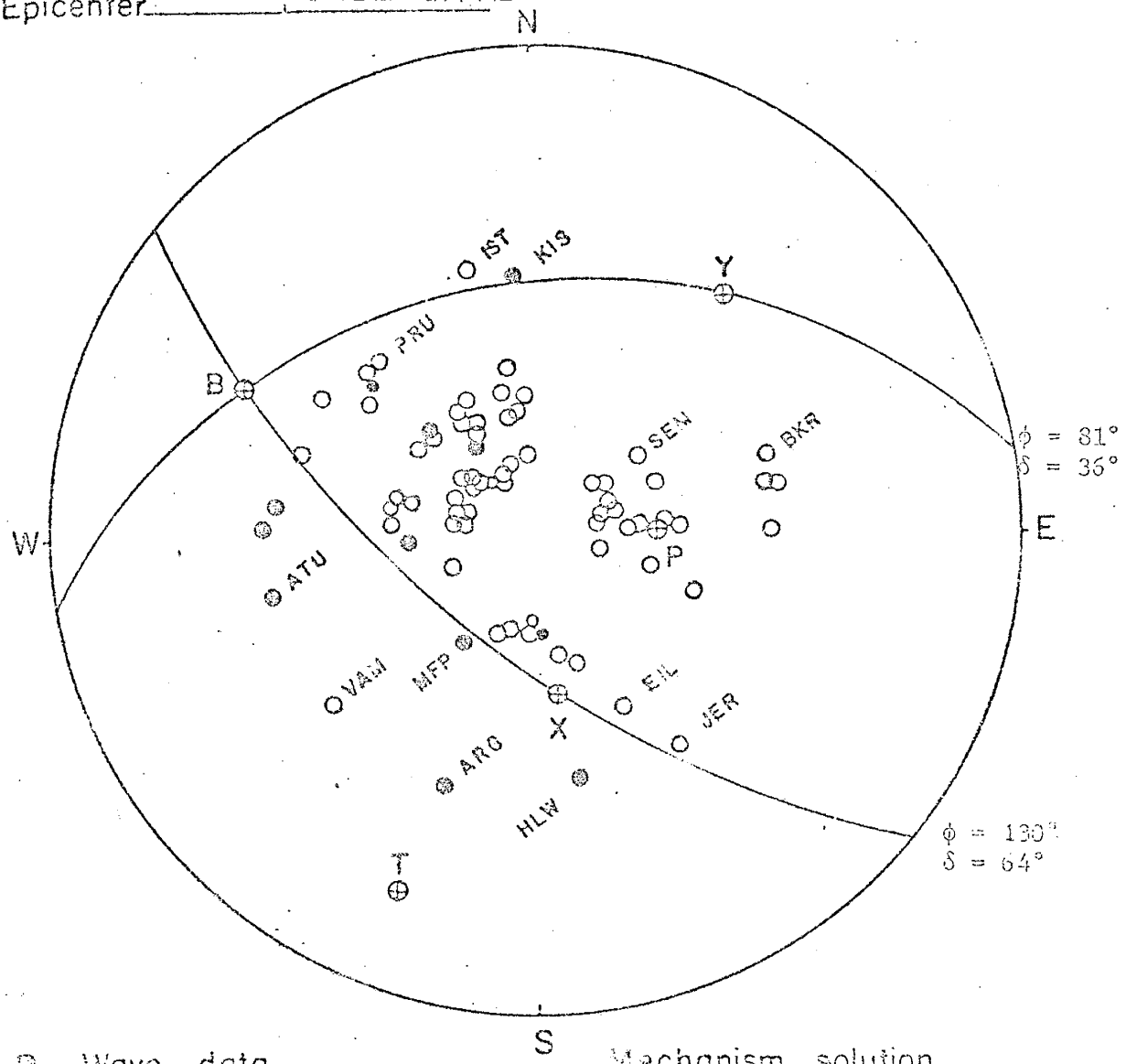

P Wave data

Compression

Dilatation

Mechanism solution

Axis	P	T	B	X	Y
A.Z.	90	200	297	174	40
Plunge	62	13	23	53	26

Figure 3.30a. Fault-plane solutions illustrating the effect of P wave velocity on a normal fault solution. P wave velocities of 6.6 km/sec and 7.5 km/sec were used in the projections for the diagrams (a) and (b) respectively. Notice the stronger component of dip-slip motion in (b).

Event No. : 7
Date : March 28, 1970
Origin time : 21:02:23.4 G.M.T.
Epicenter : 39.18N 29.48E

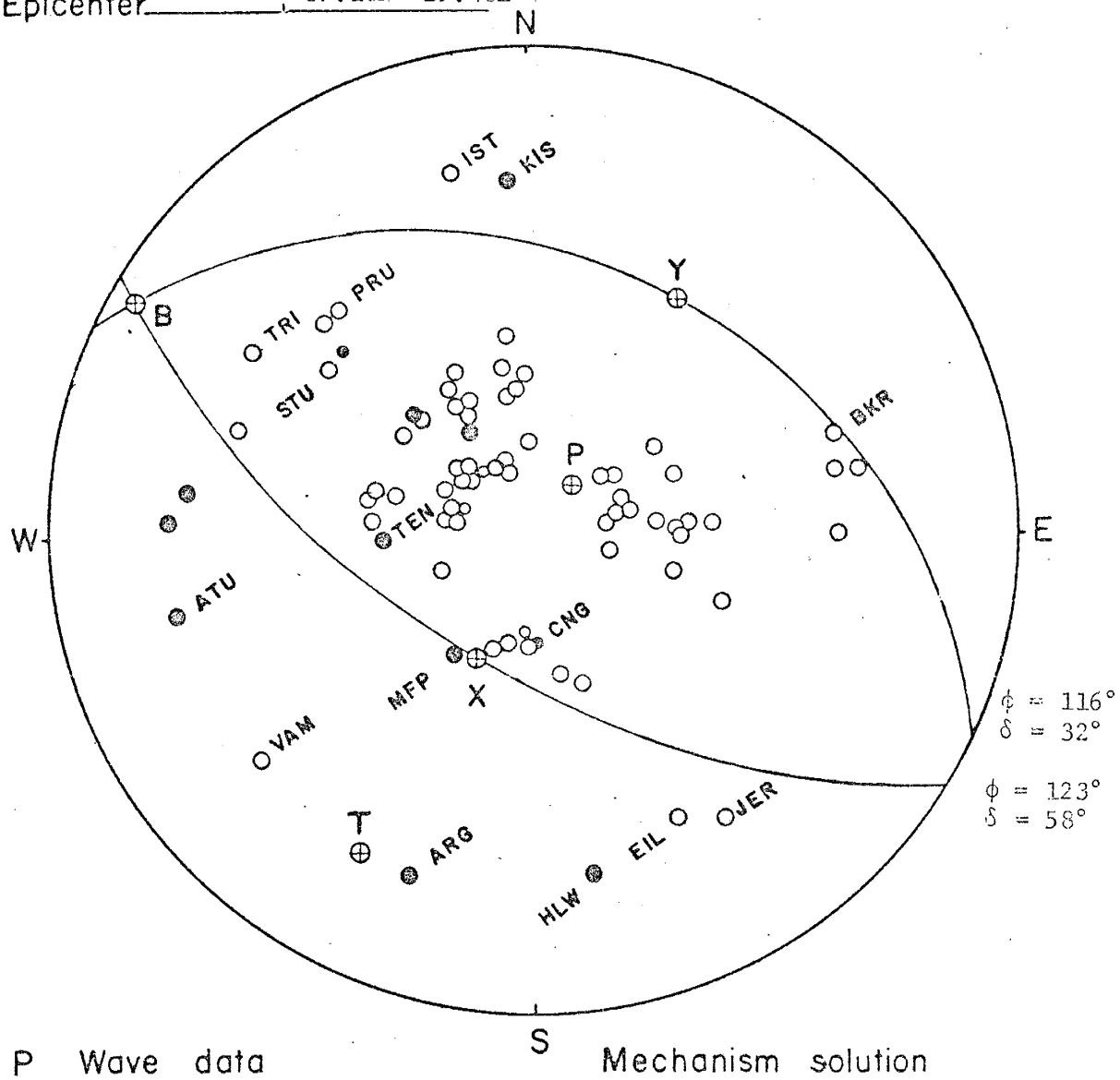

P Wave data

● Compression

○ Dilatation

Mechanism solution

Axis	P	T	B	X	Y
AZ.	42	208	301	204	32
Plunge	76	15	3	57	31

Figure 3.30b. (See figure caption for Figure 3.30a.)

component of dip-slip motion in both normal and reverse fault solutions (see Figures 3.28, 3.29 and 3.30). However, small variations in velocity do not completely change the character of the solutions.

Shortcomings

Fault-plane solutions provide the average characteristics of displacements at the focus. Some details of the deformation within the focus are lost because only a small percentage of the focal sphere can be sampled by using the direct or refracted waves (Ritsema, 1967). Figure 3.31A is a cross-section of the earth showing the distance ranges that first motions from Pg, Pn, P and PKP waves can be used for rault-plane solutions. The PKP first motions can only be used for very strong shocks and do not affect the solution very much, because they always plot within a small area toward the center of the fault-plane diagram. The best station coverage is obtained for P waves. However this does not mean that the greatest information on fault movement can be obtained from P waves. Indeed the percentage of the focal sphere sampled by P waves is surprisingly small (~20%) as seen from Figure 3.31B which shows a vertical cross-section of a focal sphere located in the crust. Direct waves (Pg) on the other hand can sample a larger percentage of the focal sphere. However to incorporate first motions from the direct waves, a large number of stations within a small area around the epicenter would be necessary. This condition can rarely be satisfied.

The percentage of the focal sphere sampled could be increased to above 50 percent if first motions from both direct and refracted waves

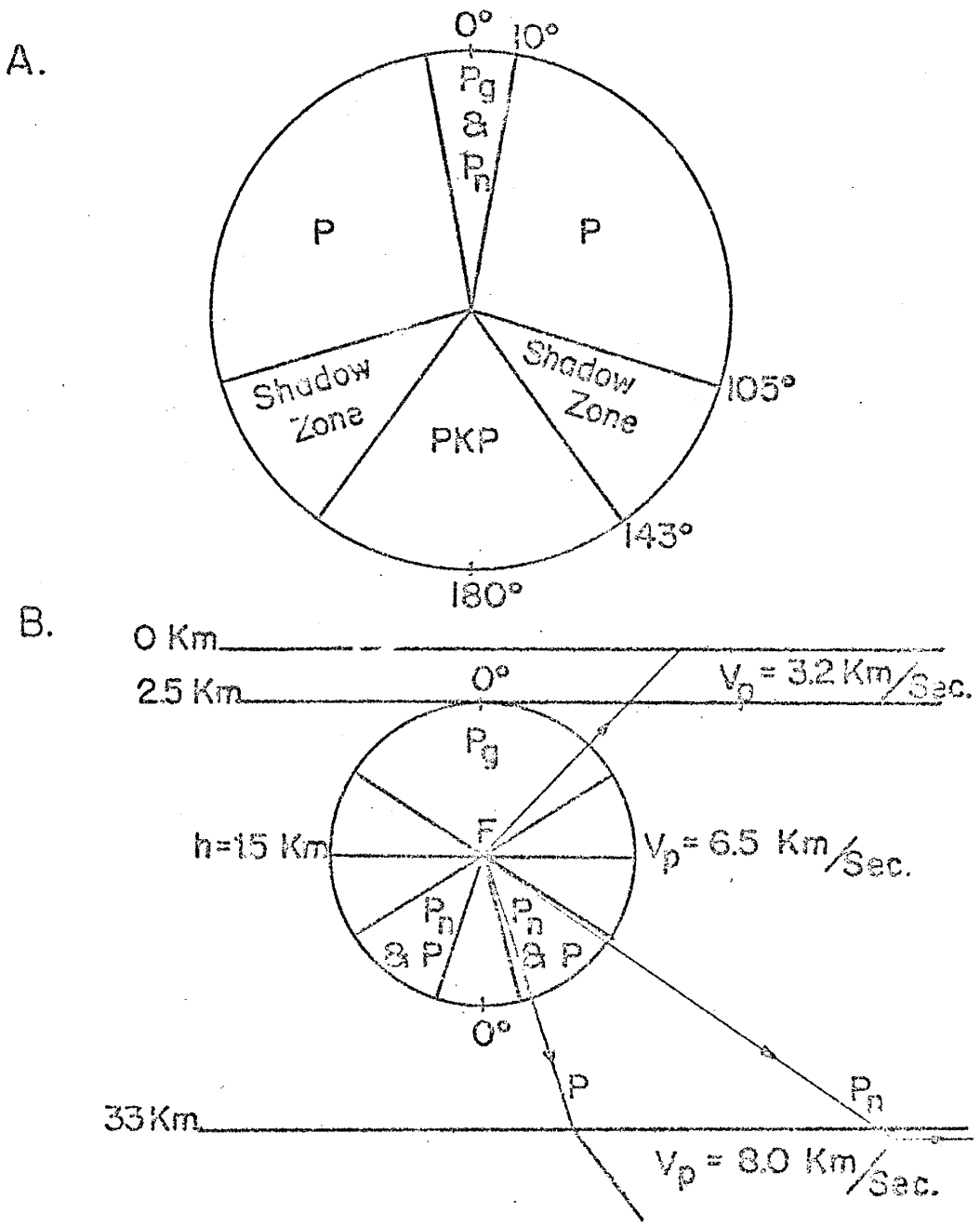

Figure 3.31.A. Cross-section of the earth indicating the distance ranges for different type of waves that can be used in first motion studies. B. Cross-section of a focal sphere, located in the crust, indicating the percentage of the focal sphere that can be sampled within a distance range of $\Delta = 0°$ to $\Delta = 100°$.

could be used together. However difficulties arise in projecting them on the focal sphere. A distinction between upgoing and downgoing waves is absolutely essential and therefore first motions from upgoing waves (first motions within the critical distance) must be projected on the upper focal hemisphere.

The most fundamental difficulty in interpreting the fault-plane solutions is the difficulty in selecting the fault-plane. An attempt has been made in this study to solve the ambiguity on the basis of several observational criteria cited earlier in this section. However, this choice cannot be made with certainty unless the earthquake has produced surface faulting or occurred on a known fault or produced a clear pattern of aftershocks. In the case of multiple fracturing arising from the primary shock and strong secondary shocks the use of surface faulting and aftershocks may be very difficult. This appears to be the case during the Gediz earthquake of March 28, 1970 (Earthquake # 7).

McKenzie and Parker (1967) suggested that plate tectonics could be used to solve the ambiguity in the case of strike-slip faulting. But in areas where plate motions are complex, this could be difficult and dangerous.

Summary and Conclusions to Fault-Plane Solutions

The fault-plane solutions discussed in the previous sections are summarized in Table 3.7. The wide variety of fault-plane solutions indicates complex crustal movements in the eastern Mediterranean and western Turkey. The northern boundary of the broad seismic zone in this region is represented by right-lateral strike-slip faulting. On the other hand the southern boundary is characterized by low-angle reverse and strike-slip faulting. Between these two regions, the fault-plane solutions obtained in this study provide clear evidence of normal faulting indicative of present vertical movements.

TABLE 3.7. Summary of Fault-Plane Solutions

No.	Date	Origin Time (G.M.T.)	Location ϕ_N	Location λ_E	Fault-plane Strike	Fault-plane Dip	Auxillary plane Strike	Auxillary plane Dip	Type of Faulting
1	Feb.19,1968	22:45:41.2	39°.4	25°.0	N40°E	80°NW	S49°E	86°NE	Strike-slip
2	Jan.14,1969	23:12:07.9	36°.2	29°.2	N66°E	22°NW	S89°E	70°S	Thrust
3	Mar.23,1969	21:08:42.6	39°.2	28°.5	S71°E	58°NE	S26°E	42°SW	Normal
4	Mar.28,1969	01:48:30.4	38°.6	28°.5	S62°E	64°SW	S00°E	44°E	Normal
5	Apr. 6, 1969	03:49:33.5	38°.5	26°.4	S79°E	66°N	N41°E	40°SE	Normal
6	June 12,1969	15:13:31.1	34°.4	25°.0	N54°E	18°NW	N76°E	74°SE	Thrust
7	Mar.28,1970	21:02:23.4	39°.2	29°.5	S50°E	64°SW	N81°E	36°N	Normal
8	Apr.19,1970	13:29:36.3	39°.0	29°.8	S83°E	70°N	S21°E	36°SW	Normal
9	Apr.19,1970	13:47:35.2	39°.0	29°.8	S75°E	66°N	S25°E	34°SW	Normal
10	May 12,1971	06:25:13.0	37°.6	29°.8	N27°E	66°NW	S71°E	72°SW	Strike-slip

4. EARTHQUAKE MECHANISMS AND ACTIVE TECTONICS

Introduction

In this section, the earthquake mechanisms, seismicity, and available geologic information in Turkey and the eastern Mediterranean are used to explain the active tectonics of the region. Fault-plane solutions published by Canitez and Ucer (1967), Papazachos and Delibasis (1969) Nowroozi (1972), and Canitez and Toksoz (1971) are used in addition to the solutions obtained in this study.

Recently McKenzie (1972b) published fault-plane solutions for the Mediterranean region from 15°W to 60°E. Unfortunately his paper appeared toward the final stages of the present work and a direct comparison of fault-plane solutions published by him and those obtained in this study could not be made. However, the fault-plane solutions determined in this study are based on more data and thus have greater control than those presented by McKenzie. Also the main conclusions arrived in this study are somewhat different from the conclusions of McKenzie (1970 and 1972b). These differences are pointed out at appropriate places in this section.

Earthquake Mechanisms

Selected fault-plane solutions for Turkey and the neighboring areas in the eastern Mediterranean are shown in Figure 4.1. The main criteria in selecting these solutions was the number of observations that were used in the solutions. The numbers in the figure refer to the earthquakes listed in Table 4.1. The P, T, and B axes for the fault-plane solutions are also listed in this table. The last column gives the

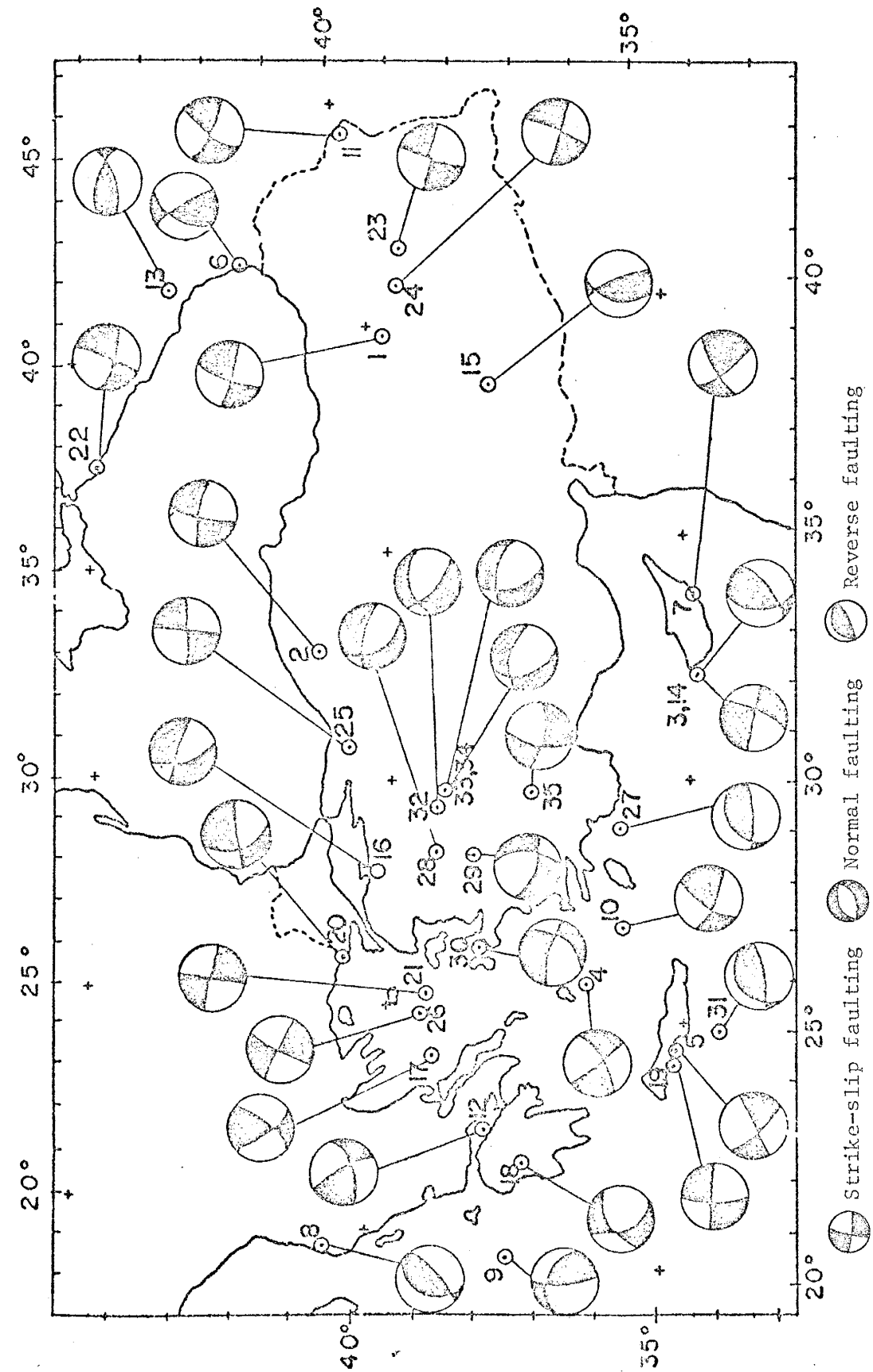

Figure 4.1. Mechanisms of earthquakes in Turkey and neighboring areas. Dark areas represent compressional regions and numbers indicate the earthquakes listed in Table 4.1.

TABLE 4.1. Summary of Focal Mechanisms of Earthquakes in Eastern Mediterranean and Turkey.

No.	Date	Time (GMT)	Epicenter ϕ°N	Epicenter λ°E	M	h	P Str.	P Plg.	T Str.	T Plg.	B Str.	B Plg.	Reference*
1	Dec.26,1939	23:57:16	39.7	39.7	8.1	S	158	17	61	22	280	62	1 (43)
2	Sept.7,1953	03:58:58	41.2	32.8	6.2	S	142	27	51	2	317	62	1 (36)
3	Sept.10,1953	04:06:00	34.9	32.2	6.2	S	249	12	347	24	135	63	1 (42)
4	July 9,1956	03:11:40	36.7	25.8	7.5	S	21	25	284	15	166	60	2 (104)
5	May 14,1959	16:36:56	35.1	24.6	6.5	S	6	3	98	41	272	48	2 (58)
6	May 20,1959	19:49:13	41.8	41.9	5.7	S	66	22	183	32	330	32	1 (30)
7	Sept.15,1961	01:46:09	34.9	33.8	6.0	S	205	11	99	53	302	35	1 (45)
8	Mar.18,1962	15:30:33	40.6	19.5	6.2	S	134	22	5	61	236	20	2 (41)
9	Apr.10,1962	21:37:13	37.6	20.1	6.3	S	240	22	121	51	346	30	2 (24)
10	Apr.28,1962	11:18:53	36.1	27.0	6.0	S	165	6	71	41	261	49	2 (28)
11	Sept.4,1962	22:59:19	39.9	44.2	5.8	S	178	13	83	21	298	66	1 (36)
12	Oct. 4,1962	19:46:10	38.1	22.6	5.2	S	29	8	289	55	125	35	2 (16)
13	July 16,1963	18:27:18	43.1	41.4	6.8	S	175	14	312	71	82	13	1 (67)
14	Sept.12,1963	08:18:58	34.9	32.2	5.6	S	129	19	356	64	225	17	1 (31)
15	June 14,1964	12:15:31	38.0	38.5	5.8	S	210	67	69	17	335	13	1 (59)
16	Oct. 6,1964	14:31:20	40.2	28.1	7.1	S	144	63	41	6	308	27	1 (72)

TABLE 4.1 Continued

No.	Date	Time (GMT)	Epicenter ϕ° N	Epicenter λ° E	M	h	P Str.	P Plg.	T Str.	T Plg.	B Str.	B Plg.	Reference
17	Mar. 9,1965	17:57:53	39.1	24.0	6.3	S	281	2	13	32	189	58	2 (57)
18	Apr. 5,1965	03:12:55	37.4	21.9	6.2	S	101	20	205	36	347	49	2 (38)
19	Apr. 9,1965	23:57:03	35.1	24.3	6.5	S	141	31	37	22	278	51	1 (51)
20	Aug.23,1965	14:08:59	40.7	26.1	5.2	S	140	39	19	31	264	27	3 (36)
21	Nov. 2,1965	03:27:12	39.3	25.5	5.6	S	53	5	145	9	297	81	2 (17)
22	July 12,1966	18:53:10	44.6	37.4	5.9	26	328	12	64	30	218	58	4 (19)
23	Aug.19,1966	12:22:09	39.2	41.7	6.1	26	151	13	240	0	326	76	4 (20)
24	Aug.20,1966	11:59:12	39.3	40.9	5.4	37	329	16	238	2	148	73	4 (17)
25	July 22,1967	16:56:53	40.7	30.8	6.0	4	139	0	45	0	0	90	4 (26)
26	Feb.19,1968	22:45:41	39.4	25.0	7.1	7	85	6	176	10	333	80	5 (73)
27	Jan.14,1969	23:12:08	36.2	29.2	6.0	50	176	25	18	64	268	9	5 (63)
28	Mar.23,1969	21:08:43	39.2	28.5	5.6	12	148	64	37	21	297	25	5 (74)
29	Mar.28,1969	01:48:30	38.6	28.5	6.4	9	343	54	236	13	139	32	5 (79)
30	Apr. 6,1969	03:49:33	38.5	26.4	5.5	14	227	62	339	11	86	30	5 (66)
31	June 12,1969	15:13:31	34.4	25.0	5.8	25	161	28	359	61	254	6	5 (72)
32	Mar.28,1970	21:02:23	39.2	29.5	7.1	20	90	62	200	13	297	23	5 (91)

TABLE 4.1. Continued

No.	Date	Time (GMT)	Epicenter ϕ°N	Epicenter λ°E	M	h	P Str.	P Plg.	T Str.	T Plg.	B Str.	B Plg.	Reference
33	Apr.19,1970	13:29:36	39.0	29.8	5.6	20	145	55	30	17	290	28	5 (69)
34	Apr.19,1970	13:47:35	39.0	29.8	5.5	26	156	60	34	17	296	22	5 (58)
35	May 12,1971	06:25:13	37.6	29.8	5.9	23	66	29	159	5	255	59	5 (73)

1 Canitez and Ucer (1967)

2 Papazachos and Delibasis (1969)

3 Canitez and Toksoz (1971)

4 Nowroozi (1972)

5 Solutions determined in this study (see section 3).

* Numbers in parentheses indicate the total number of observations.

reference, and the number of observations used in the solutions. Because the original first motion data were not available (except for the solutions obtained from Canitez and Toksoz (1971) and Nowroozi (1972)) solutions shown in Figure 4.1 were obtained by plotting the published P, T, and B axes on the Wulff stereonet.

The large variety of solutions in Figure 4.1 indicates that every kind of faulting occurs in this region. However, the directions of motion and the orientations of fault-planes are not random in each sub-region. Strike directions of fault planes are generally parallel to the local trends of the seismic zones and the geologic structures (compare Figures 4.1, 2.3, and 2.2). An examination of fault-plane solutions and the tectonic lines indicated that displacements at the focus are either parallel or perpendicular to the strike of geologic structures. This behavior of displacements at the focus has been found for other regions of the Alpide seismic belt (Keilis-Borok, et al., 1960).

Fault-plane solutions presented in Figure 4.1 represent the tectonic character of the following sub-regions: Caucasus, southeastern Turkey, north Anatolian fault, western Turkey, northern Aegean, Aegean and the Cyprian arcs. The seismicity and geology of these regions, except the Caucasus, were discussed in section 2. Seismicity of the Caucasus is discussed below in connection with the sub-regional discussion of earthquake mechanisms for the area of study.

Nowroozi (1971) studied the seismicity of the Caucasus region. He recognized three transverse seismic zones within the general NW-SE trend of regional seismicity. He pointed out that these variations in the trend may be indicative of recent changes in the tectonic regime of the region. The most apparent transverse zone is the Abul-Samsar zone (Nowroozi, 1971)

which may be connected to the seismic zone of southeastern Turkey (Figure 2.3). However this relation is not very clear from present seismicity and the earthquake mechanisms. Fault-plane solutions in the Caucasus (6, 13, and 22) generally indicate thrust faulting , indicative of crustal shortening. Solution 22 may seem not to confirm this statement, however McKenzie (1972b) published a new solution for the same shock, and his solution indicated pure dip-slip motion. Shirokova (1962) also has found dominantly thrust fault solutions in the Caucasus region.

There is one thrust-fault solution of poor quality (15) for the southeastern Turkey. This solution is not compatible with the left-lateral motions suggested from the history of plate bordering faults.

Focal mechanism solutions 1, 2, 23, 24 and 25 are associated with the north Anatolian fault. All of these solutions indicate pure right-lateral strike-slip motion and are in complete accord with the ground offsets associated with them (Ketin and Roesli, 1953; Ambraseys and Zatopek, 1968 and 1969; Wallace, 1968). Solution 1 is the fault-plane solution for the earthquake of Dec. 26, 1939. This earthquake is the strongest shallow focus shock (M = 8.0) to have occurred in the Mediterranean region (Karnik, 1971) and marks the beginning of westward migration of earthquakes along the north Anatolian fault zone. Solutions 23 and 24 are the fault-plane solutions for the Varto earthquake of April 19, 1966, and one of its aftershocks. These solutions indicate that right-lateral motions continue toward Iran.

The western continuation of north Anatolian fault appears to be complex. Both strike-slip and normal fault solutions are found in northwestern Turkey and the northern Aegean Sea. McKenzie (1972b) found

normal and thrust fault solutions in Greece. Strike-slip solutions (21, 26) in the northern Aegean Sea indicate the continuation of right-lateral motions in the west. Notice that fault planes along the north Anatolian fault and the northern Aegean gradually change their strikes from approximately S 80°E in the east, to N 30°E in the west.

All fault-plane solutions in western Turkey represent normal faulting, indicative of crustal extension. However, normal faulting does not extend southward beyond the epicenter of May 12, 1971, shock (35). Fault planes for the earthquakes in western Turkey have been selected on the basis of several criteria discussed in section 3 (see individual discussion of fault-plane solutions). All solutions indicate that fault planes are aligned parallel to the trend of structures, and that a small horizontal component of motion has occurred. However the directions of these horizontal motions do not show any regularity.

Fault-plane solutions along the Aegean and the Cyprian arcs indicate low-angle thrust faulting which is compatible with the idea that the Mediterranean sea floor is underthrusting the Aegean Sea and western Turkey. Strike-slip solutions like 3, 5 and 19 may be in error due to inappropriate velocities being used in these solutions. Solution 35 at the eastern termination of the Aegean arc is different from others and represents the motion along an arc-to-arc transform fault between the Aegean and Cyprian arcs.

Slip Vectors

Slip vectors, for the strike-slip solutions that a selection of fault-plane was made, are plotted in Figure 4.2. The length of the arrow in the figure is not the absolute value of slip but is proportional

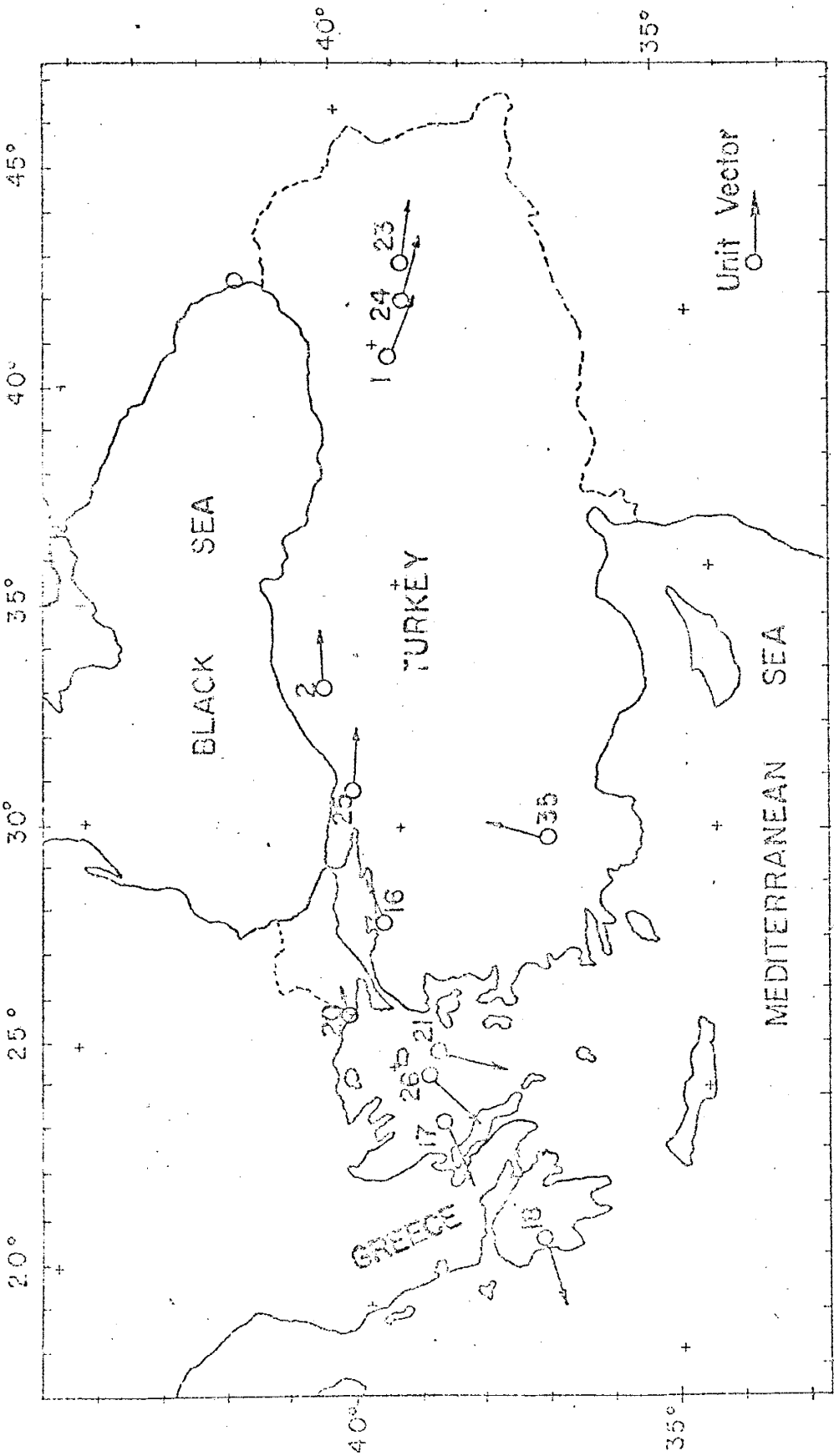

Figure 4.2. Horizontal component of slip vectors.

to the cosine of the angle between the slip vector and the horizontal. Slip vectors along the north Anatolian fault indicate that the relative motion between the north and south sides of the fault is right-lateral. Slip vectors in the northern Aegean indicate that the Aegean-Turkish block is moving toward the west with respect to Eurasia. A slip vector for earthquake 35 is compatible with motion along an arc-to-arc transform fault.

Directions of Principal Stresses

The compressional and the tensional axes are plotted in Figures 4.3 and 4.4. The lengths of the axes in these figures are proportional to the cosine of the angles which the axes make with the horizontal. Directions of principal stresses do not show any regularity if the whole region is considered. However, there is a preferred orientation in each sub-region. Tensional and compressional axes for strike-slip solutions are both horizontal as would be expected from Anderson's dynamic theory of faulting (Anderson, 1951). Compressional axes for the fault-plane solutions on the north Anatolian fault are almost perpendicular to the folds located in the northern side of the fault. This may suggest possible crustal shortening in this block (Nowroozi, 1972). For normal fault solutions found in western Turkey the compressional axes are nearly vertical and tensional axes are nearly horizontal. Tensional axes for these solutions are perpendicular to the strike of geologic structures. For thrust faulting or faulting having a strong component of thrusting as shown by the solutions for the Caucasus, the Aegean and the Cyprian arcs, the compressional axes are perpendicular to the trend of structures, and tensional axes are dipping steeply.

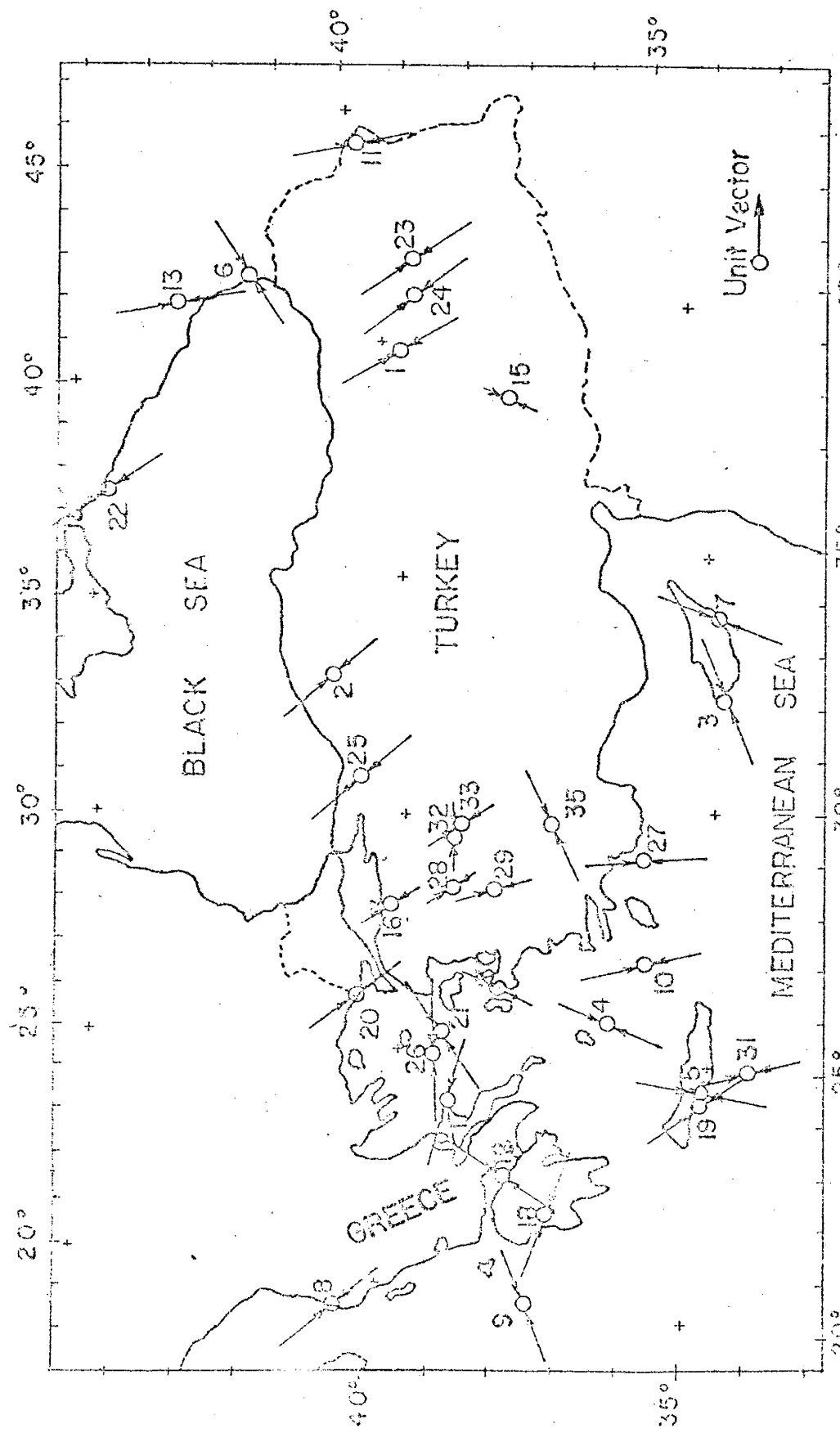

Figure 4.3. Horizontal component of the compressional axis.

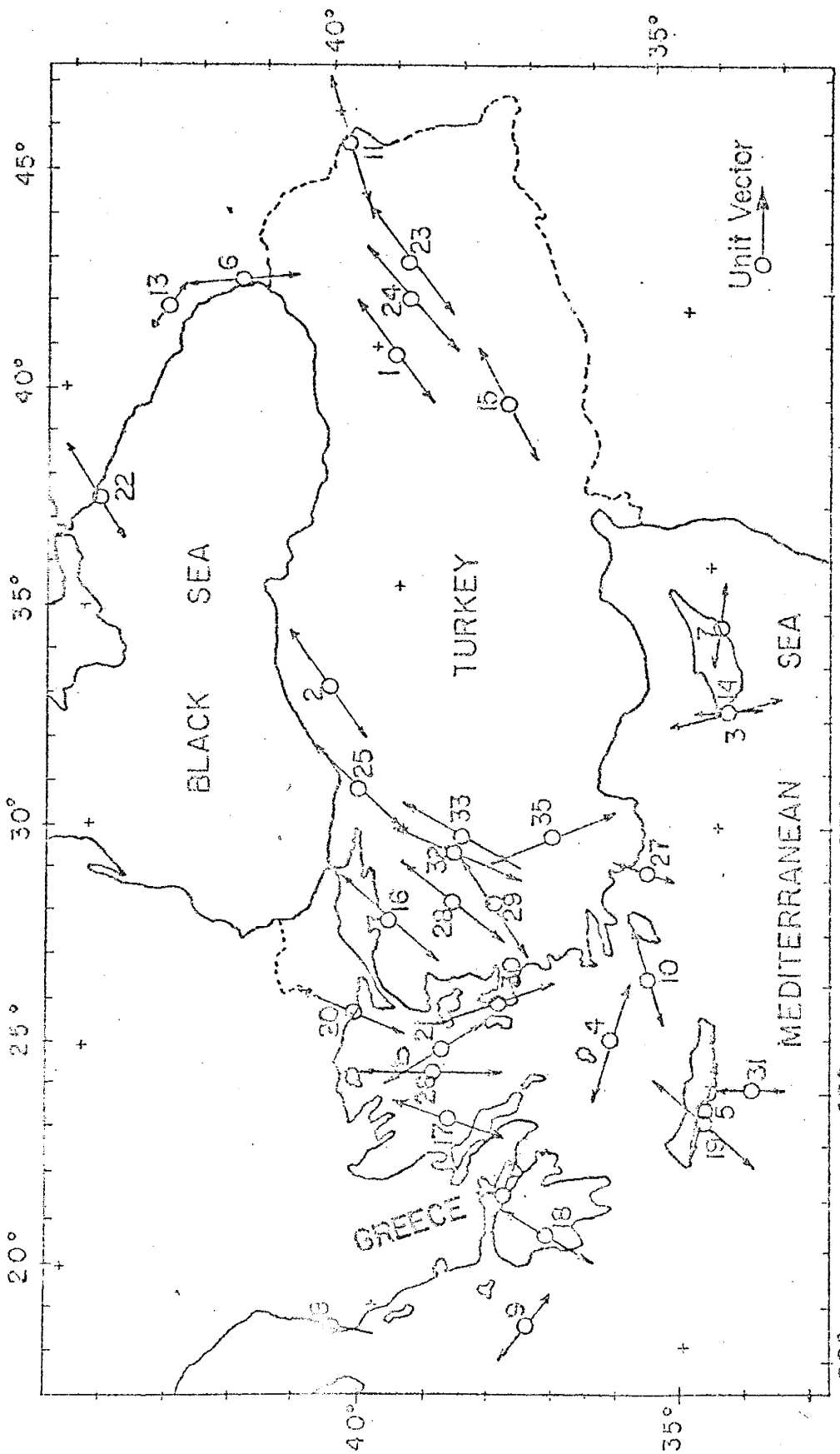

Figure 4.4. Horizontal component of the tensional axis.

A Model of Plate Tectonics

The basic concepts of plate tectonics were discussed in the introduction to the dissertation. Now its application to Turkey and the adjacent areas in the eastern Mediterranean is discussed.

Morgan (1968) and LePichon (1968) recognized three major plates of importance in the tectonics of the eastern Mediterranean. These are the now well recognized African, Arabian and the Eurasian plates. Morgan and LePichon considered the broad seismic belt in this region as the boundary between the African and the Eurasian plates. McKenzie (1970) more closely defined this boundary and introduced two small plates, namely the Aegean and the Turkish plates. Recently he further refined the position of the boundary between African and Eurasian plates and suggested a complex model for the eastern Mediterranean and Middle East (McKenzie, 1972b). His model is shown in Figure 4.5. The major difficulty with this model is the explanation for the seismicity and the earthquake mechanisms in western Turkey and the northern Aegean Sea. McKenzie suggested that horizontal motions between the Aegean and the Turkish plates are taken up in a broad zone of normal faulting in western Turkey. It is rather difficult to explain how the horizontal motions of two small plates can produce normal faulting inside such a broad zone without producing horizontal motions. Furthermore, McKenzie's model cannot explain the slow uplift of western Turkey (Arpat and Bingol, 1969)

McKenzie (1972b) admits that the northern boundary of the Aegean plate in his model is uncertain. According to the model the motion along this boundary is taken up on a series of parallel grabens connect-

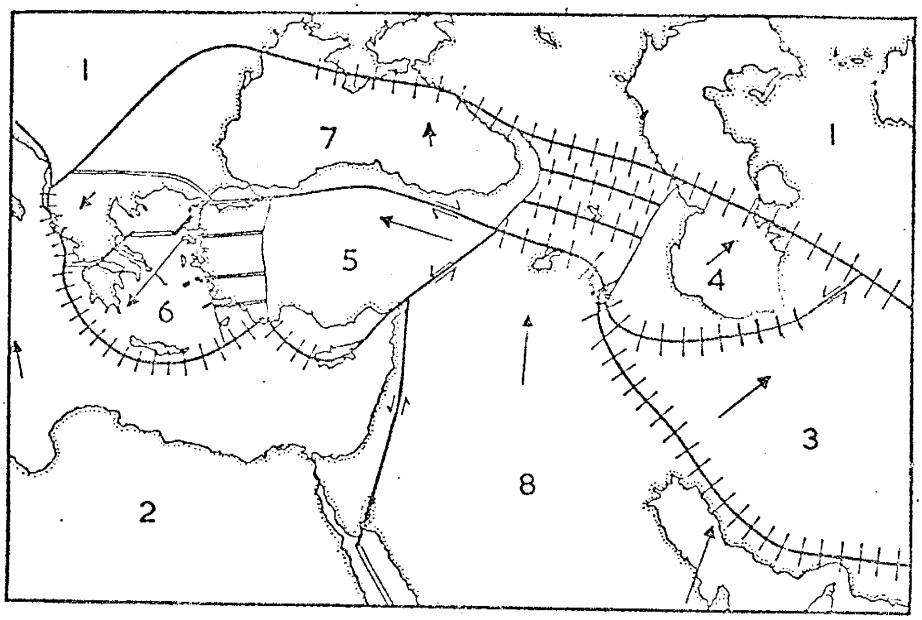

Figure 4.5. Plate tectonics model of McKenzie (1972b). Plate boundaries across which extension is occurring are shown by double line, transform faults by a single heavy line, and boundaries across which shortening is occurring by a solid line crossed by short lines. The numbers represent the following plates: 1 - Eurasian, 2 - African, 3 - Iranian, 4 - South Caspian, 5 - Turkish, 6 - Aegean, 7 - Black Sea, 8 - Arabian. Activity in western Turkey and Caucasus represent the general nature of deformation (After McKenzie, 1972b).

by strike-slip faults. Focal mechanisms of earthquakes do not clearly substantiate this idea. In addition, the thrust and the normal fault solutions found in Greece along this boundary (McKenzie, 1972b) are difficult to explain with this model. Also, the seismicity of the northern Aegean Sea indicates an offset near to the epicenter of February 19, 1968, earthquake where McKenzie (1972b) suggested a ridge (compare Figures 3.6 and 4.5). The continuation of strike-slip mechanism toward the north (strike-slip solution given by McKenzie (1972b) for April 11, 1964, shock) suggests that this offset could be related to a strike-slip fault striking approximately north-south.

A simpler plate tectonics model, based on the data presented earlier in this section, is shown in Figure 4.6. The principal plates involved in this model are the African, Arabian, Eurasian and the Aegean-Turkish plates. The Black Sea was considered by McKenzie (1972b) and Nowroozi (1972) as a single plate. However the northern and the western boundaries of this plate are not clearly defined from seismicity and the earthquake mechanisms, and only the eastern boundary is shown in Figure 4.6.

The relative motions of plates with respect to Eurasia are shown by arbitrarily scaled arrows in Figure 4.6. The African and the Arabian plates are moving northward and northeastward respectively. The Aegean and the Turkish plates of McKenzie (1970 and 1972b) are considered as a single plate moving westward as suggested from the slip vectors shown in Figure 4.2. The broad seismic zone of western Turkey is the result of deformation inside the Aegean-Turkish plate. Seismicity in this area is not directly related to the horizontal motions of plates but is associated with vertical movements inside the Aegean-Turkish plate. Relative motion between the Arabian and the Aegean-

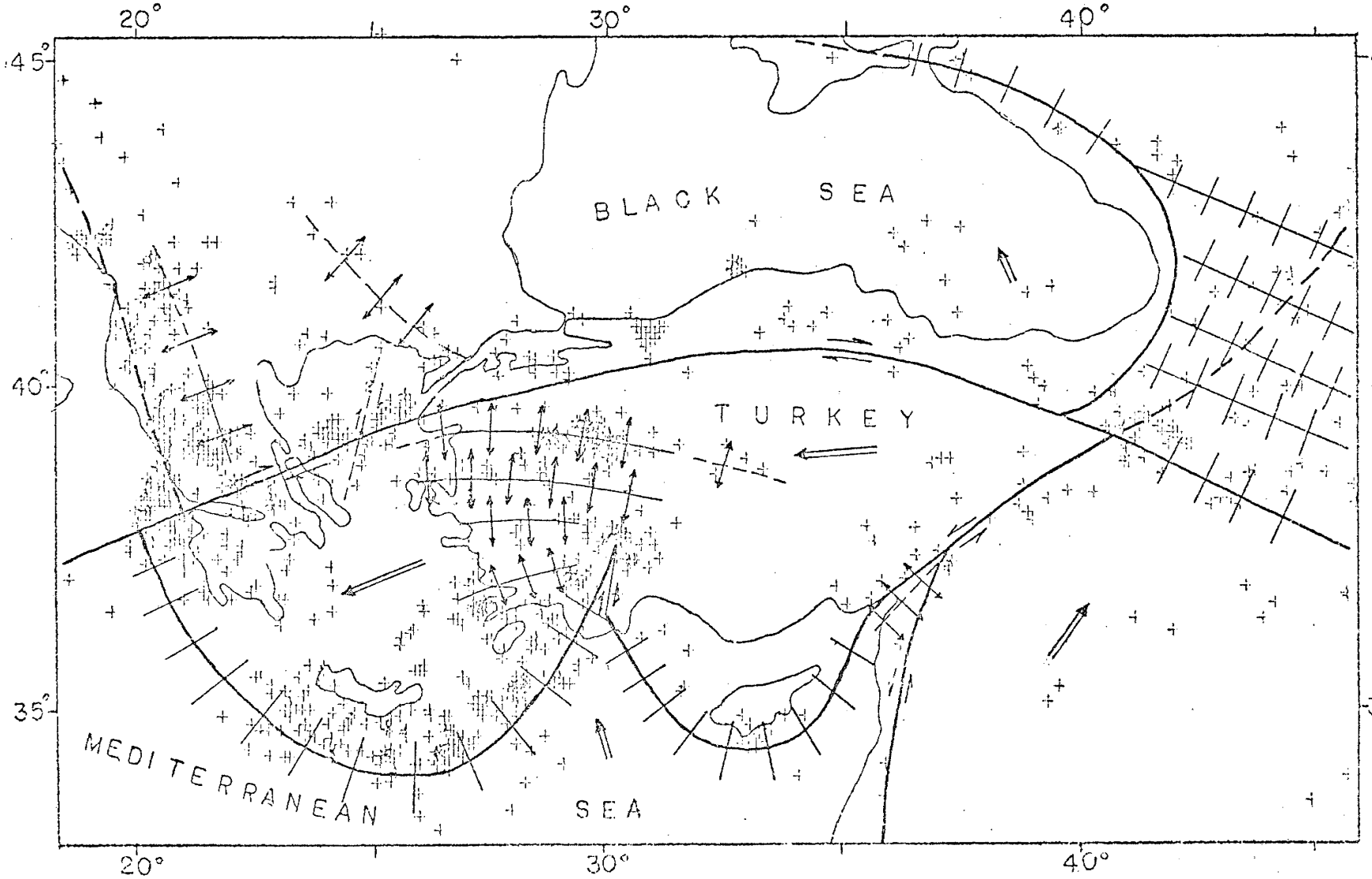

Figure 4.6. A plate tectonics model for Turkey and the neighboring areas in the eastern Mediterranean. Crosses represent the epicenters of shallow focus earthquakes. Lines crossed with diverging arrows indicate tensional features, others crossed with bars indicate compressional features.

Turkish plates produces a local tension in southeastern Turkey where the border faults and the Levant fracture zone intersect. The normal and thrust fault mechanisms found in the northern Aegean and Greece are probably related to uplifting caused by the underthrusting Mediterranean lithosphere.

The northern boundary of the Aegean-Turkish plate is the north Anatolian fault and its possible continuation in the Aegean Sea. Right-lateral motions along this boundary represent the relative motion between the Eurasian and the Aegean-Turkish plates. The eastern boundary of the Aegean-Turkish plate is defined by the border faults of southeastern Turkey. The southern boundary is defined by the Aegean and the Cyprian arcs. The Mediterranean lithosphere, which is a part of the African plate is underthrusting the Aegean-Turkish plate along this boundary. Among several geophysical evidences for the underthrusting are the presence of intermediate focus earthquakes (Figure 2.3b), negative free-air gravity anomalies (Rabinowitz and Ryan, 1970), volcanism on the concave sides of the arcs (Figure 2.3b), low heat-flow values in the eastern Mediterranean (Ryan, et al., 1970), low P_n velocities (Papazachos, et al., 1966) and the inefficient transmission of S_n waves (Molnar and Oliver, 1969), on the concave side of the Aegean arc.

The geometry of the underthrusting beneath the Aegean-Turkish plate is complex. Figures 4.8 to 4.14 show the projections of hypocenters on a vertical plane along several profiles drawn in Figure 4.7. The length and the width of the profiles vary from 400 km to 600 km, and 200 km to 300 km respectively. As can be inferred from these figures, the geometry of underthrusting in the western part of the Aegean arc is different than the eastern part. Vertical sections suggest an average dip of 30° in the

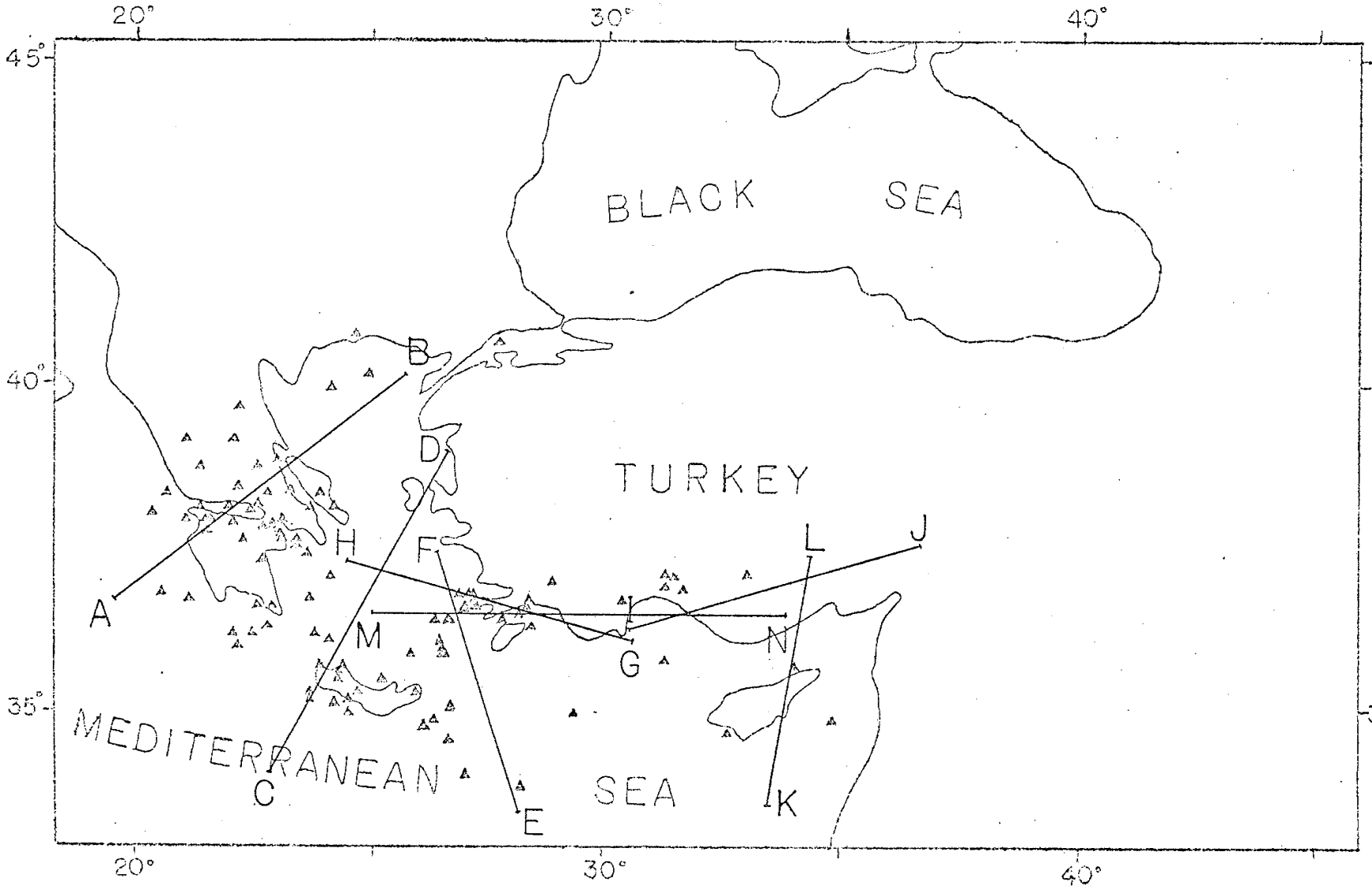

Figure 4.7. Locations of profiles along which the hypocenters are projected on a vertical plane. Triangular symbols represent the epicenters for intermediate focus (h > 70 km) earthquakes.

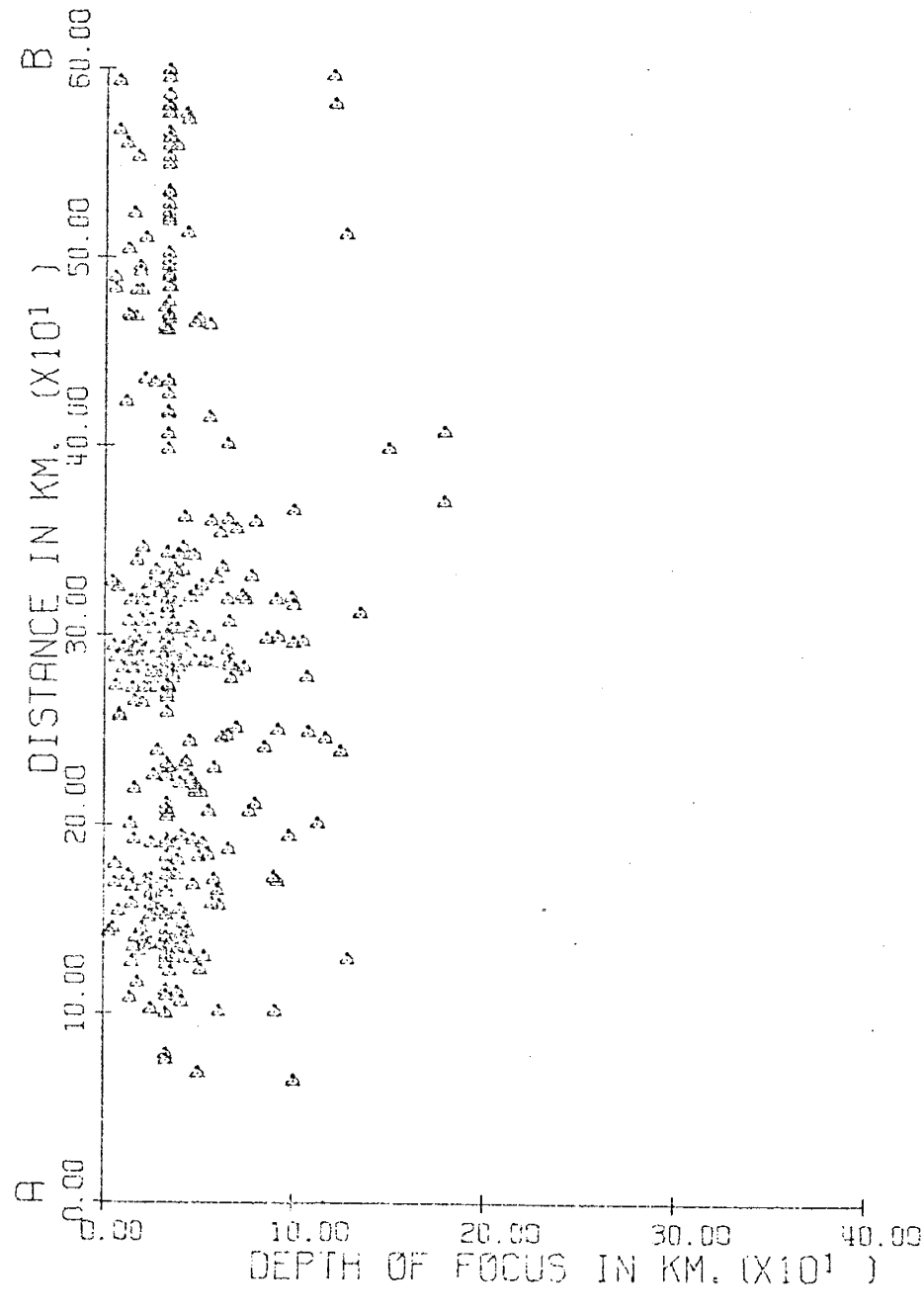

Figure 4.8. PROJECTION OF HYPOCENTERS ON A VERTICAL PLANE ALONG THE PROFILE AB. ALL HYPOCENTERS WITHIN A 150 KM. PERPENDICULAR DISTANCE FROM THE PLANE WERE PROJECTED.

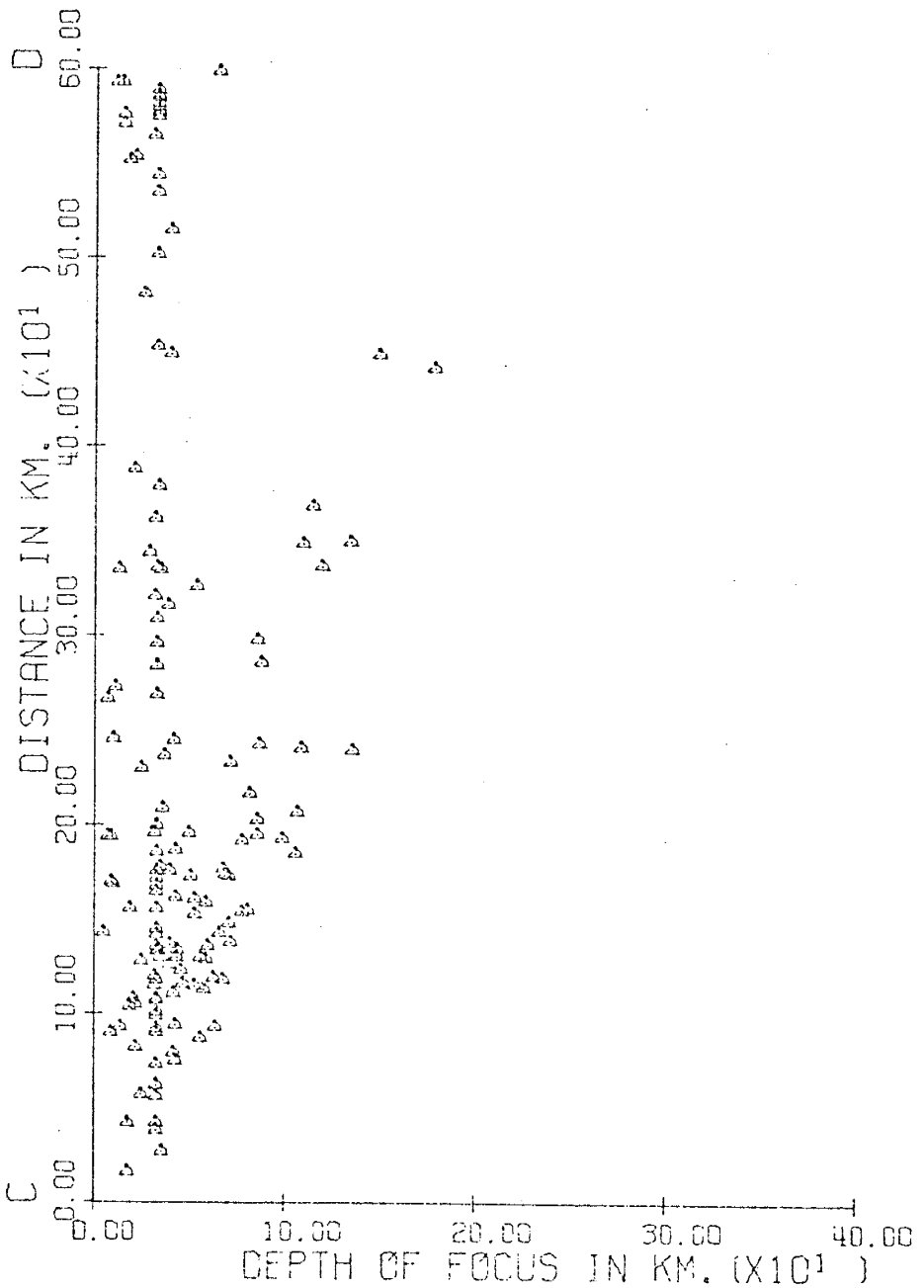

Figure 4.9. PROJECTION OF HYPOCENTERS ON A VERTICAL PLANE ALONG THE PROFILE CD. ALL HYPOCENTERS WITHIN A 150 KM. PERPENDICULAR DISTANCE FROM THE PLANE WERE PROJECTED.

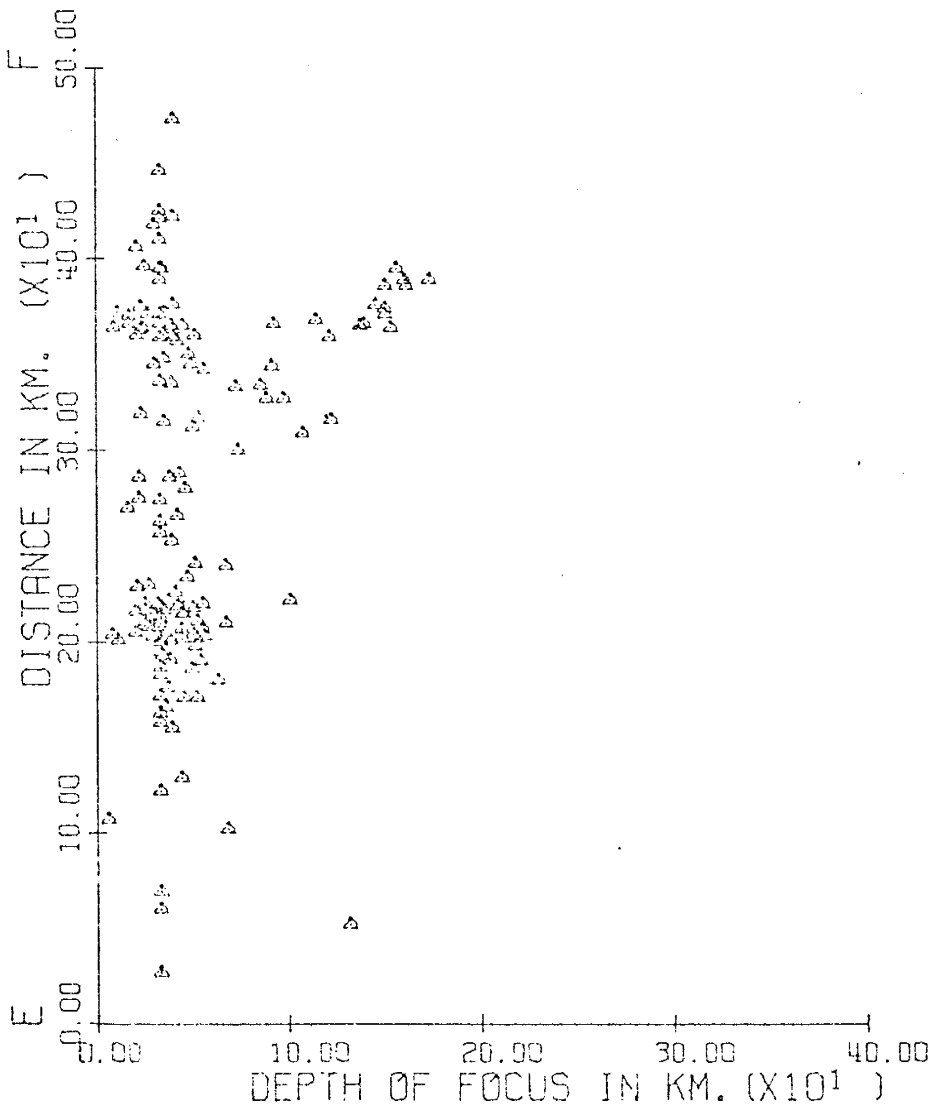

Figure 4.10. PROJECTION OF HYPOCENTERS ON A VERTICAL PLANE ALONG THE PROFILE EF. ALL HYPOCENTERS WITHIN A 100 KM. PERPENDICULAR DISTANCE FROM THE PLANE WERE PROJECTED.

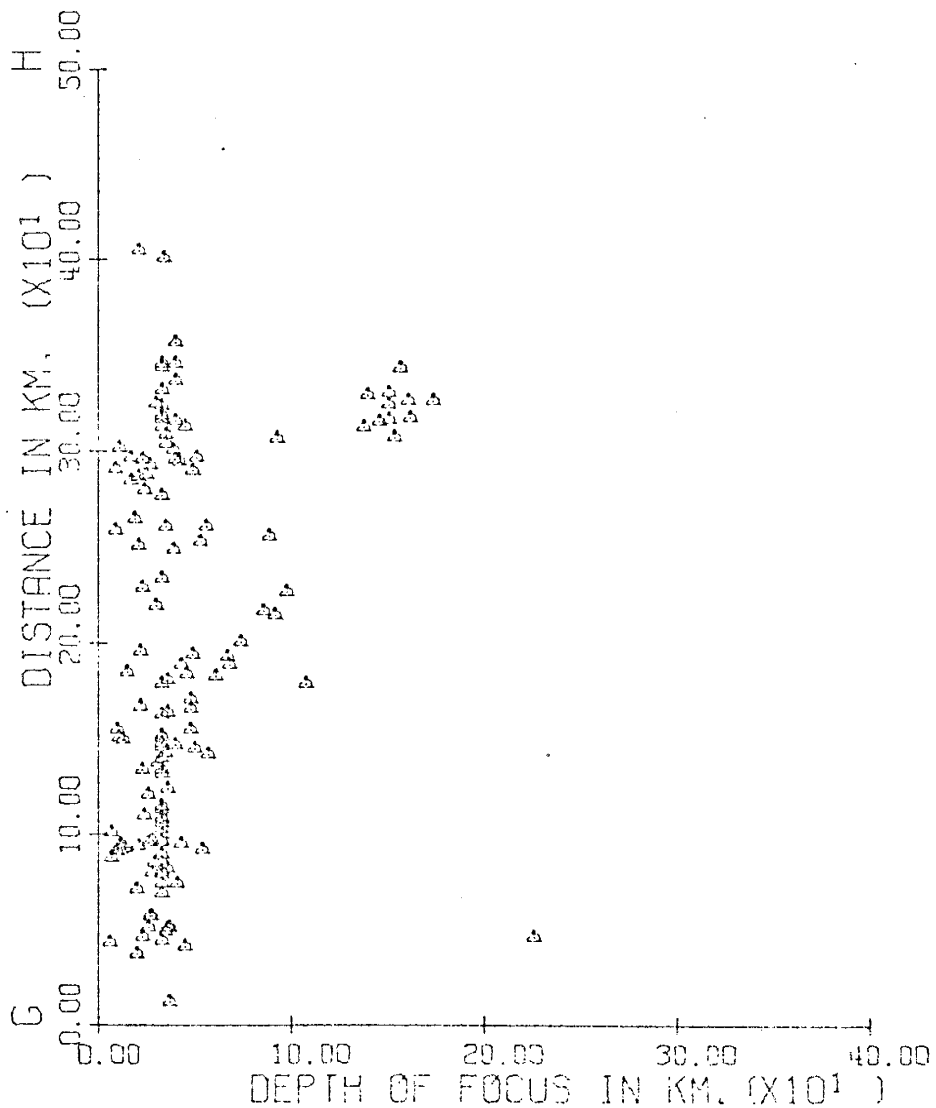

Figure 4.11. PROJECTION OF HYPOCENTERS ON A VERTICAL PLANE ALONG THE PROFILE GH. ALL HYPOCENTERS WITHIN A 100 KM. PERPENDICULAR DISTANCE FROM THE PLANE WERE PROJECTED.

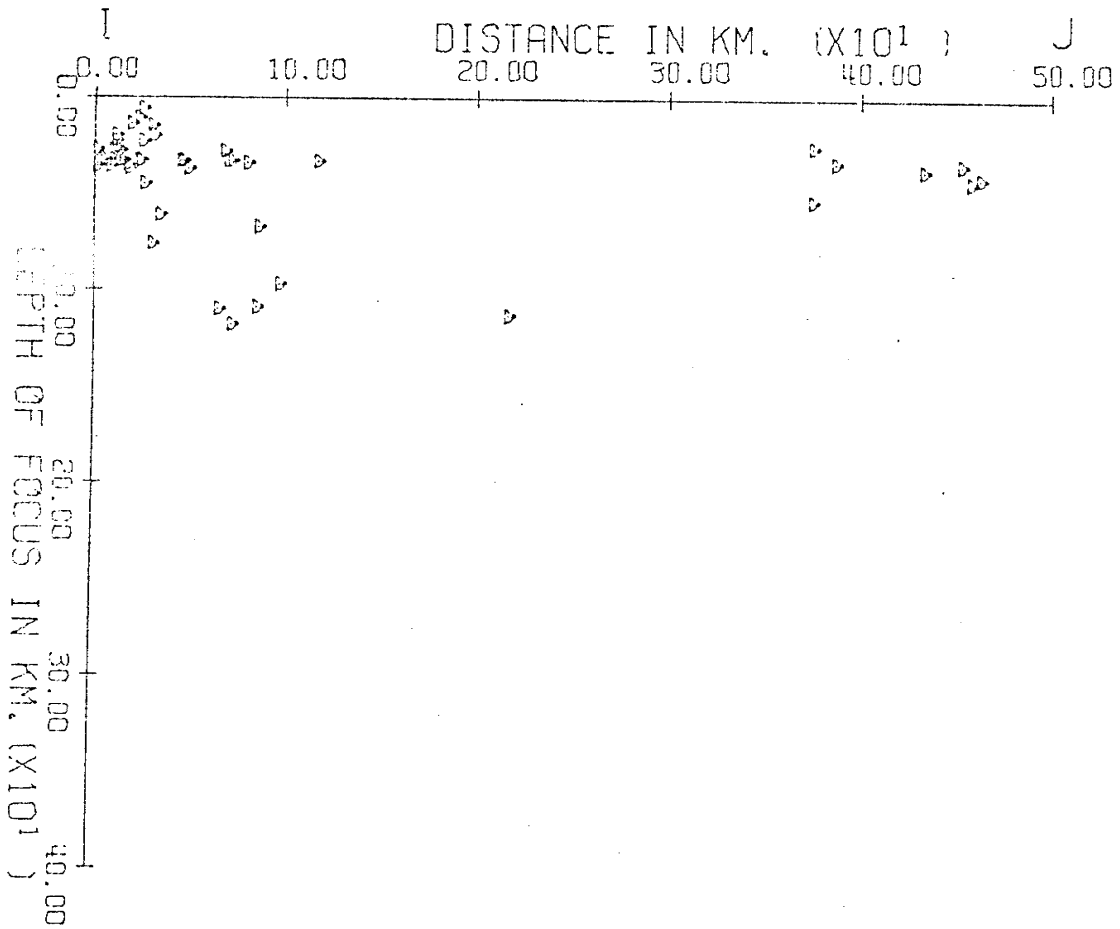

Figure 4.12. PROJECTION OF HYPOCENTERS ON A VERTICAL PLANE ALONG THE PROFILE IJ. ALL HYPOCENTERS WITHIN A 125 KM. PERPENDICULAR DISTANCE FROM THE PLANE WERE PROJECTED.

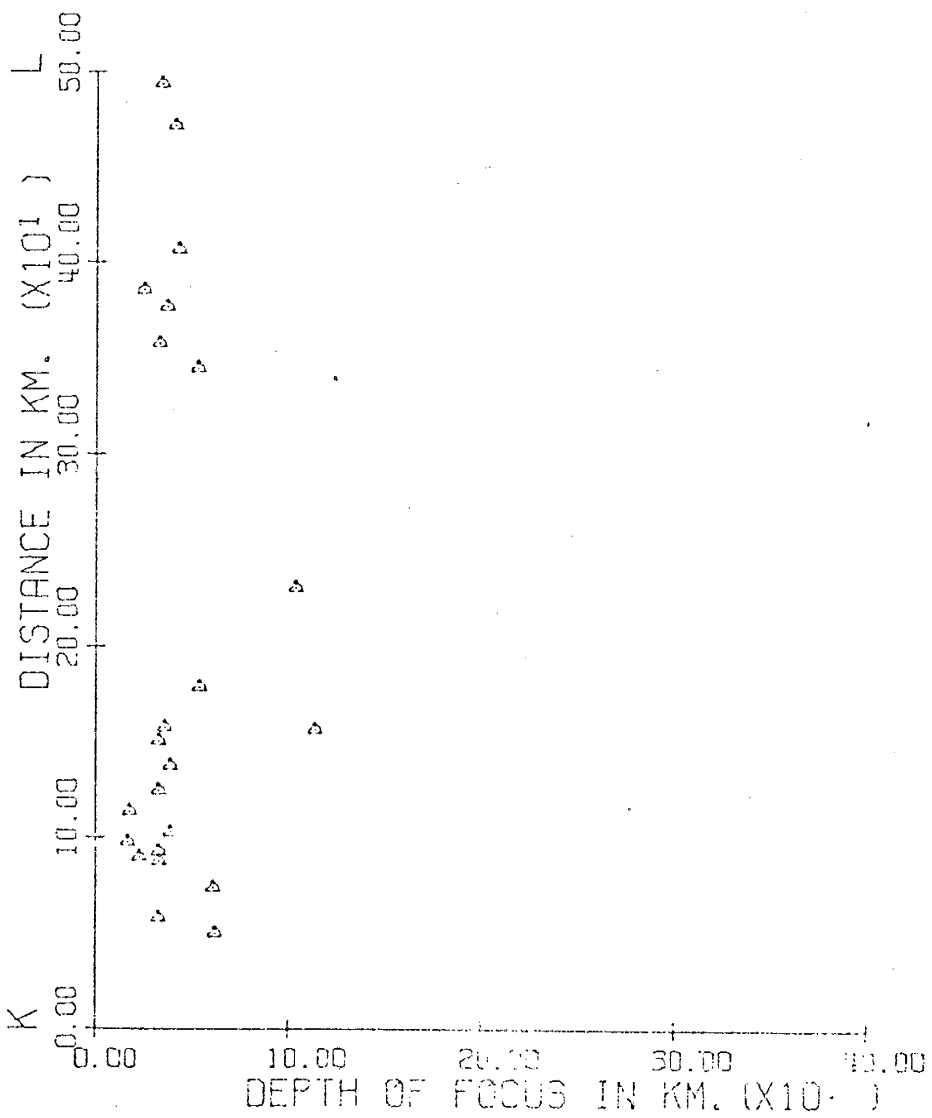

Figure 4.13. PROJECTION OF HYPOCENTERS ON A VERTICAL PLANE ALONG THE PROFILE KL ALL HYPOCENTERS WITHIN A 125 KM. PERPENDICULAR DISTANCE FROM THE PLANE WERE PROJECTED.

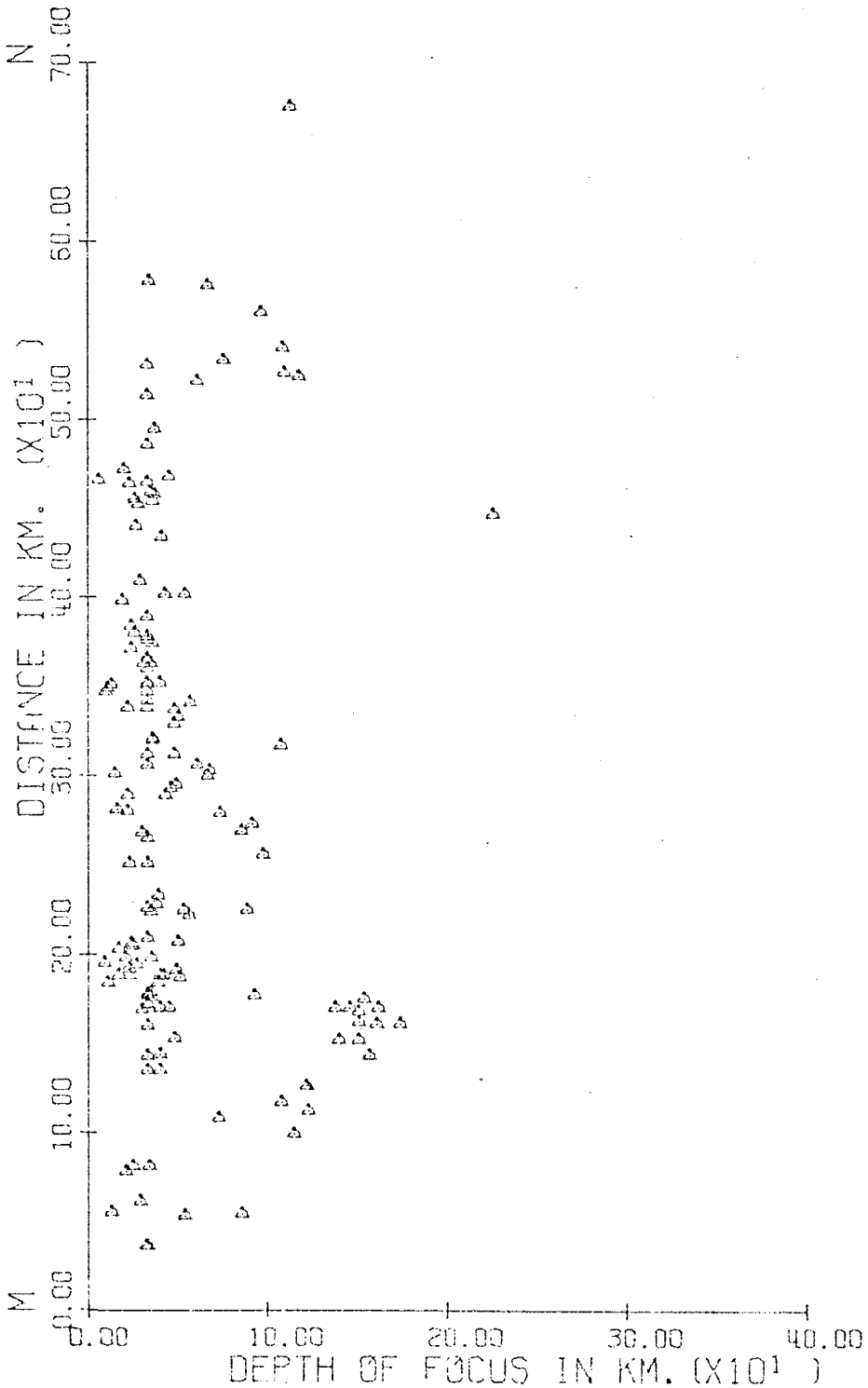

Figure 4.14. PROJECTION OF HYPOCENTERS ON A VERTICAL PLANE ALONG THE PROFILE MN. ALL HYPOCENTERS WITHIN A 100 KM. PERPENDICULAR DISTANCE FROM THE PLANE WERE PROJECTED.

west and 45° in the east for the downgoing lithosphere. The vertical section along the profile MN indicates that the rate of subductions are different along the Aegean and the Cyprian arcs. This suggests that the eastern termination of the Aegean arc is an arc-to-arc transform fault as indicated from the focal mechanism of earthquake 35 in Figure 4.1.

The areal distributions of intermediate focus earthquakes (Figures 2.3b and 4.7) and the projections of hypocenters on vertical planes indicate a thick zone of intermediate focus earthquakes at the eastern and the western ends of the Aegean arc. The broadness of the zone in the west is due to the low angle underthrusting of the Mediterranean lithosphere. The geometry of underthrusting at the eastern end of the Aegean arc is shown in Figure 4.15. This figure is a north-south vertical section of the proposed model across western Turkey, as suggested from the profiles EF and GH (Figures 4.10 and 4.11). Other supporting evidence for the geometry shown in Figure 4.15 comes from the free-air gravity anomalies (Figure 4.16) associated with two parallel trenches (Figure 2.4). Also Rabinowitz and Ryan(1970) have suggested a similar model on the basis of free-air gravity anomalies.

If we assume that underthrusting started 10 m.y. ago (LePichon, 1968) a subduction rate of 4.2 cm/yr. is obtained from the average dip (~38°) and the average width of the intermediate earthquake zone (~250 km), taking the overlapping section of the undergoing slabs into account. This is close to the rate (3.7 cm/yr.) suggested by McKenzie (1972b) but is higher than the rate of 2.6 cm/yr inferred by LePichon (1968). This discrepancy can be explained with the probable changes in the rate of plate consumption or an earlier beginning of underthrusting in the eastern Mediterranean.

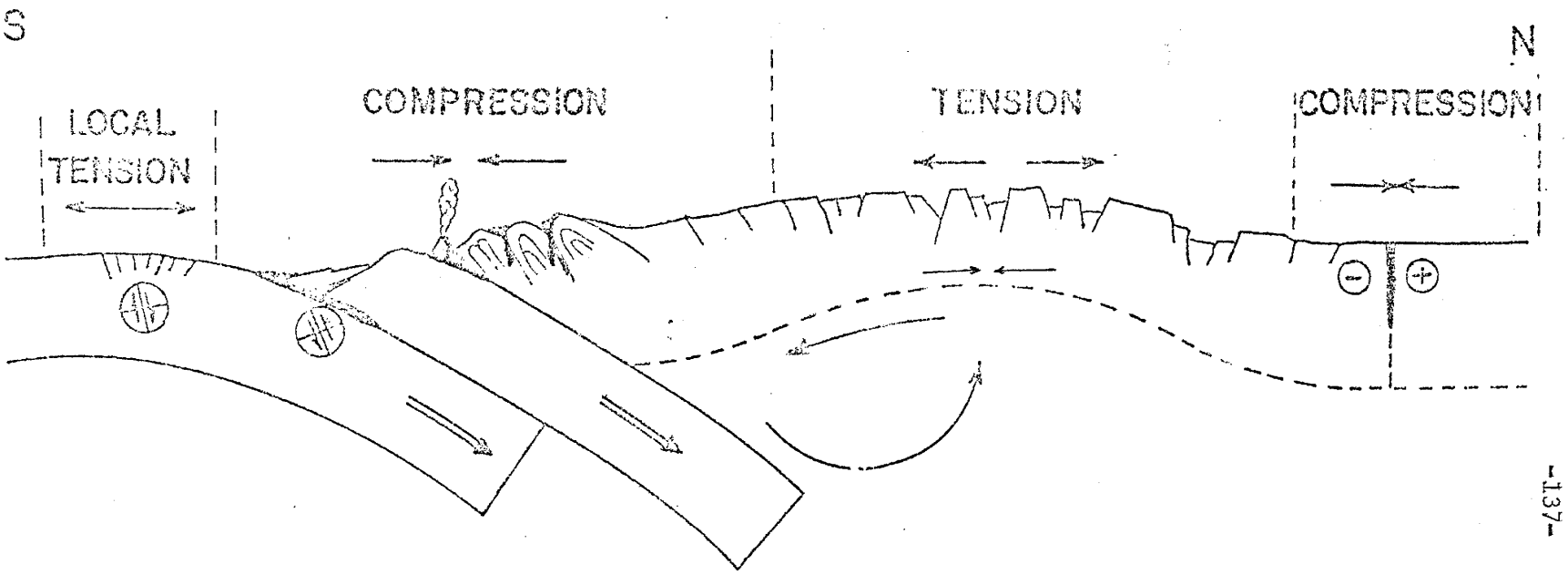

Figure 4.15. A vertical section of the proposed Plate Tectonics model across western Turkey. Uplifting in western Turkey is exaggerated to show the development of normal faults. Uplift is the result of upper mantle material rising beneath the overriding plate. + and - signs indicate the eastward and westward motions respectively along the north Anatolian fault.

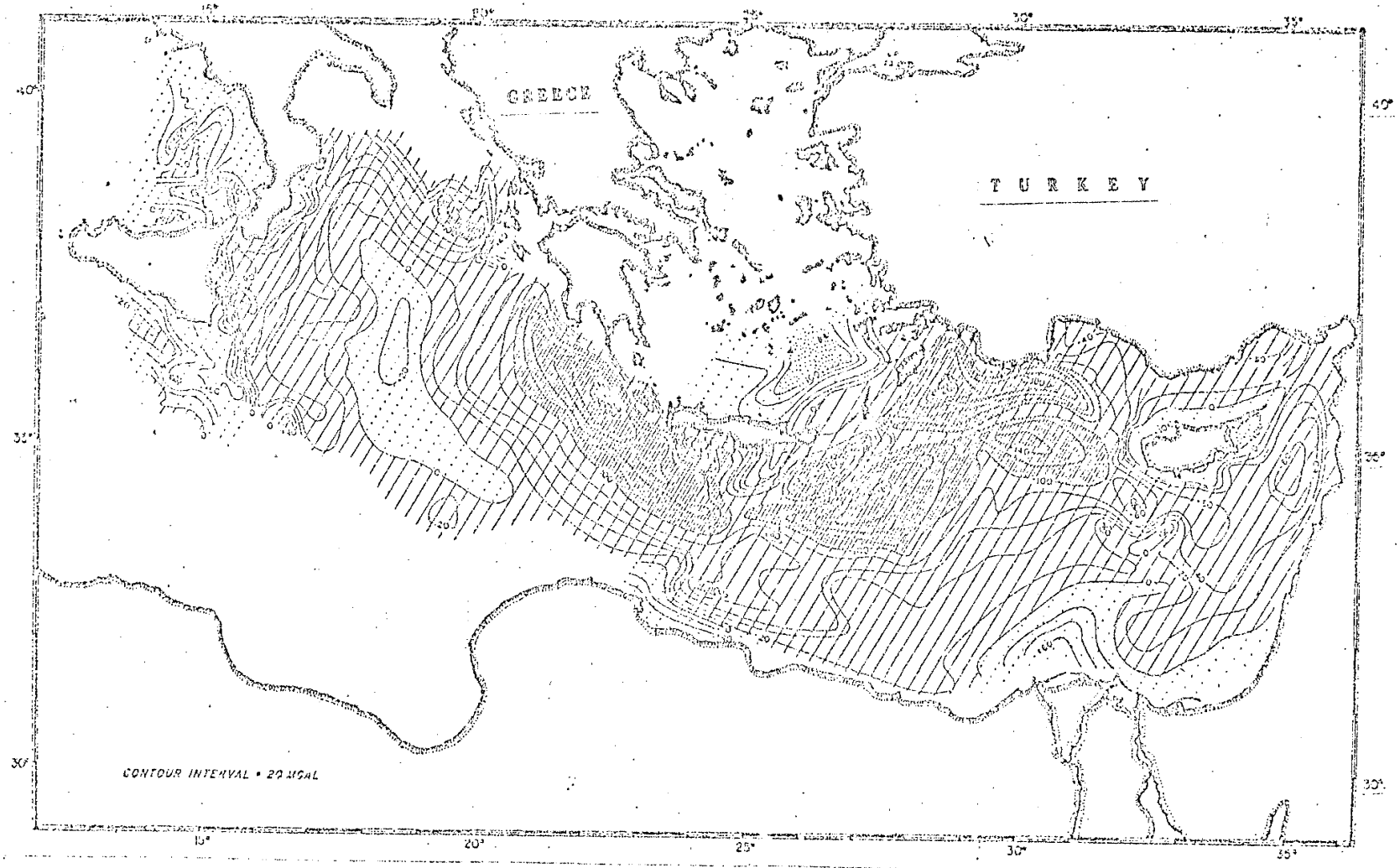

Figure 4.16. Free-air gravity anomaly map of the eastern Mediterranean Sea (After Rabinowitz and Ryan, 1970).

Discussion

Relative motions between the plates in the proposed model can explain the strike-slip and thrust fault solutions along the northern and the southern boundaries of the Aegean-Turkish plate. The normal fault solutions found in western Turkey, northern Aegean and Greece however cannot be explained with horizontal motions. It is believed that this type of faulting is the result of vertical movements within the plate.

A good analogy to the development of normal faults in western Turkey is the sand box experiments of Sanford (1959). In his experiments, Sanford demonstrated that a sinusoidal uplift at the basement can produce a series of normal faults at the crest and progressively greater distances from the crest of a fold. The average dip for these faults was 65° which is in good agreement with the average dip for the fault planes determined in section 3. The analogy can be seen better from Figure 4.15.

It is believed that the oceanic lithosphere cannot be projected downward without disturbing the surrounding upper mantle. As the lithosphere plunges into the mantle, it displaces mantle material. The displaced mantle material must go somewhere, and the path of least resistance is upward beneath the overriding continental lithosphere. This uprising of upper mantle coupled with the compression due to the relative motions of African and the Eurasian plates cause slow uplifting in the central portions of the Aegean-Turkish plate. Among several geologic evidences for uplifting the following are the most important (Arpat and Bingol, 1969): (1) The structure of the area is a series of grabens parallel to the general trend of Alpine folding, (2) Mesozoic rocks have been removed from the top of massifs by rapid erosion,

(3) Some old gneisses occur in elevated areas, (4) Young sedimentary units have been found at high elevations, (5) River erosion in the area has been more rapid vertically than laterally.

The driving mechanism for plates is by no means clear. Among several possibilities, convection in the upper mantle is the most probable one. Fault-plane solutions in this study indicate that most of the Aegean-Turkish plate is under compression. The tensional stresses are rather localized. Intra-plate compressional stresses are consistent with pushing from ridges. Nowroozi (1972) has suggested a thermal hot spot exists in eastern Turkey and western Iran. If his suggestion is true, then the westward movement of the Aegean-Turkish plate could be explained by convective motion in the mantle beneath the eastern end of the plate.

Conclusions

Earthquake mechanisms in Turkey and the Aegean region indicate complex deformations in this area. The Aegean-Turkish block is a westward moving plate undergoing internal deformation as the result of overriding the African plate. The driving mechanism may be mantle convection beneath a thermal hot spot in eastern Turkey.

Focal mechanisms of earthquakes in western Turkey indicate that intra-plate deformations arising from vertical movements are occurring inside the Aegean-Turkish block. Similar deformations are probably occurring in the northern Aegean and Greece.

Earthquake mechanisms and the vertical distribution of hypocenters along the Aegean and the Cyprian arcs indicate that the Mediterranean lithosphere is underthrusting the Aegean-Turkish plate. The geometry of underthrusting is complex. The eastern termination of the Aegean

arc is an arc-to-arc transform fault.

SUMMARY AND CONCLUSIONS

Turkey and the adjacent areas in the eastern Mediterranean comprise, seismicly, the most active section of the Alpine orogenic belt. Seismic activity in this region shows a close relation to Tertiary folding and Quaternary differential movements. A majority of the earthquakes occur around the Aegean Sea and along the north Anatolian fault. Intermediate focus earthquakes occur on the concave sides of the Aegean and the Cyprian arcs.

The large variety of fault-plane solutions in Turkey and the surrounding areas indicates complex deformation. A close relation exists between the focal mechanisms of earthquakes and sub-regional structures. Displacements at the focus are either parallel or perpendicular to the strike of geologic structures.

Fault-plane solutions are strongly affected by the choice of P wave velocity at the focus. Use of too low a velocity can change the character of dip-slip solutions, and introduce a strong strike-slip component of motion.

All fault-plane solutions in western Turkey represent normal faulting, indicative of crustal extension. Tensional axes for these solutions are nearly horizontal and perpendicular to the general east-west trend of graben structures.

The focal mechanism of the destructive Gediz earthquake of March 28, 1970, in western Turkey was normal faulting. The complexity of surface faulting and the occurrence of strong secondary shocks associated with this earthquake suggest multiple fracturing. A comparison of the fault-plane solutions for the main shock and the secondary shocks

indicates that both the east-west and the southeast-northwest tectonic lines in the Gediz region were reactivated during these earthquakes.

The focal mechanism of the northern Aegean earthquake of February 19, 1968, was strike-slip faulting. This earthquake indicates that the right-lateral motions associated with the north Anatolian fault continue in the Aegean Sea.

The focal mechanisms of earthquakes and the vertical distributions of hypocenters along the Aegean and the Cyprian arcs indicate that the Mediterranean lithosphere is underthrusting the Aegean-Turkish block. The geometry of underthrusting and the focal mechanism of the Burdur earthquake of May 12, 1971, suggest that the eastern termination of the Aegean arc is an arc-to-arc transform fault.

Seismicity, earthquake mechanisms, and the geology of the eastern Mediterranean and Turkey suggest that the Aegean-Turkish block is a westward moving plate undergoing internal deformation as the result of overriding the African plate. The driving mechanism may be mantle convection beneath a thermal hot spot in eastern Turkey. The diffuse seismic activity in western Turkey is not directly the result of horizontal motions but is a consequence of vertical movements inside the plate induced from the interaction of the African and the Eurasian plates.

Application of the concepts of Plate Tectonics to continental areas is difficult. The diffuse seismic activity in continental interiors cannot be explained very easily with horizontal motions of a large number of small plates. Focal mechanisms of intraplate earthquakes, such as the earthquakes of western Turkey, indicate that local variations

in the state of stress inside plates may produce intraplate deformations. This may have great importance in understanding the evolution and the present behavior of plates.

APPENDIX I

Summary of Station Parameters and First Motion Data

The station parameters and all available P wave first motion data are presented in this appendix. The calculation of station parameters, and the angle of incidence i_h at the focus, is discussed in the text (p. 29). All P wave first motions reported in this appendix were observed on the WWSSN long-period vertical-component records, unless otherwise noted. The first motion data for the stations outside the WWSSN were obtained by either correspondence or from the station bulletins. The following number designations were adapted to indicate the sources of first motions for the stations outside the WWSSN:

(1) First motion observed on short-period vertical-component record.

(2) First motion obtained by correspondence.

(3) First motion obtained from station bulletins.

(4) First motion obtained from the NOAA (formerly USCGS) earthquake data reports.

The observed P wave first motions were graded according to the quality of first arrivals and the quality of seismograms. The following letter designations were adopted to indicate the quality of first motions:

Ex = Excellent.

VG = Very Good.

G = Good.

F = Fair.

P = Poor.

* = First motions observed on short-period and long-period records contradict.

The grading of the first motions was not entirely based on personal judgment, but was also based on comparison of seismograms. However, the grading was not intended to be extremely precise, and therefore first motions might be graded to a higher or lower quality in some cases. To give a better feeling about the quality of first motions and the grading system, some graded samples of first motions are presented. Figure A.I.1 shows small portions of the WWSSN long-period and short-period vertical-component records and indicates the quality of first motions. Note that Fig. A.I.1 does not compare the first motions on long-period records against the first motions on short-period records. The first motions for stations outside the WWSSN could not be graded and the assumptions were made that impulsive arrivals were good, and emergent arrivals were fair or poor.

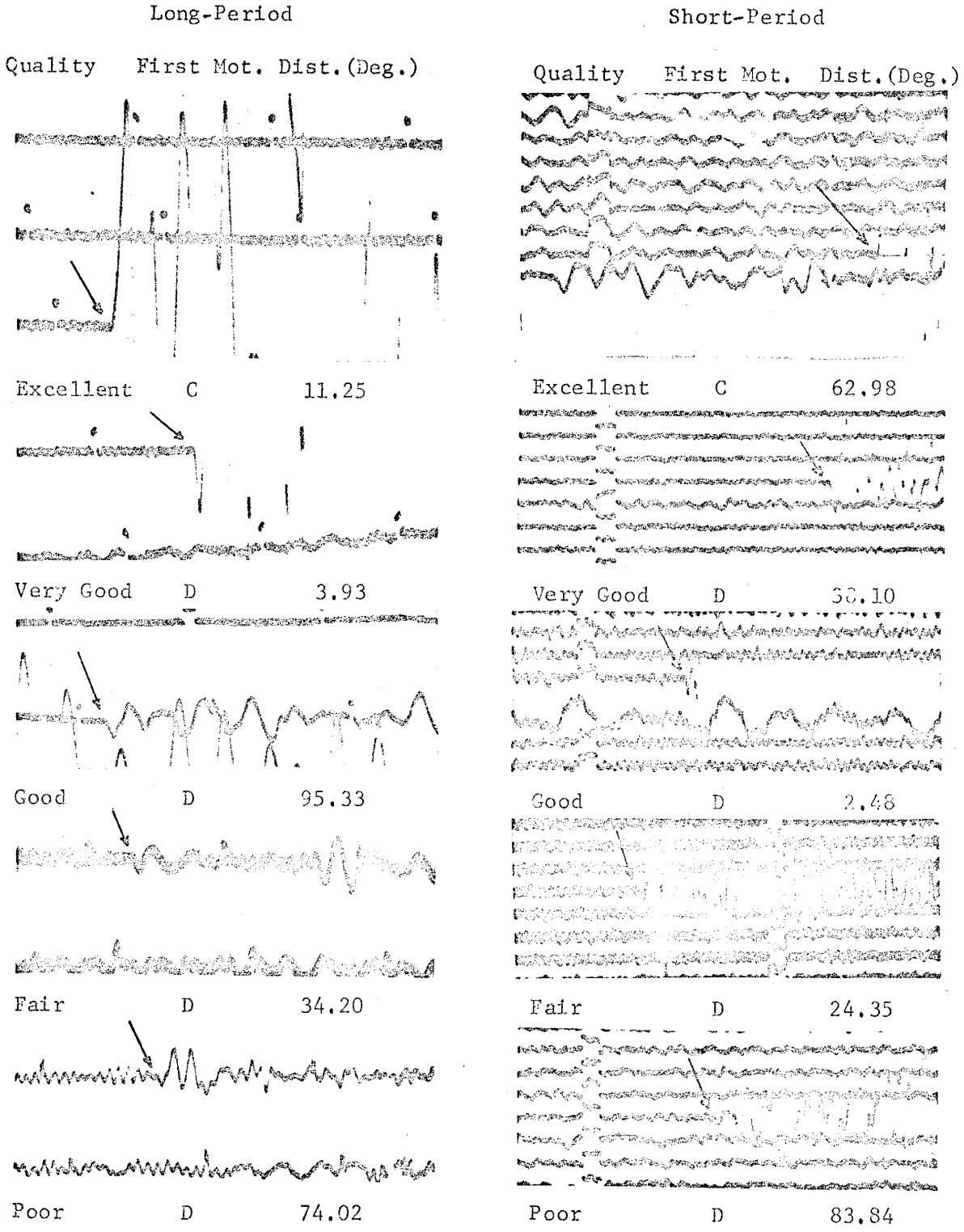

Figure A.I.1. Sampled portions of the WWSSN long-period and short-period vertical-component seismograms, indicating the quality of first motions. The arrow indicates the beginning of event.

TABLE A.I.1. Summary of Station Parameters and the First Motion Data for the Earthquake of Feb. 19, 1968.

Station	Distance (degrees)	Azimuth	i_h Vp=6.6 (km/sec)	i_h Vp=7.5 (km/sec)	P Wave First Motion	Quality
AAB	38.87	67.	29.8	34.8	D	(2)
AAE	32.77	154.	31.3	36.2	C	Ex
AAM	75.85	314.	19.9	22.8	C	G
AKU	35.83	331.	30.6	35.3	C	VG
ALQ	93.20	322.	15.9	18.2	D	VG
ANP	79.CO	66.	18.9	21.7	D	Ex
ATL	82.17	307.	18.0	20.6	D	Ex
ATU	1.74	215.	59.2	77.6	C	Ex
BAG	83.84	74.	17.4	19.9	D	Ex
BEC	69.90	296.	21.5	24.6	D	G
BHP	95.33	286.	15.8	18.0	D	G
BKS	97.07	335.	15.8	18.0	C	G
BLA	77.27	308.	19.5	22.2	D	Ex
BOG	94.02	276.	15.8	18.1	D	G
BUL	59.63	176.	24.1	27.7	C	Ex
CAR	84.82	279.	17.1	19.5	D	G
CHG	66.02	85.	22.6	25.8	D	Ex
COL	75.54	357.	19.9	22.8	C	G
COP	18.29	337.	45.5	54.2	C	Ex
DAL	89.86	314.	17.2	19.6	D	G
DAV	93.57	78.	15.9	18.1	D	G
DUG	91.58	329.	16.1	18.4	D	G

TABLE A.I.1. (Continued)

Station	Distance (degrees)	Azimuth	i_h Vp=6.6 (km/sec)	i_h Vp=7.5 (km/sec)	P Wave First Motion	Quality
ESK	24.57	320.	33.9	39.4	C	F
FLO	81.96	315.	18.1	20.7	D	VG
GDH	49.61	333.	26.8	30.8	C	Ex
GEO	74.16	308.	20.3	23.2	D	VG
GOL	88.83	324.	16.3	18.6	D	G
GRM	72.72	179.	20.6	23.6	D	P(1)
GRS	16.43	83.	48.9	59.9	D	(2)
GSC	97.40	329.	15.7	17.9	C	P
HLW	10.86	149.	53.7	66.3	C	G(1)
IST	3.46	60.	57.6	73.7	D	Ex
JER	11.25	130.	53.6	66.1	C	Ex
KBS	39.86	356.	29.5	34.1	C	VG
KEV	30.37	1.	31.8	36.8	C	P(1)
KOD	54.82	107.	25.4	29.2	D	Ex
KRV	16.34	79.	48.8	59.9	D	(2)
KTG	39.22	337.	29.7	34.3	C	F
LEM	88.67	100.	16.4	18.7	D	F
LON	88.89	338.	16.3	18.6	D	G
LUB	92.01	318.	16.0	18.2	D	F
MAL	23.20	273.	35.6	41.4	D	Ex
MAT	82.34	48.	18.0	20.5	D	G
NAI	42.09	162.	29.0	33.4	C	Ex
NAT	70.86	246.	21.1	24.2	C	P

TABLE A.I.1. (Continued)

Station	Distance (degrees)	Azimuth	i_h Vp=6.6 (km/sec)	i_h Vp=7.5 (km/sec)	P Wave First Motion	Quality
NDI	43.94	88.	28.4	32.7	D	Ex
NOR	44.58	352.	28.3	32.6	C	Ex(*)
NUR	21.11	360.	39.1	45.8	C	Ex
OGD	71.35	308.	21.1	24.2	D	VG
OXF	84.46	311.	17.3	19.7	D	G
PAT	2.78	246.	57.6	75.0	C	(3)
PDA	39.11	284.	29.7	34.3	D	G
POO	46.85	102.	27.6	31.8	D	Ex
PRE	65.22	177.	22.7	26.0	C	Ex
PRK	0.99	98.	58.9	78.5	D	(3)
PTO	25.53	285.	33.1	38.3	D	Ex
QUE	35.32	92.	30.8	35.5	D	Ex
SCP	73.47	310.	20.4	23.4	D	VG
SDB	55.36	193.	25.3	29.0	C	Ex
SHA	86.39	308.	16.8	19.1	D	Ex
SHI	24.56	105.	33.9	39.4	D	Ex
SHL	56.79	83.	24.8	28.5	D	Ex
SHK	80.41	53.	18.6	21.2	D	G
SJG	79.48	285.	18.8	21.5	D	VG
STU	14.67	315.	51.6	62.9	C	VG
TAB	16.65	88.	48.5	58.4	D	Ex
TOL	22.27	281.	37.2	43.4	D	Ex
TRI	10.39	311.	56.1	70.6	D	Ex

TABLE A.I.1. (Continued)

Station	Distance (degrees)	Azimuth	i_h Vp=6.6 (km/sec)	i_h Vp=7.5 (km/sec)	P Wave First Motion	Quality
TRN	80.50	276.	18.5	21.2	D	G
TUC	97.40	324.	15.7	17.9	D	P
VAL	27.27	309.	32.2	37.3	D	VG
WES	68.59	308.	21.9	25.1	D	Ex
WIN	62.40	188.	23.4	26.8	C	Ex

TABLE A.I.2. Summary of Station Parameters and the First Motion Data for the Earthquake of Jan. 14, 1969.

Station	Distance (degrees)	Azimuth	i_h Vp=6.6 (km/sec)	i_h Vp=7.5 (km/sec)	P Wave First Motion	Quality
AAB	37.20	64.	31.0	35.1	C	(2)
AAE	28.50	160.	32.1	37.2	D	Ex
AQU	13.67	302.	52.9	65.1	C	Ex
ATL	86.78	310.	16.7	19.1	C	G(1)
ATU	4.73	294.	57.2	72.9	C	Ex
BAG	81.48	76.	18.3	20.9	C	F
BAK	10.09	62.	55.2	68.2	C	(2)
BKR	12.42	59.	54.0	65.9	C	(2)
BLA	81.89	311.	18.1	20.7	D	F
BUL	56.31	181.	25.1	28.8	D	VG
CAR	88.68	282.	16.5	18.8	D	F
CHG	62.98	86.	23.4	26.8	C	VG
CMP	9.61	342.	55.8	71.6	D	(4)
COL	78.90	359.	19.0	21.7	C	P
COP	22.59	335.	36.6	42.7	C	P
DUG	95.64	331.	15.9	18.1	C	P(1)
EIL	8.19	142.	56.6	72.1	D	(2)
ESK	29.17	321.	32.1	37.1	C	P(1)
FLO	86.59	317.	16.8	19.2	C	F(1)
GOL	93.37	327.	16.0	18.2	C	G(1)
GRM	69.52	182.	21.7	24.8	D	G
GRS	13.91	71.	51.6	64.3	C	(2)

TABLE A.I.2. (Continued)

Station	Distance (degrees)	Azimuth	i_h Vp=6.6 (km/sec)	i_h Vp=7.5 (km/sec)	P Wave First Motion	Quality
HLW	6.59	164.	56.6	72.9	D	Ex
IST	4.87	358.	57.6	73.5	D	Ex
JER	6.63	130.	56.6	71.6	D	Ex
KBL	32.30	81.	31.5	36.4	C	Ex(*)
KBS	43.33	355.	28.7	33.1	C	G
KEV	33.60	359.	31.3	36.1	C	P
KHC	17.26	323.	47.6	57.5	C	G
KOD	50.67	108.	26.6	30.6	C	P
KON	26.66	338.	32.6	37.8	C	P
KRV	14.12	66.	48.2	64.3	D	(2)
KTG	43.47	338.	28.7	33.0	D	P(1)
LAH	37.42	84.	30.6	35.2	C	G
LEM	84.79	102.	17.2	19.6	C	P(1)
LOR	21.78	308.	38.0	44.4	C	G
MAL	26.90	281.	32.4	37.5	C	G
MAT	81.95	50.	18.1	20.7	C	F
MSH	24.40	81.	34.3	40.2	C	Ex
NAI	38.10	168.	30.1	34.7	D	Ex
NDI	40.80	86.	29.4	33.9	C	Ex
NOR	48.24	352.	27.3	31.5	D	G(1)
NUR	24.51	355.	34.1	39.5	C	Ex(*)
POO	42.93	102.	28.8	33.2	C	G
PRE	61.93	181.	23.6	27.0	D	Ex

TABLE A.I.2. (Continued)

Station	Distance (degrees)	Azimuth	i_h Vp=6.6 (km/sec)	i_h Vp=7.5 (km/sec)	P Wave First Motion	Quality
PRU	17.42	327.	47.6	56.9	C	G
QUE	31.95	90.	31.6	36.5	C	Ex
SCP	78.09	312.	19.3	22.0	C	G
SDB	53.18	199.	25.9	29.8	D	Ex
SEM	38.90	52.	30.0	34.5	C	(2)
SEO	74.13	55.	20.3	23.3	C	G
SHA	91.00	310.	16.1	18.4	C	P
SHI	20.57	102.	40.5	47.5	C	Ex
SHK	79.65	55.	18.8	21.5	C	P
SHL	53.92	83.	25.7	29.5	C	VG
SJG	83.57	288.	17.7	20.2	C	F
SNG	70.79	95.	21.3	24.3	C	F
STU	19.29	317.	43.0	50.8	C	G
TAB	13.76	77.	52.8	64.9	C	Ex
TOL	26.29	288.	32.7	37.9	C	G
TRN	84.22	279.	17.4	20.1	C	F
UME	28.17	352.	32.2	37.2	C	G(1)
WIN	59.84	193.	24.1	27.7	D	VG

TABLE A.I.3. Summary of Station Parameters and the First Motion Data for the Earthquake of Mar. 23, 1969.

Station	Distance (degrees)	Azimuth	i_h Vp=6.3km/sec	P Wave First Motion	Quality
AAB	36.46	67.	28.9	D	(2)
AAM	77.92	316.	18.4	D	VG
AKU	37.32	330.	28.8	C	P
ANP	76.58	68.	18.8	D	G
ATL	84.42	309.	16.6	D	G(1)
ATU	3.93	253.	53.8	D	VG
BAG	81.28	76.	17.5	D	P
BEO	8.22	316.	51.5	C	(4)
BKR	11.68	73.	50.1	C	(2)
BLR	77.57	358.	18.5	C	(4)
BNG	35.78	197.	29.1	C	(4)
BUL	59.34	180.	23.0	D	VG
CHG	63.33	87.	22.1	D	VG
CMP	6.61	338.	52.7	C	(4)
COL	75.86	358.	18.9	D	VG
COP	19.63	332.	40.2	C	P
EIL	11.01	149.	50.5	D	(2)
ESK	26.50	318.	30.9	D	VG
GDH	51.01	333.	25.2	D	G
GEO	76.40	310.	18.8	D	G
GOL	90.54	326.	15.4	D	P
GRM	72.53	182.	19.8	C	P

TABLE A.I.3. (Continued)

Station	Distance (degrees)	Azimuth	i_h Vp=6.3km/sec	P Wave First Motion	Quality
GRS	13.77	83.	49.1	D	(2)
HKC	72.90	75.	19.6	D	G
HLW	9.62	165.	53.2	D	P
ISK	1.95	13.	54.1	C	(4)
IST	1.88	11.	54.2	C	Ex
JAN	5.92	277.	53.0	D	(3)
JER	9.20	142.	53.5	D	G
KBL	32.49	85.	29.8	D	VG(*)
KBS	40.26	355.	28.0	D	P
KEV	30.56	359.	30.2	C	F
KHC	14.59	317.	48.1	D	VG
KOD	52.19	110.	24.9	D	VG
KON	23.66	336.	33.4	D	G
KRL	17.41	311.	44.3	C	(4)
KRV	13.72	78.	49.1	D	(2)
KTG	40.47	337.	28.0	D	G
LOR	19.57	302.	40.2	D	Ex
MAL	25.92	275.	31.1	D	Ex
MAT	80.42	50.	17.7	D	G
NAI	41.18	167.	27.8	D	VG
NDI	41.24	89.	27.8	D	VG
NOR	45.16	352.	26.7	D	F
NUR	21.44	355.	36.5	C	Ex

TABLE A.I.3. (Continued)

Station	Distance (degrees)	Azimuth	i_h Vp=6.3km/sec	P Wave First Motion	Quality
OGD	73.58	310.	19.5	D	G
PAT	5.35	262.	53.2	D	(3)
PLG	4.05	288.	53.8	D	(3)
POO	44.17	105.	27.0	D	G
PRA	14.77	322.	48.5	C	(4)
PRE	64.95	180.	21.7	D	F
PRK	1.72	272.	54.9	C	(3)
PRU	14.66	322.	48.7	D	P
PTU	28.20	286.	30.4	D	VG
QUE	32.60	94.	29.8	C	P(1)
ROM	12.45	288.	49.9	C	(4)
SCM	79.29	358.	18.0	C	(4)
SCP	75.66	311.	19.0	D	G
SDB	55.89	197.	23.9	D	G
SEM	37.55	55.	28.7	D	(2)
SHI	21.90	109.	35.5	D	Ex
SHK	78.35	55.	18.3	D	G
SHL	54.13	84.	24.4	D	G
STU	16.79	311.	47.6	D	P
TAB	13.94	89.	49.5	D	G
TNN	75.91	0.	18.9	C	(4)
TOL	24.97	282.	31.8	D	Ex
TRI	12.64	306.	50.0	D	Ex

TABLE A.I.3. (Continued)

Station	Distance (degrees)	Azimuth	i_h Vp=6.3 (km/sec)	P Wave First Motion	Quality
TRN	83.21	278.	16.9	D	G
UME	25.09	351.	31.7	C	G(1)
VAL	29.51	308.	30.4	D	G
VAM	5.10	223.	53.8	C	(3)
WES	70.82	310.	20.1	D	G
WIN	62.68	192.	22.3	D	VG

TABLE A.I.4. Summary of Station Parameters and the First Motion Data for the Earthquake of Mar. 28, 1969.

Station	Distance (degrees)	Azimuth	i_h Vp=6.3 (km/sec)	i_h Vp=7.5 (km/sec)	P Wave First Motion	Quality
AAB	36.76	67.	28.9	35.0	D	(2)
AAM	78.29	316.	18.3	22.0	D	VG
AKU	37.81	331.	28.6	34.7	D	G
ALQ	95.42	324.	15.1	18.0	D	VG
ANP	76.87	68.	18.6	22.3	D	VG
ARG	2.39	185.	53.7	74.1	C	(3)
ATL	84.74	309.	16.3	19.6	D	Ex
ATU	3.72	262.	53.2	72.4	D	Ex
BAG	81.50	76.	17.4	20.8	D	Ex
BAK	9.80	76.	51.6	68.5	C	(2)
BEC	72.62	298.	19.7	23.7	D	G
BHP	98.09	288.	15.0	18.0	D	P
BLA	79.83	310.	17.8	21.3	D	Ex
BOG	96.76	281.	15.0	18.0	D	G
BUL	58.74	180.	23.1	27.9	D	VG
CAR	87.56	282.	15.8	18.9	D	Ex
CHG	63.44	86.	22.1	26.6	D	Ex
COL	76.45	358.	18.7	22.5	D	Ex
COP	20.13	333.	38.9	48.3	D	Ex
COR	92.98	340.	15.2	18.2	D	G
DAV	91.13	80.	15.3	18.4	D	VG
DUG	93.21	331.	15.2	18.2	D	G

TABLE A.I.4. (Continued)

Station	Distance (degrees)	Azimuth	i_h Vp=6.3 (km/sec)	i_h Vp=7.5 (km/sec)	P Wave First Motion	Quality
EIL	10.54	147.	51.5	68.5	C	(2)
ESK	26.90	319.	30.7	38.2	D	Ex
GDH	51.51	333.	25.0	30.2	D	VG
GEO	76.72	310.	18.7	22.4	D	VG
GOL	91.00	326.	15.3	18.4	D	G
GRM	71.93	182.	19.9	23.9	D	VG
GRS	13.93	81.	48.8	63.0	D	(2)
HLW	9.07	164.	53.2	72.4	C	(4)
IST	2.48	10.	53.7	73.7	D	VG
JER	8.79	139.	53.3	72.4	D	VG
KBL	32.62	84.	29.8	36.3	D	Ex
KBS	40.86	355.	27.8	33.8	D	Ex
KHC	15.00	319.	48.2	62.0	D	VG
KEV	31.16	359.	30.1	36.6	D	P
KOD	52.06	110.	24.9	30.1	D	Ex
KON	24.17	337.	32.8	40.1	D	Ex
KRV	13.93	76.	48.8	63.0	C	(2)
KTG	40.99	337.	27.8	33.7	D	Ex
LIS	29.23	282.	30.5	37.2	C	(4)
LON	90.59	340.	15.4	18.4	D	G
LOR	19.84	304.	40.2	50.2	D	Ex
MAL	25.90	276.	31.1	38.6	D	Ex
MAN	82.96	77.	16.9	20.3	D	Ex

TABLE A.I.4. (Continued)

Station	Distance (degrees)	Azimuth	i_h Vp=6.3 (km/sec)	i_h Vp=7.5 (km/sec)	P Wave First Motion	Quality
MAT	80.87	50.	17.5	21.0	D	Ex
MFP	39.45	212.	28.2	34.3	C	(4)
MSH	24.76	85.	32.0	39.2	D	P(1)
NAI	40.61	167.	27.9	33.9	D	VG
NAT	72.99	249.	19.6	23.5	D	G
NDI	41.33	89.	27.8	33.7	D	Ex
NOR	45.74	352.	26.6	32.2	D	Ex
NUR	22.03	355.	35.5	43.8	D	Ex
OGD	73.91	310.	19.4	23.3	D	Ex
PDA	41.87	286.	27.6	33.5	D	Ex
PLG	4.21	296.	53.7	74.2	D	(3)
POO	44.10	104.	27.0	32.7	D	G(1)
PRE	64.35	180.	21.9	26.3	D	G
PRK	1.77	292.	54.9	77.5	C	(3)
PRU	15.10	323.	48.2	62.1	D	VG
PTO	28.29	287.	30.4	37.1	D	VG
QUE	32.64	93.	29.8	36.3	D	Ex
SDB	55.29	198.	24.1	29.1	D	G
SEM	37.96	55.	28.7	34.6	D	(2)
SHA	88.95	310.	15.5	18.6	D	Ex
SHI	21.80	107.	35.7	44.0	D	Ex
SHK	78.76	54.	18.1	21.7	D	VG
SJG	82.24	287.	17.2	20.6	D	VG

TABLE A.I.4. (Continued)

Station	Distance (degrees)	Azimuth	i_h Vp=6.3 (km/sec)	i_h Vp=7.5 (km/sec)	P Wave First Motion	Quality
STU	17.13	313.	44.9	57.2	D	VG
TAB	14.05	87.	49.0	64.0	D	Ex
TOL	25.02	283.	31.8	38.9	D	Ex
TRI	12.94	308.	51.8	66.0	D	Ex
TRN	83.22	278.	16.9	20.2	D	F
TUC	99.57	326.	15.0	18.0	D	P
UME	25.68	352.	31.3	38.3	D	Ex
VAL	29.83	309.	30.3	36.9	D	VG
VLS	6.13	268.	52.9	72.4	C	(2)
WES	71.15	310.	20.2	24.2	D	Ex
WIN	62.07	192.	22.4	27.0	D	P

TABLE A.I.5. Summary of Station Parameters and the First Motion Data for the Earthquake of Apr. 6, 1969.

Station	Distance (degrees)	Azimuth	i_h Vp=6.6km/sec	P Wave First Motion	Quality
AAB	38.24	66.	30.1	D	(2)
AAM	77.26	315.	19.5	D	F
AKU	37.14	331.	30.3	C	G(1)
ALQ	94.57	323.	15.9	D	G(1)
ARG	2.66	148.	58.2	C	(3)
ATL	83.58	308.	17.6	D	F
ATU	2.17	257.	59.0	D	Ex
BAG	83.04	75.	17.7	C	P
BEC	71.28	297.	21.1	D	P
BLA	78.69	309.	18.4	D	G
BNG	34.71	194.	31.0	C	(4)
BKR	13.45	71.	52.9	C	(2)
BUL	58.68	178.	24.4	C	P
CAR	86.05	280.	16.9	D	G(1)
CHG	65.01	85.	22.8	D	VG
CMP	6.84	352.	56.5	C	(4)
COL	76.50	357.	19.7	D	G(1)
COP	19.55	336.	42.6	D	F
DUG	92.52	329.	16.0	D	G(1)
ESK	25.96	320.	32.8	C	P(1)
GDH	50.90	333.	26.5	D	F
GEO	75.57	309.	19.9	D	F(1)

TABLE A.I.5. (Continued)

Station	Distance (degrees)	Azimuth	i_h Vp=6.6km/sec	P Wave First Motion	Quality
GRS	15.49	80.	50.7	D	(2)
GOL	90.19	325.	16.2	D	G
HKC	74.66	73.	20.2	C	P
HLW	9.55	153.	55.2	C	G
IST	3.23	37.	57.8	C	Ex
KBL	34.19	83.	31.0	D	G
KBS	40.83	356.	29.3	C	P
KEV	31.25	0.	31.7	C	G(1)
KON	23.67	339.	34.9	C	G(*)
KRL	16.68	315.	49.0	C	(4)
KTG	40.47	337.	29.4	D	F(1)
LOR	18.60	305.	44.8	D	VG
MAL	24.35	275.	34.4	D	VG
MAT	82.12	49.	18.1	D	P
NAI	40.91	164.	29.3	D	G
NAT	71.50	247.	21.0	D	P(1)
NDI	42.89	87.	28.8	D	G(1)
NOR	45.62	352.	28.0	D	G(1)
NUR	22.03	358.	37.4	C	F
OGD	72.77	309.	20.6	D	P
OXF	85.87	312.	17.0	D	G
PDA	40.40	286.	29.5	D	P
PLG	2.95	310.	58.2	D	(2)

TABLE A.I.5. (Continued)

Station	Distance (degrees)	Azimuth	i_h Vp=6.6km/sec	P Wave First Motion	Quality
POO	45.60	102.	28.1	D	G
PRE	64.27	178.	23.0	D	G
PTO	26.83	287.	32.4	D	G(1)
QUE	34.20	92.	31.0	D	F
SCP	74.88	311.	20.2	C	F
SDB	54.76	195.	25.4	D	G(1)
SEM	39.29	54.	29.8	D	(2)
SHA	87.80	308.	16.5	D	F
SHI	23.27	104.	35.9	D	VG
SHL	55.83	83.	25.2	D	VG
SJG	80.76	286.	18.4	D	P
SNG	73.20	94.	20.6	D	G
STU	16.07	315.	49.8	C	P
TAB	15.61	85.	50.6	D	VG
TOL	23.52	283.	35.2	D	VG
TRI	11.80	312.	55.8	D	F
TUC	98.76	324.	15.8	D	P(1)
UME	25.58	354.	33.1	C	VG(1)
VAM	3.55	210.	57.7	C	(3)
WES	70.00	309.	21.5	D	P
WIN	61.68	190.	23.6	D	G(1)

TABLE A.I.6. Summary of Station Parameters and the First Motion Data for the Earthquake of June 12, 1969.

Station	Distance (degrees)	Azimuth	i_h Vp=7.5km/sec	P Wave First Motion	Quality
AAB	41.02	61.	33.9	C	(2)
AAE	28.31	150.	37.2	D	G
AAM	79.37	315.	21.6	C	VG
AKU	40.30	334.	34.0	C	F(*)
ALQ	97.16	322.	18.0	C	F
ANP	81.00	66.	21.1	C	VG
AQU	12.09	315.	66.2	C	VG
ARG	3.09	53.	74.2	C	(3)
ATL	85.26	308.	19.5	C	VG
ATU	3.73	344.	74.2	C	Ex
BAG	85.21	73.	23.8	C	VG
BAK	13.90	60.	64.3	C	(2)
BEC	72.20	298.	23.9	C	P
BKR	16.23	58.	60.4	C	(2)
BLA	80.42	309.	21.2	C	VG
BNG	30.49	193.	37.0	D	(4)
BUL	54.64	176.	29.3	D	F
CAR	85.70	280.	19.4	C	VG
CHG	66.52	83.	25.7	C	VG
CIN	4.02	37.	74.2	C	(4)
COL	80.54	357.	21.2	C	VG
COP	22.99	342.	41.9	C	Ex

TABLE A.I.6. (Continued)

Station	Distance (degrees)	Azimuth	i_h Vp=7.5km/sec	P Wave First Motion	Quality
COR	95.95	338.	18.0	C	P
DAV	94.57	78.	18.1	C	G
EIL	9.68	117.	69.5	D	(2)
ESK	28.58	326.	37.2	C	VG
ERZ	14.04	62.	64.9	C	(4)
GDH	54.11	335.	29.5	C	G
GRS	17.70	67.	56.3	C	(2)
HLW	6.99	129.	72.9	D	Ex
ISK	7.36	24.	72.2	C	(4)
KBL	35.96	77.	35.4	C	VG
KBS	44.85	356.	32.6	C	VG
KER	18.19	84.	54.5	D	(4)
KEV	35.37	1.	35.7	C	VG
KON	27.19	343.	37.4	C	Ex
KTG	43.88	339.	32.9	C	VG
LAH	41.02	80.	33.7	D	G
LEM	87.77	100.	18.9	D	G(1)
LIS	27.71	289.	37.5	D	(4)
MAL	23.99	284.	40.2	C	Ex
MAN	86.60	75.	19.1	C	G
MAT	85.65	48.	19.4	C	G
NAT	68.93	248.	25.0	C	P
NDI	44.33	82.	32.7	C	VG(*)

TABLE A.I.6. (Continued)

Station	Distance (degrees)	Azimuth	i_h Vp=7.5km/sec	P Wave First Motion	Quality
NOR	49.54	353.	31.0	C	VG
NUR	26.11	360.	38.1	C	VG
OGD	74.53	310.	23.1	C	Ex
OXF	87.79	311.	18.9	C	P
PAT	4.67	326.	74.2	D	(3)
PDA	40.63	290.	33.9	C	VG
PLG	6.10	348.	72.2	C	(3)
POO	45.97	97.	32.2	C	VG
PRK	4.94	11.	74.2	C	(3)
PTO	27.26	294.	37.4	C	VG
QUE	35.41	85.	35.6	C	Ex
SCP	76.73	311.	22.5	C	VG
SDB	50.52	194.	30.6	D	P
SEM	42.64	51.	33.3	C	(2)
SHA	89.49	308.	18.6	C	VG
SHI	23.68	94.	40.7	C	Ex
SHK	83.42	52.	20.2	C	VG
SHL	57.53	79.	28.4	C	VG
SJG	80.84	286.	21.1	C	F
STU	18.56	326.	53.4	C	Ex
TAB	17.50	72.	56.4	C	Ex
TOL	23.72	292.	40.6	C	Ex
TRI	14.20	326.	69.8	C	Ex

TABLE A.I.6. (Continued)

Station	Distance (degrees)	Azimuth	i_h Vp=7.5km/sec	P Wave First Motion	Quality
TRN	81.11	277.	21.0	C	VG
UME	29.56	356.	37.1	C	Ex
VAL	30.68	316.	36.8	C	Ex
WES	71.75	309.	24.0	C	Ex

TABLE A.I.7. Summary of Station Parameters and the First Motion Data for the Earthquake of Mar. 28, 1970.

Station	Distance (degrees)	Azimuth	i_h Vp=6.6 (km/sec)	i_h Vp=7.5 (km/sec)	P Wave First Motion	Quality
AAB	35.74	68.	30.8	35.6	D	(2)
AAE	31.29	162.	31.7	36.6	D	VG
AAM	78.46	316.	19.2	21.9	D	G
AKU	37.71	330.	30.2	34.9	D	G
ALQ	95.43	325.	15.8	18.1	D	VG
ANP	75.86	69.	19.9	22.8	D	Ex
AQU	12.56	290.	53.4	65.8	D	VG
ARG	3.17	200.	57.8	74.1	C	(3)
ATL	85.01	310.	17.2	19.6	D	VG
ATU	4.68	257.	57.8	74.1	C	Ex
BAG	80.52	76.	17.9	20.4	D	Ex
BAK	8.83	79.	55.3	69.2	D	(2)
BEC	73.09	298.	19.9	22.8	D	VG
BHP	98.71	289.	15.8	18.0	D	F
BKR	10.94	72.	54.3	67.2	D	(2)
BKS	98.66	338.	15.8	18.0	D	F
BOG	97.48	282.	15.8	18.0	D	G
BUL	59.34	181.	23.5	26.9	D	G
CAR	88.28	282.	16.2	18.5	D	VG
CHG	62.56	87.	23.4	26.9	D	Ex
CNG	65.18	177.	22.8	26.2	C	(4)
COL	75.87	359.	19.2	21.9	D	Ex

TABLE A.I.7. (Continued)

Station	Distance (degrees)	Azimuth	i_h Vp=6.6 (km/sec)	i_h Vp=7.5 (km/sec)	P Wave First Motion	Quality
COP	20.00	331.	32.9	38.1	D	Ex
COR	92.70	341.	15.9	18.1	D	G
DAV	90.19	81.	16.0	18.3	D	Ex
DUG	93.80	332.	15.8	18.1	D	G
DUR	26.02	317.	33.2	38.0	C	(4)
EIL	10.64	153.	54.6	67.5	D	(2)
ESK	27.02	317.	32.3	37.4	D	VG
FBC	58.95	329.	24.3	27.8	C	(4)
FLO	84.53	317.	17.3	19.8	D	VG
GDH	51.36	333.	26.4	30.4	D	VG
GEO	77.00	310.	19.6	22.4	D	VG
GOL	90.97	327.	16.2	18.4	D	VG
GRF	16.70	315.	49.0	57.6	C	(4)
GRM	72.56	183.	20.8	23.8	D	P(1)
HKC	72.15	75.	20.9	23.9	D	VG
HLW	9.46	170.	55.3	71.7	C	Ex
IST	1.88	348.	59.1	74.8	D	Ex
JAN	6.69	277.	56.5	71.5	C	(3)
JCT	95.88	318.	15.8	18.0	D	F
JER	8.75	146.	56.5	71.5	D	G
KBL	31.72	86.	31.6	36.5	D	Ex
KBS	40.33	355.	29.3	33.7	D	G(1)
KEV	30.58	358.	31.8	36.8	D	VG

TABLE A.I.7. (Continued)

Station	Distance (degrees)	Azimuth	i_h Vp=6.6 (km/sec)	i_h Vp=7.5 (km/sec)	P Wave First Motion	Quality
KIS	7.84	357.	56.5	72.0	C	(4)
KHC	15.11	316.	51.3	63.0	D	Ex
KON	23.98	335.	34.6	40.2	D	Ex
KRV	12.97	78.	53.2	65.4	D	(2)
KTG	40.78	336.	29.3	33.8	D	VG
LAH	36.96	88.	30.4	34.2	D	Ex
LEM	85.22	103.	17.0	19.5	D	G
LON	90.31	341.	16.2	18.5	D	VG
MAL	26.69	275.	32.2	37.3	D	Ex
MAN	81.99	78.	18.1	20.7	D	Ex
MAT	79.83	51.	18.8	21.4	D	Ex
MFP	40.39	213.	29.5	34.0	C	(4)
MSH	23.85	87.	34.6	41.2	D	Ex
NAI	41.02	169.	29.3	33.8	D	VG
NAT	74.00	249.	20.4	23.3	D	G
NDI	40.46	90.	29.5	34.0	D	Ex
NOR	45.28	351.	28.1	32.4	D	G
NUR	21.52	353.	38.4	44.9	D	Ex
OGD	74.17	311.	20.4	23.3	D	Ex
OXF	87.16	314.	16.7	19.1	D	Ex
PDA	42.52	286.	28.9	33.3	D	VG
POO	43.42	105.	28.6	33.0	D	Ex
PRE	64.96	181.	23.0	26.3	D	VG

TABLE A.I.7. (Continued)

Station	Distance (degrees)	Azimuth	i_h Vp=6.6 (km/sec)	i_h Vp=7.5 (km/sec)	P Wave First Motion	Quality
PRK	2.50	272.	58.2	74.1	C	(3)
PRU	15.13	320.	51.3	63.0	D	VG
PTO	28.94	286.	32.1	37.1	D	Ex
SCP	76.24	312.	19.9	22.7	D	VG
SDB	56.13	199.	25.1	28.8	D	VG
SEM	36.91	55.	30.4	35.1	D	(2)
SEO	72.21	56.	20.9	23.9	D	Ex
SHA	89.22	310.	16.3	18.6	D	VG
SHI	21.17	110.	39.1	45.8	D	Ex
SHL	53.35	85.	25.9	29.8	D	Ex
SJG	82.87	288.	17.9	20.5	D	VG
STU	17.38	310.	47.3	56.7	D	Ex
TAB	13.17	90.	53.0	65.2	D	Ex
TEN	39.10	268.	29.8	34.4	C	(4)
TOL	25.72	282.	33.1	38.3	D	Ex
TRI	13.27	304.	55.3	69.2	D	Ex
TRN	83.98	279.	17.5	20.0	D	VG
TUC	99.55	327.	15.8	18.0	D	G
UME	25.22	350.	33.5	38.8	D	Ex
VAL	30.12	308.	31.9	36.9	D	VG
VAM	5.66	230.	57.2	72.7	D	(3)
WES	71.42	310.	21.1	24.1	D	Ex
WIN	62.84	193.	23.4	26.8	D	VG

TABLE A.I.8. Summary of Station Parameters and the First Motion Data for the First Earthquake of Apr. 19, 1970.

Station	Distance (degrees)	Azimuth	i_h Vp=6.6km/sec	P Wave First Motion	Quality
AAE	31.09	163.	31.7	D	G
AKU	37.94	330.	29.5	C	P
ALE	51.81	350.	25.3	C	(4)
ALM	25.45	275.	33.2	C	(4)
AQU	12.82	290.	53.4	C	G
ARG	3.13	205.	57.8	C	(3)
ATL	85.27	310.	17.1	D	P
ATU	4.87	259.	57.2	D	VG
BAG	80.34	77.	18.6	D	G
BEC	73.36	299.	20.5	C	P
BKR	10.77	71.	54.1	C	(2)
BNS	19.83	314.	41.6	C	(4)
BUL	59.21	181.	24.3	D	P
CAR	88.53	282.	16.4	C	VG(1)
CHG	62.34	88.	23.5	D	G
CMP	7.13	332.	56.5	C	(4)
COL	76.01	359.	19.9	D	G(1)
COP	20.23	331.	41.0	C	G
DUG	94.03	332.	15.9	D	G(1)
EIL	10.42	154.	54.9	D	(2)
ESK	27.28	317.	32.3	C	F
FLO	84.78	317.	17.2	D	F

TABLE A.I.8. (Continued)

Station	Distance (degrees)	Azimuth	i_h Vp=6.6km/sec	P Wave First Motion	Quality
FUR	16.16	310.	50.8	C	(4)
GOL	91.20	327.	16.1	D	P(1)
GRM	72.44	183.	20.8	D	P
GRS	12.79	83.	53.2	D	(2)
HKC	71.97	76.	20.9	D	P
HLW	9.29	172.	55.3	D	(4)
IFR	28.56	270.	32.1	C	(4)
IST	2.07	343.	57.8	C	Ex
[illegible]	6.93	278.	56.5	C	(3)
KEV	30.72	358.	31.7	C	G
KBS	40.49	355.	29.4	C	G
KBL	31.50	86.	31.6	D	G
KON	24.20	335.	34.3	C	G
KRL	18.24	310.	45.6	C	(4)
KTG	40.99	336.	29.3	C	G
LEM	84.97	103.	17.2	D	P
MAT	79.74	51.	18.8	D	G
MAL	26.93	276.	32.4	D	P
MSH	23.63	87.	35.2	D	VG
NAI	40.85	169.	29.3	D	F
NDI	40.24	90.	29.5	D	G
NOR	45.44	351.	28.1	C	G
NUR	21.68	353.	38.1	C	G

TABLE A.I.8. (Continued)

Station	Distance (degrees)	Azimuth	i_h Vp=6.6km/sec	P Wave First Motion	Quality
PLG	5.05	287.	57.8	D	(3)
POO	43.16	105.	28.7	D	G
PRE	64.83	182.	22.9	C	G(*)
PRK	2.73	275.	57.8	D	(3)
PTO	29.20	287.	32.1	C	G
QUE	31.59	95.	31.6	D	G
SRI	15.63	92.	50.8	C	(4)
SCP	76.49	312.	19.7	D	G(1)
SEM	36.80	55.	30.4	C	(2)
SHI	20.91	110.	39.4	D	Ex
SHL	53.14	85.	25.9	D	G
SJG	83.13	288.	17.8	D	G
SLM	85.11	317.	17.2	C	(4)
STU	17.64	310.	46.8	D	G
TAB	12.94	89.	53.2	D	VG
TOL	25.97	283.	32.8	D	VG
TRI	13.54	305.	51.3	C	P(1)
TRN	84.22	279.	17.4	D	G
UME	25.39	350.	33.2	C	Ex
UPP	22.19	343.	37.2	C	(4)
VKA	13.38	318.	57.2	C	(4)
VLS	7.24	266.	56.5	C	(3)
WES	71.68	310.	21.0	D	G
WIN	62.76	193.	23.4	D	G

TABLE A.I.9. Summary of Station Parameters and the First Motion Data for the Second Earthquake of Apr. 19, 1970.

Station	Distance (degrees)	Azimuth	i_h Vp=6.6km/sec	P Wave First Motion	Quality
AAB	35.55	68.	30.9	D	(2)
AAE	31.08	163.	31.8	D	VG(1)
AAM	78.74	316.	19.2	D	G
AKU	37.95	330.	29.5	C	P(1)
ALQ	95.69	325.	15.8	D	P(1)
AQU	12.85	290.	53.5	D	P(1)
ARG	3.15	206.	57.9	D	(3)
ATL	85.30	310.	17.1	D	G
ATU	4.90	259.	57.3	D	G
BAG	80.30	77.	18.6	D	G
BEC	73.38	299.	20.6	D	P(1)
BUL	59.21	181.	24.3	D	G
CAR	88.56	282.	16.5	D	VG
CHG	62.31	88.	23.6	D	G
CMP	7.14	322.	56.6	C	(4)
COL	76.02	359.	19.9	D	G
COP	20.24	331.	41.0	C	P
DUG	93.34	332.	16.0	D	P
FLO	84.80	317.	17.2	D	VG
FUR	16.19	310.	50.8	C	(4)
GOL	91.22	327.	16.1	D	P(1)
GRF	16.98	315.	48.1	C	(4)

TABLE A.I.9. (Continued)

Station	Distance (degrees)	Azimuth	i_h Vp=6.6km/sec	P Wave First Motion	Quality
GRM	72.44	183.	20.8	D	P(1)
GRS	12.76	83.	53.2	C	(2)
IFR	28.60	270.	32.1	C	(4)
IST	2.08	342.	59.5	C	VG
JAN	6.96	278.	56.6	C	(3)
KBL	31.47	86.	31.7	D	VG(1)
KBS	40.49	355.	29.5	C	P(1)
KEV	30.72	358.	31.8	C	P(1)
KON	24.21	335.	34.4	C	G(1)
KTG	41.00	336.	29.3	D	P
LEM	84.94	103.	17.2	D	P
MAT	79.71	51.	18.8	D	VG
NAI	40.84	169.	29.4	D	P
NDI	40.21	90.	29.6	D	P
NOR	45.45	351.	28.1	D	G(1)
NUR	21.68	353.	38.1	C	G
OGD	74.45	311.	20.2	D	G(1)
PLG	5.03	287.	57.9	D	(3)
POO	43.13	106.	28.8	D	G(1)
PRE	64.83	182.	22.9	D	G
PRK	2.76	275.	57.9	D	(3)
PTO	29.23	287.	32.1	C	P
SCP	76.52	312.	19.7	D	G

TABLE A.I.9. (Continued)

Station	Distance (degrees)	Azimuth	i_h Vp=6.6km/sec	P Wave First Motion	Quality
SEO	72.07	56.	20.9	D	G(1)
SHI	20.88	110.	39.4	D	VG(1)
SHL	53.11	85.	26.0	D	G
SJG	83.16	288.	17.8	D	P(1)
STU	17.66	310.	46.8	D	VG(1)
TAB	12.91	89.	53.2	D	F
TOL	26.00	283.	32.9	D	VG
TRI	13.56	305.	51.4	C	G
TRN	84.26	279.	17.4	D	G
TUC	99.80	327.	15.8	D	G(1)
UME	25.39	350.	33.3	C	G(1)
WES	71.70	310.	21.0	D	P
WIN	62.77	193.	23.4	D	G

TABLE A.I.10. Summary of Station Parameters and the First Motion Data for the Earthquake of May 12, 1971.

Station	Distance (degrees)	Azimuth	i_h Vp=6.6 (km/sec)	i_h Vp=7.5 (km/sec)	P Wave First Motion	Quality
AAE	29.69	162.	32.5	37.6	C	G
AAM	79.75	316.	18.9	21.5	D	G
AKU	39.20	331.	30.0	34.6	C	F
ANP	76.29	69.	19.8	22.6	D	P
AQU	13.35	296.	53.4	65.9	C	Ex
ARG	1.86	223.	59.3	77.3	C	(3)
ATU	4.75	277.	57.8	74.2	C	Ex
BAG	80.74	76.	18.5	21.1	D	VG
BEC	74.02	299.	20.4	23.3	D	P
BLA	81.28	311.	18.3	21.0	D	G
BNG	34.61	200.	31.0	35.8	C	(4)
BNS	20.87	317.	39.6	46.5	C	(4)
BUC	7.35	339.	56.7	72.0	C	(4)
BUL	57.73	181.	24.7	28.3	C	G(1)
CAR	88.79	282.	16.4	18.7	C	P
CHG	62.47	87.	23.5	26.9	D	VG
CMP	8.45	337.	56.5	71.5	C	(4)
CNG	63.58	177.	23.2	26.6	C	(4)
COL	77.50	359.	19.4	22.2	D	G
COP	21.51	333.	38.5	45.0	C	P
DAV	90.28	81.	16.2	18.5	D	F
DUG	94.60	332.	15.9	18.1	D	G(1)

TABLE A.I.10. (Continued)

Station	Distance (degrees)	Azimuth	i_h Vp=6.6 (km/sec)	i_h Vp=7.5 (km/sec)	P Wave First Motion	Quality
ESK	28.35	319.	32.2	37.2	C	P
EIL	9.13	150.	55.4	69.2	C	(2)
FLO	85.84	317.	17.0	19.3	D	G
FUR	17.13	314.	48.2	61.7	C	(4)
GEO	78.17	310.	19.3	22.0	D	G
GRS	13.11	76.	53.0	65.7	D	(2)
HKC	72.40	75.	20.8	23.8	D	F
HIW	7.83	170.	56.5	72.8	C	(4)
HYB	47.13	101.	27.6	31.8	C	(4)
IAS	9.73	351.	54.0	68.5	C	(4)
IST	3.51	351.	57.8	74.2	C	Ex
JCT	97.19	318.	15.8	18.0	D	P
JER	7.34	141.	56.6	71.5	C	G
KBL	31.70	83.	32.5	37.6	D	Ex
KEV	32.20	358.	31.5	36.5	D	VG
KHC	16.43	320.	49.3	59.1	C	G
KON	25.52	336.	33.2	38.5	C	VG
KRV	13.23	71.	53.3	65.7	D	(2)
KTG	42.33	337.	29.0	33.4	C	P
LAH	36.93	86.	30.4	35.2	D	G
LEM	84.69	103.	17.3	19.7	D	P
MAL	27.06	279.	32.9	38.1	D	G
MAT	80.72	51.	18.5	21.1	D	VG

TABLE A.I.10. (Continued)

Station	Distance (degrees)	Azimuth	i_h Vp=6.6 (km/sec)	i_h Vp=7.5 (km/sec)	P Wave First Motion	Quality
MSH	23.80	84.	34.9	40.6	D	Ex
NAI	39.40	169.	29.7	34.3	C	F
NAT	73.60	250.	20.4	23.4	D	G
NDI	40.32	88.	29.5	34.0	D	G
NOR	46.90	352.	27.7	31.9	D	G
NUR	23.15	354.	35.8	41.6	D	G
OGD	75.36	311.	20.0	22.9	D	G
OXF	88.41	314.	16.5	18.8	D	VG
POO	42.84	104.	28.8	33.2	D	G
PTO	29.60	289.	32.0	37.1	C	G
PRK	3.17	303.	57.8	74.2	C	(3)
PRU	16.52	323.	49.1	59.1	C	G
QUE	31.56	92.	31.6	36.6	D	VG
RBA	29.77	274.	32.0	37.1	C	(4)
SCP	77.45	312.	19.4	22.2	D	G
SEM	37.72	54.	30.3	34.9	D	(2)
SHA	90.40	311.	16.2	18.4	D	G
SHI	20.51	106.	40.4	47.5	D	VG
SJG	83.53	288.	17.7	20.2	D	G
SRO	13.22	324.	53.0	65.2	C	(4)
STU	18.58	314.	44.7	53.1	D	F
TAB	13.11	83.	53.1	65.3	D	G
TAN	58.64	160.	24.4	28.0	C	(4)

TABLE A.I.10. (Continued)

Station	Distance (degrees)	Azimuth	i_h Vp=6.6 (km/sec)	i_h Vp=7.5 (km/sec)	P Wave First Motion	Quality
TIR	8.51	299.	55.5	69.8	C	(4)
TRI	14.38	309.	52.0	66.4	C	Ex
TRN	84.40	279.	17.3	19.8	D	G
VAL	31.27	310.	31.7	36.7	C	VG
VKA	14.49	322.	52.0	72.8	C	(4)

REFERENCES CITED

Aki, K., Study of earthquake mechanism by a method of phase equalization applied to Rayleigh and Love waves, J. Geophys. Res., 65, 729-740, 1960.

Aki, K., Earthquake mechanism, in The Upper Mantle, pp. 423-466, edited by A. R. Ritsema, Tectonophysics, 13(1-4), 1972.

Allen, C. R., Active faulting in northern Turkey, Division of Geological Sciences, Contribution 1577, 10 p., California Institute of Technology, Pasadena, California, 1969.

Ambraseys, N. N., and A. Zatopek, The Varto Ustukran (Anatolia) earthquake of 1966, August 19: a summary of a field report, Bull. Seismol. Soc. Amer., 58, 47-102, 1968.

Ambraseys, N. N., and A. Zatopek, The Mudurnu valley, west Anatolia, Turkey, earthquake of 1967, July 22, Bull. Seismol. Soc. Amer., 59, 521-289, 1969.

Ambraseys, N. N., and J. S. Thalenko, The Gediz (Turkey) earthquake of 1970, March 28, Nature, 227, 592-593, 1970.

Ambraseys, N. N., On the value of historical records of earthquakes, Nature, 232, 375-379, 1971.

Anderson, E. M., The Dynamics of Faulting, 206 p., Oliver and Boyd, Edinburgh, 1951.

Archambeau, C. B., General theory of elastodynamic source fields, Rev. Geophys., 6, 241-288, 1968.

Arpat, E., and E. Bingol, The rift system of the western Turkey; thoughts on its development, Bull. Min. Res. and Explor. Inst. Turkey, 73, 1-9, Ankara, 1969.

Beloussov, V. V., Earth's tectonosphere (results and further problems for investigation), Intern. Geol. Rev., 11 (12), 1368-1381, 1969.

Berry, M. J., and L. Knopoff, Structure of the upper mantle under the western Mediterranean basin, J. Geophys. Res., 72, 3613-3626, 1967.

Blumenthal, M., Geologie der Taurusketten im Hinterland von Seydisehir und Beysehir: Maden Tetkik Arama Enst., Publ. ser.D, n.2, Ankara, 1947.

Brunn, J. H., J. H. Dumont, P. C. Graciansky, M. Gutnic, T. Juteau, J. Marcoux, O. Monod and A. Poisson, Outline of the geology of the western Taurids, in Geology and History of Turkey, pp. 225-255, edited by A. S. Campbell, The Petrol. Explor. Soc. Libya, Tripoli, 1971.

Bullen, K. E., An Introduction to the Theory of Seismology, 3rd ed., pp. 154-155, Cambridge University Press, London, 1963.

Bune, V. J., N. A. Vvedenskaya, I. V. Gorbunova, N. V. Kondorskaya, N. S. Landyreva, and I. V. Federova, Correlation of M_{LH} and M_{pv} by data of the network of seismic stations of the USSR, Geophys. J. R. astr. Soc., 19, 533, 1970.

Burridge, R., and L. Knopoff, Body force equivalents for seismic dislocations, Bull. Seismol. Soc. Amer., 57, 341-371, 1964.

Campbell, A. S. (Editor), Geology and History of Turkey, 511 p., Petrol. Explor. Soc. Libya, Tripoli, 1971.

Canitez, N., and M. N. Toksoz, Focal mechanism and source depth of earthquakes from body and surface wave data, Bull. Seismol. Soc. Amer., 61, 1369-1379, 1971.

Canitez, N., and S. B. Ucer, Computer determinations for the fault plane solutions in and near Anatolia, Tectonophysics, 4, 235-244, 1967a.

Caputo, M., G. F. Panza, D. Postpischl, Deep structure of the Mediterranean basin, J. Geophys. Res., 75, 4919-4922, 1970.

Cash, D. J., The Dulce, New Mexico, earthquake of January 23, 1966: Location, focal mechanism, magnitude, and source parameters, Ph.D. Thesis, 89 p., New Mexico Institute of Mining and Technology, Socorro, New Mexico, 1971.

DeSitter, L. U., Structural Geology, 551 p., McGraw-Hill, New York, 1964.

Drakopoulos, J. C., and A. C. Ekonomides, Aftershocks of February 19, 1968 earthquake in northern Aegean Sea and related problems, Pure and Appl. Geophys., 95, 100-115, 1972.

Elsasser, W. W., Convection and stress propagation in the upper mantle, Princeton University Tech. Rept. 5, 1967.

Ergin, K., U. Guclu, and Z. Uz, A catalog of earthquakes for Turkey and surrounding area (11 A.D. to 1964 A.D.), Technical University of Istanbul, Faculty of Mining Engineering, 1967.

Erinc, S., The Gediz earthquake of 1970; in Geology and History of Turkey pp. 443-457, edited by A. S. Campbell, The Petrol. Explor. Soc. Libya, Tripoli, 1971.

Evison, F. F., Seismogenesis, Tectonophysics, 9, 113-128, 1970.

Ewing, J. and M. Ewing, Seismic refraction measurements in the Atlantic Ocean basins, in the Mediterranean Sea, on the Mid-Atlantic ridge and in the Norwegian Sea, Bull. Geol. Soc. Am., 70, 291-318, 1959.

Galanopoulos, A. G., The seismotectonic regime in Greece, Ann. Geofis. (Rome), 20, 109-119, 1967.

Gaskell, T. F., M. N. Hill, J. C. Swallow, Seismic measurements made by H.M.S. Challenger in the Atlantic, Pacific, and Indian Oceans and Mediterranean Sea, 1950-1953, Phil. Trans. Roy. Soc., A255, 417-465, 1958.

Gilluly, J., Tectonics involved in the evolution of mountain ranges, in The Nature of the Solid Earth, pp. 406-439, edited by E. C. Robertson, McGraw-Hill, New York, 1972.

Gutenberg, B., and C. F. Richter, Seismicity of the Earth, 273 p., Princeton University Press, Princeton, New Jersey, 1954.

Hanson, M. E., A. R. Sanford, A two-dimensional source function for a dynamic brittle bilateral tensile crack, Bull. Seismol. Soc. Amer., 60, 1209-1219, 1970.

Hanson, M. E., A. R. Sanford and R. J. Shaffer, A source function for a dynamic bilateral brittle shear fracture, J. Geophys. Res., 76, 3375-3385, 1971.

Herrin, E. (chairman), E. P. Arnold, B. A. Bolt, G. E. Clawson, E. R. Engdahl, H. W. Freedman, D. W. Gordon, A. L. Hales, J. L. Lobdell, O. Nuttli, C. Romney, J. Taggart, and W. Tucker, 1968 Seismological tables for P phases, Bull. Seismol. Soc. Amer., 58, 1193-1241,1968.

Hess, H. H., Evolution of ocean basins, Report to Office of Naval Research on research supported by ONR Contract Nonr. 1858(10), 38 pp., 1960.

Hodgson, J. H., and W. Milne, Direction of faulting in certain earthquakes of the north Pacific, Bull. Seismol. Soc. Amer., 41, 221-242, 1951.

Honda, H., Earthquake mechanism and seismic waves, J. Phys. Earth., 10, 1-97, 1962.

Ilhan, E., Earthquakes in Turkey, in Geology and History of Turkey, pp. 431-441, edited by A. S. Campbell, The Petrol. Explor. Soc. Libya, Tripoli, 1971.

Ilhan, E., The structural features of Turkey, in Geology and History of Turkey, pp. 159-170, edited by A. S. Campbell, The Petrol. Explor. Soc. Libya, Tripoli, 1971.

Isacks, B., J. Oliver, and L. Sykes, Seismology and the new global tectonics, J. Geophys. Res., 75, 5011-5027, 1968.

Isacks, B. L., L. R. Sykes, and J. Oliver, Focal mechanisms of deep and shallow earthquakes in the Tonga-Kermadec region and the tectonics of island arcs, Geol. Soc. Amer. Bull., 80, 1443, 1969.

Jeffreys, H., and K. E. Bullen, Seismological tables, Brit. Assn. Gray-Milne Trust, 1958.

Karnik, V., Seismicity of the European area, 2 vols, D. Reidel Publ. Co., Dordrecht-Holland, 1969 and 1971.

Karnik, V., Seismicity of the European area, Amer. Geophys. Union monograph 13, 139-144, 1969.

Keilis-Borok, V. I., E. N. Bessonova, O. D. Gotsadze, I. V. Kirillova, S. D. Kogan, T. I. Kikhtikova, L. N. Malinovskaya, G. I. Pavlova, and A. A. Serskii, Investigation of the Mechanism of Earthquakes, 210 p., English translation published by Amer. Geophys. Union, 1960.

Ketin, I., and F. Roesli, Makroseismische Untersunchungen über das nordwestanolische Beben Vom 1953 Marz 18, Eclogae Geol. Helv., 46, 187, 1953.

Ketin, I., Relations between general tectonic features and the main earthquake regions of Turkey, Bull. Min. Res. and Explor. Inst. (M.T.A.), 71, 63-67, Ankara, 1968.

Le Pichon, X., Sea-floor spreading and continental drift, J. Geophys. Res., 73, 3661-3697, 1968.

McKenzie, D. P., and R. L. Parker, The north Pacific: an example of tectonics on a sphere, Nature, 216, 1276-1280, 1967.

McKenzie, D. P., The relation between fault plane solutions for earthquakes and the directions of the principal stresses, Bull. Seismol. Soc. Amer., 59, 591-601, 1969b.

McKenzie, D. P., The plate tectonics of the Mediterranean region, Nature, 226, 239-243, 1970.

McKenzie, D. P., Plate tectonics, in The Nature of the Solid Earth, pp. 323-360, edited by E. C. Robertson, McGraw-Hill, New York, 1972a.

McKenzie, D. P., Active tectonics of the Mediterranean region, Geophys. J. R. astr. Soc., 30, 109-185, 1972b.

Molnar, P., and J. Oliver, Lateral variations of attenuation in the upper mantle and discontinuities in the lithosphere, J. Geophys. Res., 74, 2648-2682, 1969.

Morgan, W. J., Rises, trenches, great faults and crustal blocks, J. Geophys. Res., 73, 1959-1982, 1968.

Morgan, W. J., Convection plumes in the lower mantle, Nature, 230, 42-43, 1971.

Moskalenko, V. N., New data on the structure of the sedimentary strata and basement in the Levant Sea, Oceanologiya, 6, 828-836, 1966.

Nakano, H., Notes on the nature of the forces which give rise to the earthquake motions, Central Meteor. Observ. Japan, Seismol. Bull., 1, 92-130, 1923.

Nowroozi, A. A., Seismo-tectonics of the Persian plateau, Eastern Turkey, Caucasus, and Hindu Kush regions, Bull. Seimol. Soc. Amer., 61, 317-341, 1971.

Nowroozi, A. A., Focal mechanism of earthquakes in Persia, Turkey, west Pakistan, and Afghanistan and plate tectonics of the middle east, Bull. Seismol. Soc. Amer., 62, 823-850, 1972.

Papazachos, B. C., P. E. Comniakis, and J. Drakopoulos, Preliminary results of an investigation of the crustal structure in southeastern Europe, Bull. Seismol. Soc. Amer., 56, 1241-1268, 1966.

Papazachos, B. C., Phase velocities of Rayleigh waves in southeastern Europe and eastern Mediterranean Sea, Pure and Appl. Geophys., 75, 47-55, 1968.

Papazachos, B. C., and N. D. Delibasis, Tectonic stress field and seismic faulting in the area of Greece, Tectonophysics, 7(3), 231-255, 1969.

Payo, G., Crustal structure of the Mediterranean Sea by surface waves, Part I, group velocity, Bull. Seismol. Soc. Amer., 57, 151-172, 1967.

Price, N. J., Fault and joint development in brittle and semi-brittle rock, Pergamon Press, 176 p., 1966.

Rabinowitz, P. D., and W. B. F. Ryan, Gravity anomalies and crustal shortening in the eastern Mediterranean, Tectonophysics, 10, 585-608, 1970.

Ramsay, J. G., Folding and Fracturing of Rocks, McGraw-Hill, New York, 568 p., 1967.

Randal, M. J., On the mechanism of earthquakes, Bull. Seismol. Soc. Amer., 54, 1283-1289, 1964a.

Reid, H. F., The mechanics of the earthquake: the California earthquake of April 18, 1906, Report of the state investigation committee, v. 2, Carnegie Institution of Washington, D. C., 1910.

Richter, C. F., Elementary Seismology, W. H. Freeman and Co., San Francisco, 768 p., 1958.

Ritsema, A. R., Mechanisms of European earthquakes, Tectonophysics, 4, 247-259, 1967.

Ryan, W. B. F., D. J. Stanley, J. B. Hersey, D. A. Fahlquist, T. D. Allan, The tectonics and geology of the Mediterranean Sea, in The Sea, v. 4, pp. 387-492, edited by A. E. Maxwell, Wiley-Interscience, 1970.

Sanford, A. R., Analytical and experimental study of simple geologic structures, Geol. Soc. Amer. Bull., 70, 19-52, 1959.

Savage, J. C., A theory of creep waves propagating along a transform fault, J. Geophys. Res.,76, 1954-1966, 1971.

Shirokova, E. I., Stresses effective in earthquake foci in the Caucasus and adjacent districts, Izv. Akad. Nauk USSR, Ser. Geophiz, 10, 809, 1962.

Stauder, W. J., The focal mechanism of earthquakes, Adv. in Geophysics, 9, 1-76, 1962.

Stauder, W. J., Mechanism of Rat island earthquake sequence of February 4, 1965, with relation to island arcs and sea-floor spreading, J. Geophys. Res., 73, 3847-3858, 1968.

Sykes, L. R., Mechanism of earthquakes and nature of faulting on mid-oceanic ridges, J. Geophys. Res., 72, 2131-2153, 1967.

Sykes, L. R., and M. L. Sbar, Intra-plate earthquakes, contemporary stresses, and the driving mechanism of plate tectonics (Abs.), Transactions, Amer. Geophys. Union, v. 54, n. 4, 455, 1973.

Tasdemiroglu, M., The 1970 Gediz earthquake in western Anatolia, Turkey, Bull. Seism. Soc. Amer., 61, 1507-1527, 1971.

Toksoz, M. N., D. G. Harkrider, and A. Ben-Menahem, Determination of source parameters by amplitude equilization of seismic surface waves, 2, Release of tectonic strain by underground nuclear explosions and mechanisms of earthquakes, J. Geophys. Res., 70, 907-922, 1965.

Udias, A., A study of the aftershocks and focal mechanism of the Salinas-Watsonville earthquakes of August 31, and September 14, 1963, Bull. Seismol. Soc. Amer., 55, 85-106, 1965.

Vening Meinesz, F. A., The Earth's Crust and Mantle, Developments in Solid Earth Geophysics, v. 1, 124 p., Elsevier Publ. Co., 1964.

Vine, F. J., and D. H. Matthews, Magnetic anomalies over ocean ridges, Nature, 199, 947-949, 1963.

Vogt, P. R., and R. H. Higgs, An aeromagnetic survey of the eastern Mediterranean Sea and its interpretation, Earth and Planet. Sci. Letters, 5, 439-448, 1969.

Vvedenskaya, A. V., Determination of the displacement fields following an earthquake, employing dislocation theory, Bull. (IZV.) Acad. Sci. USSR, Geophys., 3, 277-284, 1956.

Wallace, R. E., Earthquake of 1966 August 19 Varto area, eastern Turkey, Bull. Seismol. Soc. Amer., 58, 11-45, 1968.

Wegener, A., The Origin of Continents and Oceans (Transl.), 4th ed., Dover, New York, 220 p., 1966.

Wilson, J. T., A new class of faults and their bearing on continental drift, Nature, 207, 343-347, 1965.

This dissertation is accepted on behalf of the faculty of the Institute by the following committee:

Allan R. Sanford
Adviser

C. W. Hahn

C. J. Pridding

Marvin N. Wilkening

May 11, 1973
Date